Title
Biomechanics and evolution of flight in stick insects

Author
Zeng, Yu

Publication Date
2013

Peer reviewed|Thesis/dissertation

Biomechanics and evolution of flight in stick insects

by

Yu Zeng

A dissertation submitted in partial satisfaction
of the requirements for the degree of

Doctor of Philosophy

in

Integrative Biology

in the

GRADUATE DIVISION

of the

UNIVERSITY OF CALIFORNIA, BERKELEY

Committee in charge:

Professor Robert Dudley, Co-Chair
Professor David Wake, Co-Chair
Professor Ronald Fearing
Professor Kipling Will

Fall 2013

Biomechanics and evolution of flight in stick insects

by

Yu Zeng

Abstract

Biomechanics and evolution of flight in stick insects
by
Yu Zeng
Doctor of Philosophy in Integrative Biology
University of California, Berkeley
Professor Robert Dudley, Co-Chair
Professor David Wake, Co-Chair

Many unresolved questions in animal flight evolution relate to the transition between flightless and volant forms. Functional analysis of transitional modes using anatomical intermediates may help to assess the biomechanical underpinnings to such transitional processes. The group of stick insects exhibits tremendous diversity in wing sizes, which is potentially correlated with selection gradient for wing size. This dissertation work uses stick insects as a model system to address the ecological context of controlled aerial behaviors and the evolutionary consequences of flight loss.

Chapter 1 explores the behavioral context of controlled aerial descent in the newly hatched larvae of an Australian stick insect *Extatosoma tiaratum*, which exhibit ephemeral ant-mimicry and hyperactive dispersal activities. Through lab experiments, we documented the ontogenetic variation in various taxic behaviors and voluntary drop as an escaping response. Chapter 2 explores the visual ecology of directed aerial descent in larval *E. tiaratum*. We investigated how visual contrasts are used as locomotor references during directed aerial descent. Our results suggest the use of vertically constant contrast edges is a major component of directional targeting. The utility of contrast as visual cues was further shown to be dependent on both the heterogeneity of the visual environment and the quality of perceived signals. Chapter 3 addressed the biomechanics of aerial righting behaviors in larval *E. tiaratum*. Through high–speed filming and three–dimensional motion reconstruction, the results showed highly controlled leg movements are involved in righting maneuvers. Through posture control, the insects achieve effective righting rotation. More subtle leg movements were also shown in stroke–like patterns, which are instantaneously correlated with whole–insect rotation. This study provided useful information for understanding the ecology and evolution of controlled aerial behaviors in invertebrates. Chapter 4 addressed the functional consequences of progressive wing size reduction along an altitudinal gradient in three populations of a stick insect *Asceles tanarata* native to Malay Peninsula. We investigated how wing and body morphology change along the altitudinal gradient, and further studied the biomechanics of flight in each flight morph. The results indicate the reduction of fight apparatus leads to changes in wing design and wing kinematics. Reduced flapping fight performances resemble parachuting and gliding. Due to both altered kinematics and flight trajectories

different from conventionally recognized flapping flight, the aerodynamics of wing flapping is characterized by large advance ratio and reduced half–stroke asymmetries. Although the reduction in flight performance is closely correlated with the reduction of wing size, wing aerodynamics shows more complex pattern along the performance gradient.

Acknowledgments

First, I would like to express my gratitude to my major advisor, Robert Dudley, for his continuous support since my undergraduate years, and for his inspiration, insights, patience, knowledge and trust. He stimulated my curiosity on aerial behaviors in insects when we first met in 2004, which eventually led to my undergrad research on directed aerial descent in nymphal stick insects *Extatosoma tiaratum* and graduate researches on stick insects flight.

I also would like to give the deepest appreciation to my co-advisor David Wake, who has been patiently advising and supporting me with enormous encouragement over the past six and a half years. Without his wise guidance and significant help I would never have overcome various mental difficulties encountered at different stages of my life in graduate school.

I would like to offer my special thanks to two other members of my dissertation committee: Ronald Fearing and Kipling Will, for their advice over the past four years and for their prompt responses and insightful comments during my writing phase.

To Francis Seow-Choen: thank you for hosting my multiple visits to Singapore and generously offering your stick insects to film. You also have shared with me your experience on stick insect biology and field collection skills, without which I wound not be able to complete my researches.

I am also deeply grateful to the members of my qualifying exam committee: Marvalee Wake, Mimi Koehl, Rosemary Gillespie and Kipling Will, who gave me valuable advice and enormous encouragement.

I have received help from other graduate student. I thank Dennis Evangelista for always standing on my side and helping on different aspects of my researches. I thank Henry Jacobs for generously spending substantial amount of time to help me learn and practice motion analyses on the aerial righting project. Also, I thank Sonal Singhal, who has kindly helped sequencing *Asceles tanarata* genes for building a molecular phylogeny. My greatest thanks also goes to colleagues. I thank Sven Bradler and Thomas Buckley, who have commented on my work and helped me refining the analyses. I thank Bo Cheng and Sanjay Sane for commenting on my analyses. Also, I thank collaborator Faszly Rahim for organizing field trips at Malaysia.

To my undergraduate assistants: Kenrick Lam, Grisanu Matt Naing, Harry Nunns, 'Jenny' Jia Tang, Sehoon Park, Camille Gonzales, Nina Gnong, Sofia Chang, Joan Chen, Yvonne Lin, Arianna Abundo, Mengsha Gong, 'Polly' Yuexiang Chen, Stephanie Yom, Manu Vaish, Vivian Lu, Julie Ray, Brenda Chen, Chandni Kazi, Hanson Zhao, Juliana Olsson, Te Su, Danny Jan, Jizel Emralino, Katie O'Connell, Lynn Nhi Ng uyen, Sebastian Ruf, Faye Pon, Connor O'Malley, Pauline Luong, Sharon Liu, Angela Chuang, and Stephanie Rotter, without your dedication and enthusiasm my research would have never been possible. I would like to thank my labmates: Sofia Chang, Marc Badger, Leeann Louis, Erica Kim, Jose Fernandez, Chris Clark, Greg Byrnes, Matt Medeiros, Yonatan Munk, Marta Wolf, Nir

Sapir, and Victor Ortega for their support through the past many years.

Furthermore, I would like to thank Douglas Ewing, the greenhouse manager of University of Washington, for introducing me to the world of stick insects when I was studying at University of Washington, which led me to exploration in the world of stick insect over the past eight years. I sincerely thank Thomas Daniel for advising me on studying directed aerial descent biomechanics in *E. tiaratum*, which was my earliest observations of different aerial behaviors. I thank Tyson Hedrick for teaching me how to use MatLab when I first started motion reconstruction and analyses.

I would like to thank my high school geography teacher Ying Xie for being a dedicated advisor during my earliest practices in science. I also would like to thank my high school biology teacher Anze Yu for his trust and encouragement, which had tremendously strengthened my confidence of pursuing a life-long career in biology.

To Tom Libby, director of Berkeley Center for Integrative Biomechanics Education and Research (CIBER), who have provided me countless technical support and valuable advice over the past six years. To Azuan Aziz, Juhaida Harun, Shi-Fu Huang, Talia Yuki Moore and Xiaolin Chen, who have helped my field trips. To aunt Nan Lv, thank her solicitude throughout my PhD years. To Lixin Eow, for her warm support when I was under the stress of finishing this dissertation.

To my mother for the her support over the last twenty nine years. You have not only been the greatest mother but also the best friend. Even under the worst financial stress of the family, you had done all you can to ensure my education and health. It was you who first introduced me to the wonder of nature and have supported my hobby for animals for many years. You also spent substantial amount of money on my training in painting, which had been a priceless lesson on aesthetics and benefited my practices in sciences.

Lastly, I would like to thank the Forestry Department of Pahang, Malaysia and Universiti Kebangsaan Malaysia for providing facilities for my field work. Funding has been provided by Museum of Vertebrate Zoology, National Science Foundation, Department of Integrative Biology, Sigma Xi, Society for Integrative and Comparative Biology, and Graduate Division of UC Berkeley.

Dedicated to my mother, Yufeng Peng

Contents

List of Figures

List of Tables

Chapter 1

The ontogenetic variation of navigational strategy in a gliding larval stick insect (*Extatosoma tiaratum*)

Newly hatched larvae of a stick insect, *Extatosoma tiaratum*, exhibit ephemeral ant-mimicry and hyperactive dispersal activities. Here we quantitatively investigated ontogenetic variation in cursorial and taxic behaviors in order to understand the underlying shifts in behavioral ecology during early life history. We first studied the ontogenetic variation in phototaxis and negative gravitaxis behaviors, and found that larval *E. tiaratum* integrate both signals for directed navigation and that the intensity of taxic behaviors changes ontogenetically within the first instar stage. Comparisons of the endurance of dispersal across different ages within the first molt showed a peak of dispersal hyperactivity immediately after hatching, which is followed by a decline. The use of voluntary drop as an escaping response is mostly adopted during this stage of active dispersal. A hyperactive diurnal dispersing phase, with high sensitivity to perturbation, develops immediately after hatching, whereas a subsequent cryptic phase is developed after settling on host plants. A series of ontogenetic shifts in adaptive behaviors through different phases of the early life history in *E. tiaratum* provides insights into the evolution and ecological setting of gliding behaviors in larval *E. tiaratum*.

1.1 Introduction

Forest canopies are complex ecological arenas with three-dimensionally variable physical environments, e.g., spatial heterogeneity, lighting and temperature, and the activities, e.g., navigation, predation and niche partitioning, within arboreal communities can differ substantially from those of purely terrestrial ecosystems. The behavioral niches in arboreal ecosystems may be related, but not restricted, to the temporal occupation of vegetative resources as substrates for resources or as channels for accessing resources [123, 84]. Nonetheless, behavioral ecology of arboreal invertebrates is largely understudied. The uses of physical environments and behavioral adaptation on canopies by arboreal invertebrates are addressed here by using comparative approaches.

As an adaptation among arboreal animals, the uses of gliding, or controlled aerial locomotion, are generally related to reaching resources, escaping from predation, exploratory travel or as mechanisms to avoid falling into unfamiliar habitats [36]. Multiple evolutionary origins of gliding suggest a common demand of such locomotion in different arboreal taxa. However, our current knowledge of the behavioral correlates of gliding remains limited to a few vertebrate species [21, 21, 125, 116], and less is known about arthropods. Documentation of arboreal ant workers falling from trees indicates the initiation of aerial phases is associated with potential predatory risk and disturbances [52, 79, 131]. Studies on the role of visual cues in directed aerial descent of arboreal bristletails, wingless ant workers and larval stick insects suggest their use of visual cues for targeting tree trunks [143, 141]; *E. tiaratum*, which requires a certain level of environmental brightness. Behavioral correlates of directed descent among other arboreal arthropods remain undiscovered. Given the logistic difficulties of conducting behavioral experiments on tree canopies our research possibilities have been restricted; nevertheless, the functionality of gliding may be assessed through experimental studies on laboratory animals.

Macleay's Spectre Stick Insect *E. tiaratum* is native to coastal rainforests along Eastern Australia (Figure 1.1-A). The colony used in this study has red-headed new hatchlings, and thus likely originated from the rainforests of Northeast Queensland [16]. Mainly feeding on local Eucalyptus vegetation, *E. tiaratum* adults are generally arboreal. Mature females drop eggs to the forest floor with no further care [27]. Since the eggs of *E. tiaratum* are decorated with lipid and organic compounds that attract ants, they can be collected, dispersed, stored and protected by foraging ants on the forest floor [59]. Therefore, incubation likely occurs on the forest floor or in ant nests, and newly hatched instars should first appear at the forest floor. In the native habitat, hatching occurs during the rainy season (November to January, [17]). The hatching rhythm of *E. tiaratum* differs from other stick insects in that it occurs during the midday instead of early morning or nighttime [25, 26]. Besides high air humidity, increased environmental temperature has also been recognized as a cue that stimulates hatching. The new hatchlings are diurnally active, and are recognized as mimics of the red-headed and black-bodied workers of several local ant species of the genus

Leptomyrmex, which are ground or log-dwelling and diurnally active on both forest floor and trees [133] (Andrea Lucky, pers. comm.). Immediately after hatching, *E. tiaratum* larvae start running rapidly, and actively searching for vertical surfaces on which to climb upward, presumably for the purpose of reaching the tree canopies and searching for the right host plants,[103]. The rapid-running and ant-mimicking stage only lasts for the first 3-5 days, after which a gradual transition in coloration, behavior and daily rhythm occurs [16, 18]. It takes on average 15 days for young *E. tiaratum* to enter the second molt. Nymphal and adult *E. tiaratum* beyond the second molt are leaf or lichen mimics, and are nocturnally active, indicating a life style of high crypticity typical among stick insects [54]. A recent study (unpublished data) has documented the capability of directed aerial descent in newly hatched larval *E. tiaratum*, indicating both morphological capability and ecological feasibility of such behavior during the immediate post-hatching period. Among all larval stages of *E. tiaratum*, only newly hatched larvae exhibit the maximal gliding performance, i.e. the smallest gliding angle and thus the least height loss. Newly hatched *E. tiaratum* larvae may be under high predatory risk when migrating vertically from understories towards the tree canopies in their native ecosystem [96], and their Batesian ant-mimicry and various behavioral displays used under disturbances may thus be parts of an anti-predation strategy, especially for exposed travel in the day time [104, 97, 18].

Navigation through highly complex vegetative structures during dispersal in larval *E. tiaratum* may require more than a single environmental cue, given the variable climate and inconsistency of environment across different canopy heights [44, 76]. The use of an environmental light gradient as a cue for directed movement has been documented from single-celled organisms to vertebrates in a wide variety of habitats for different purposes, such as foraging and dispersal [83, 112]. Two fundamental quantities of the ambient light environment may be essential to an insect's behavior: (1) the overall brightness, which indicates the average photon density at the observing point, and (2) the brightness gradient, which is a vector consisting of the direction and magnitude of brightness variation [135]. In fact, the photoreceptor sensitivity in larval stick insects is specialized for recognizing bright environments [88]. The intensity of environmental brightness generally increases vertically in forest environments [11, 44], and thus newly hatched *E. tiaratum* from low light conditions may utilize such cues for targeting tree canopies and navigating among vegetative structures. Also, gravity perception is essential to the locomotion in insects [20, 19], and the gravitational field may provide cues that serve as important direction references in exploration under the lack of other environmental cues, e.g., visual signals [108].

Furthermore, host searching can be energetically costly in forests with high plant diversity [112], and dispersal requires substantial amount of energy expenditure, and is highly dependent on the nutritional status of the insect [102, 33]. Thus, the dispersal capability can be assessed by measuring the insects' ascending performance. During ascent, the temporal patterns of pauses are important indices for understanding fatigue recovery, sensory field stabilization and detectability of intermittent locomotion [72]. Furthermore, according

to prior records and preliminary observations, the hyperactive phase of larval *E. tiaratum* is ephemeral and lasts only for a short period of time after hatching. Such hyperactivity may facilitate dispersal and host searching by enhancing the traveling speed, and its decline may be temporally correlated with settling on host plants.

Lastly, arboreal animals may voluntarily or accidentally become airborne during resource search, under potential predatory pressure or environmental disturbances, and the initiation of an airborne phase is essential to the function of subsequent aerial locomotor behaviors [36, 37]. For example, foraging ant workers on tree canopies may drop themselves in response to potential predatory risk [52, 79]. Newly hatched larval *E. tiaratum* may face the disturbances from an unsteady climate, e.g., heavy rains during the hatching season may prevent immediate success in locating a suitable microhabitat [80, 118, 13]. Larval *E. tiaratum* may escape potential danger through an aerial escape. According to preliminary observation, newly hatched *E. tiaratum* are hypersensitive to various disturbing signals, such as physical contact, airflow, substrate slipperiness and substrate vibration, to which they may respond with voluntary withdrawal of tarsi from the substrate, causing an immediate airborne phase.

Here we propose the investigation on the cursorial and taxic behaviors in the early larvae of *E. tiaratum* in order to understand the ontogenetic variation of behavioral traits and their implications for relevant perspectives of the life history. There are three main focuses of this study: (1) the use of environmental cues for directed dispersal; (2) ontogenetic variation in dispersal capabilities; (3) ontogenetic variation voluntary dropping as defensive reactions. Given that the older instars have different life history goals from the earlier ones, we hypothesize that there are ontogenetic shifts in these traits that may reflect such changes.

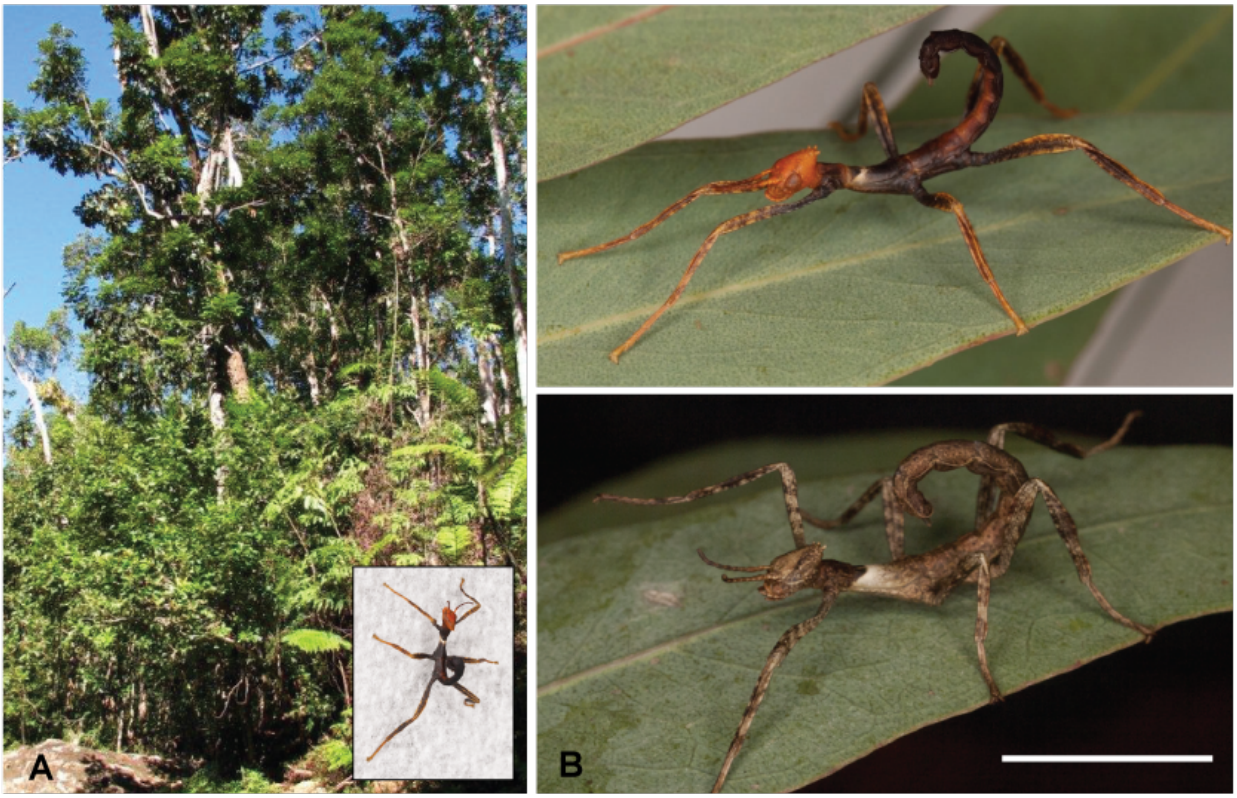

Figure 1.1: (A) Natural habitat of *E. tiaratum*. Lowland Mesophyll forest at Polly Creek, Garradunga, Queensland (Photo courtesy: Jack W. Hasenpusch). Note the complex spatial structures formed by vegetation, and the vertical variation of physical environment. Insertion: a newly born E. tiaratum larva in ascent. (B) Newly hatched (top) and 10-day-old (bottom) individuals (scale bar, 1 cm). Note the differences in coloration and abdomen size.

1.2 Materials and methods

Eggs of *E. tiaratum* from our lab colony were incubated on vermiculate substratum under 70% humidity at 25°C. Newly hatched larvae were collected every 12 hours and then transferred to individual clear plastic cups (354 ml) with caps. Each cup was offered with fresh leaves of Himalayan Blackberry (*Rubus armeniacus*) since the day of birth (0 day–after–hatch; day–after–hatch is abbreviated as DAH hereafter), and was lightly sprayed with water every 2–3 days to maintain a stable humidity. Each cup held no more than 5 individuals. During the experiments, the larval insects were temporarily transferred or kept in the same cups with a water supply.

1.2.1 Ontogenetic variation in taxic responses to light and gravity

In order to examine the role of the light environment in spatial navigation of *E. tiaratum* larvae, we experimentally studied their directionality when exposed to light gradients under different overall brightness with a binary decision setup. We combined one cardboard tunnel (diameter, 2 cm; length, 20 cm) with a thinner and shorter one (diameter, 4.5 cm; length, 10 cm) to form a T–shaped device with one entrance perpendicular to two opposite exits. This device was placed horizontally, and one paper screen (5×5 cm) was placed 3 cm apart from the exit at both ends. Natural-spectrum light bulbs (Verilux, Inc.) connected to a voltage controller for adjusting the brightness were used as the sources of light behind the screens. The brightness at each exit was calibrated with a lightmeter (401025, Extech, MA, USA; spectral range: 400°C 740 nm) prior to experimental trials (Figure 1.2). Experimental trials were conducted under constant temperature (25°C). In each trial, we released one individual at the tunnel entrance and immediately covered the entrance to prevent the insect returning. The insect's directional choices were recorded after it exited from either end, or recorded as "stop" if it did not exit after 5 minutes. Three different combinations of brightness gradients (0 and 3 Lux, 100 and 500 Lux, and 10,000 vs. 20,000 Lux) were used so as to resemble the brightness across different heights in forests, from low light understories to fully exposed canopy under average daylight [4]. Also, in order to record the ontogenetic change of phototaxis behavior, each light gradient treatment was tested for three age groups (0-1, 5, and 10 DAH) representing the early, intermediate and late stages of the first instar. The control experiment was conducted on a 0-1 DAH group in which the setup was in complete darkness, and the experiment personnel used low red light source accompanied with infrared imaging to monitor the process. We ran 5 trials on each of 5 to 20 individuals for each group. We compared the biases of directional choice under each treatment for each age group using One-Way Repeated Measured ANOVA, and compared the overall frequencies of the directional choice under each treatment within the null (1 : 1, assuming no directional bias) using the G–test with William's Correction.

Dispersing larval *E. tiaratum* likely utilize the gravity field as an indication of direction.

Here we examined the effects of gravity to the directionality of *E. tiaratum* nymphs by exposing them to a binary–choice setup in a homogeneous visual environment. We constructed a cubic chamber (40 cm, side length) of which the inner surface was covered by white felt cloth. A T-shaped device made of two wooden sticks was placed in the center of this chamber (Figure 1.3). A small window was located near the free end of the horizontal stick for releasing the experimental insects, and another small window was opened at one top corner for observation. There were also four light bulbs placed external to the top, bottom and two lateral sides to provide a uniform visual environment within the chamber. The brightness inside the chamber was set to 600 Lux. In experiments, *E. tiaratum* nymphs were transferred to the free end of horizontal stick. The movement of the insects was then monitored by the experimental personnel. If the insect turned back, it would be collected to start a new trial. After the insect reached the vertical stick and continued until reaching either ends, the choice of direction was recorded as "up", "down" or "return". Three representative age groups (0–1, 6–7 and 12–14 DAH) within the first instar were tested, as well as one group of early second instars (19–20 DAH). For each individual, we ran 5 trials with valuable data (i.e. no returning of released insects). We used One–Way Repeated Measures ANOVA to compare the results among treatments within each age group, and used the G–test with William's correction to compare the measured frequencies to null frequencies for each of the 4 trials. The null frequency for ascent in each trial is 50%, assuming the choice of vertical direction is independent of gravity.

Preliminary results from the gravitaxis experiments suggested strong negative gravitaxis behavior in vertically traveling larval *E. tiaratum* in the absence of visual cues. Previous studies indicate insects may use integrated sensory inputs in oriented dispersal or exploratory behaviors (Robie et al., 2010; Schowalter, 2000). Besides, the physical environment in the natural habitats of *E. tiaratum* is highly variable across space and time. We here further examined the negative gravitaxis behavior by exposing the newly hatched nymphs to various levels of one essential ambient physical quantity, environmental brightness. With the same experimental setup and procedure described in the previous section, we conducted trials of newly hatched *E. tiaratum* under three environmental brightness levels: 0 Lux, i.e. complete darkness, 5 Lux and 10 Lux. If the insects' judgment of vertical travel direction was independent of environmental brightness, we expected to observe no variations of negative gravitaxis behavior among three trials. The frequencies of tested insects climbing upward were compared with the null using the G–test with William's correction.

1.2.2 Ontogenetic variation of dispersal activity

We used a vertical treadmill (width 2 cm, height 28 cm) connected to a motor speed control and a light source set on top of the treadmill for attracting the experimental insects (Figure 1.4). The experiments were conducted in a dark room of constant temperature (25°C). Six groups of different age covering the early 2/3 of the first instar stage were used in this

study: 2 HAH (hour–after–hatch), 4 HAH, 48 HAH (2 DAH), 96 HAH (3 DAH), 120 HAH (5 DAH), and 240 HAH (10 DAH). In experiments, the motor speed was manually adjusted via a voltage controller such that the climbing insect was always kept near the central section of the treadmill. We used a video camera (SONY HDR-XR160) to film the movement of insects on the treadmill. We set a maximum of 60 minutes for each individual to climb, and the experiment was also terminated if an individual stopped climbing for more than 15 minutes. We used 2-6 individuals per group and conducted one run for each individual. Afterwards, we used a motion tracking software (ProAnalyst, Xcitex, MA, USA) to extract the instantaneous speeds of the insects and treadmill, and calculated the insect's instantaneous climbing speed as $U_t = u_t + v_t$, where u_t and v_t are instantaneous speeds of the insect and the treadmill, respectively, with respect to the camera frame. We used programmed scripts in MatLab [82] to analyze the variation of climbing speed of each individual through each experimental trial. Specifically, since insects involved in such vertical climbing exhibit intermittent pauses, the time periods spent in climbing and at rest were identified. For each trial, we first measured the total height climbed; we then quantified the temporal patterns of intermittent climbing, including the total time of climbing, the total time spent at rest, and the average frequency of start of climbing and pauses. We compared these parameters among all age groups by using One–Way ANOVA to evaluate the ontogenetic shifts in dispersal capability and climbing endurance.

1.2.3 Ontogenetic variation of aerial escape and accidental fall

We experimentally introduced physical contact that resembled predatory attacks to examine the behavioral responses of larval *E. tiaratum*, and used this result to predict their responses under similar situations in the wild. In the experiment, the insects were transferred to a chamber made of nylon mesh (1466C, BioQuip Products, CA), and simulations of physical attacks were introduced by rapidly touching the anterior half of the insect using a brush pen (7 mm, tip diameter) when the insects were resting or walking on the side or roof of the chamber. Attack simulations were introduced with a minimal time interval of 10 second. The responses were recorded as "drop" if the attacked individual dropped itself off from the substrate; any other response, e.g., rapid escaping or startle display, was coded as "non–drop". This experiment was conducted on 7 individuals in each of three age groups, 0-DAH, 5-DAY and 10-DAH. Also, we studied the fate of larval *E. tiaratum* encountering a slippery surface under controlled conditions, in which the accidental fall may occur due to the loss of foothold during fast oscillatory running. A cardboard (15 cm, width; 35 cm, height), painted with a horizontal band of Teflon (2 cm) near one end, was placed vertically bellow a light source. Experimental insects were released near the bottom of the board; they rapidly climbed up due to phototaxis and negative gravitaxis. We conducted the experiments on three age groups (0 DAH, 5 DAH and 10 DAH), each with 7 individuals, and recorded the frequencies of falls.

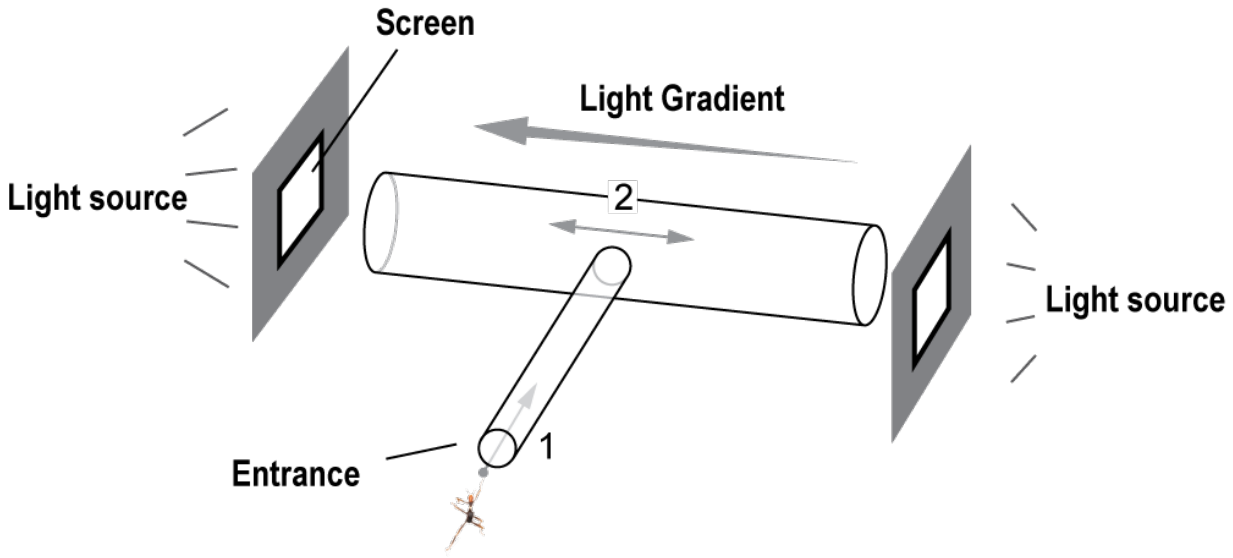

Figure 1.2: The experimental setup used for recording phototaxis behavior. The screens at both ends were set in different brightness. Experimental insects were released at the entrance (step 1), and the arrows indicate the direction of movement. After reaching the bigger tunnel, the insects choices of direction were recorded (step 2). For clarity, the black tunnels are transparent in this Figure.

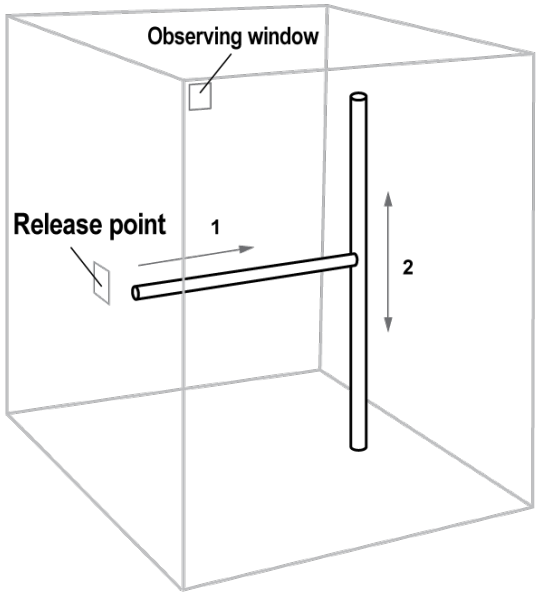

Figure 1.3: Experimental setup for studying negative gravitaxis behavior. A T-shaped device is placed in a chamber with uniform visual environment. In experiments, insects were released at the free end of the horizontal stick (step 1), and they moved forward until reaching the vertical stick, where the directional preference of movement was recorded (step 2). The chamber is shown only in skeleton for clarity.

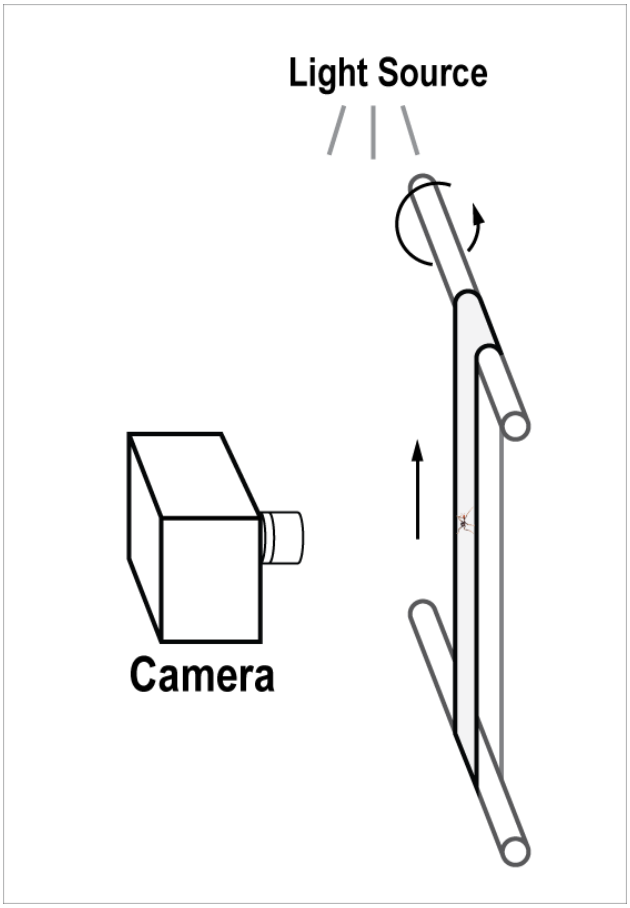

Figure 1.4: Experimental setup for recording ascending movement. See text for details.

1.3 Results

1.3.1 Taxis behaviors

For phototaxic behavior under various brightness, we recorded the direction of movement from 3 age groups, each in light gradients under 3 levels of environmental brightness, and one control experiment conducted in a 1-DAH group (0-1 DAH group, N = 50, 30 and 36 for low, median and high brightness, respectively; 5 DAH group, N = 60, 50 and 20; 10 DAH group, N = 100, 20 and 15; control group, N = 50). Results from the control experiment showed no significant difference between the frequencies of exiting from either directions under complete darkness (One-Way Repeated Measured ANOVA, P =0.489; Table 1.1). First, larval *E. tiaratum* showed significant directionality when exposed to light gradients under all treated environmental brightness (One-Way Repeated Measures ANOVA: 0-1 DAH under LB, P<0.0001, MB and HB, P < 10-5; 5 DAH under LB, P <0.0001, MB, P <0.005; 10 DAH under LB, P<0.0001). Under low brightness, all three age groups showed strong positive phototaxis. Both 5 DAH and 10 DAH groups showed reduction in phototaxis with increase in the environmental brightness (Figure 1.5). Specifically, there is no significant phototaxis observed in 5 DAH group under high brightness (G-test with William's Correction, P = 1), and in 10 DAH group under both median (P = 0.182) and high brightness (P = 0.07). In summary, the youngest group showed a strong probability of moving towards the brighter direction under all tested circumstances, the oldest group showed a preference for the median brightness, and an intermediate pattern is shown in the intermediate aged group.

For negative gravitaxis behavior under different brightness, we recorded results from successful runs under each treatment (N = 100 for groups of 0 Lux, 5 Lux and 10 Lux and N = 93 for the group of 600 Lux). All observed frequencies are significantly different from the null (Table 1.1), and the directional choice was statistically significant within each age group (One-Way Repeated Measures ANOVA, 0 Lux, P = 0.003; 5 Lux, P = 0.017; 10 Lux, P = 0.001; 600 Lux, P<0.001). The degree of negative gravitaxis was found to be positively correlated with environmental brightness. Tested *E. tiaratum* larvae exhibited negative gravitaxis (>50% in ascent frequency) under most brightness, but exhibited positive gravitaxis under complete darkness (77%, descent frequency). In contrary, even at a low level of environmental brightness (5 Lux), the negative gravitaxis behavior was significantly reinforced (70%, ascent frequency).

For the ontogenetic shift of negative gravitaxis, we recorded 93 successful runs in the 0-1 DAH group, 73 successful runs in the 6-7 DAH group, 52 successful runs in the 12-14 DAH group, and 131 successful runs in the 19-20 DAH group, which was in the second instar stage. Within each age group, the directional choices were statically significant (One-Way Repeated Measures ANOVA, 0-1 DAH and 6-7 DAH, P < 0.001; 12-14 DAH, P < 0.001; 19-20 DAH, P = 0.031). All groups exhibited negative geotaxic climbing in frequencies significant different from the null (G-test with William's Correction; 0-1 DAH, P < 10-25; 6-7 DAH, P < 10-8;

12-14 DAH, P < 0.05; 19-20 DAH, P < 10-4). Although the majority of all tested groups showed negative gravitaxis climbing, a general decrease in frequency of up-climbing is shown in the older groups (Table 1.2).

Brightness (Lux)	Ascent Frequency (%)	Gravitaxisity Type
0	23	positive
5	70	negative
10	80	negative
600	98	negative

Table 1.1: The effects of overall environmental brightness on negative gravitaxis ascent in the early first instars (0-3 DAH) of *E. tiaratum*. See text for statistical results.

Age (DAH)	Ascent Frequency (%)	Gravitaxis Type
0–1	98	negative
6–7	84	negative
12–14	63	negative
19–20	66	negative

Table 1.2: Ontogenetic shift of negative gravitaxis behavior shown by ascent frequencies in first and early second instars of *E. tiaratum* under environmental brightness of 600 Lux. See text for statistical results.

1.3.2 Ontogenetic variation of dispersal activity

We recorded climbing movements in 2 individuals of 2-HAH, 4 individuals for each of 4-HAH and 240-HAH group, and 6 individuals for each of 48-HAH, 96-HAH and 120-HAH groups. Among all tested groups, 2 HAH group had the longest climbing time (average, 57 min), within 60 minutes. We found a decrease of the overall climbed height through age (Figure 1.6-C). The youngest group had the greatest climbed height (125 ± 17 m, mean±std.), and a general trend of decline was found among other tested groups (4HAH, 61 ± 16 m; 48 HAH, 65 ± 13 m; 96 HAH, 41 ± 17 m; 120 HAH, 4 ± 3 m; 240 HAH, 0.8 ± 0.7 m). Also, different age groups exhibit similar climbing speeds (Figure 1.6-B). Besides, the youngest group also showed the longest climbing time. In general, we see a significant decrease in the total climbing time, and significant increases in the proportion of rest time and pause frequency with greater age (Figure 1.7). Overall, the newly hatched individuals exhibited the longest non-stop climbing and the greatest climbing height, and the time spent in rest and pause frequency generally increases with age.

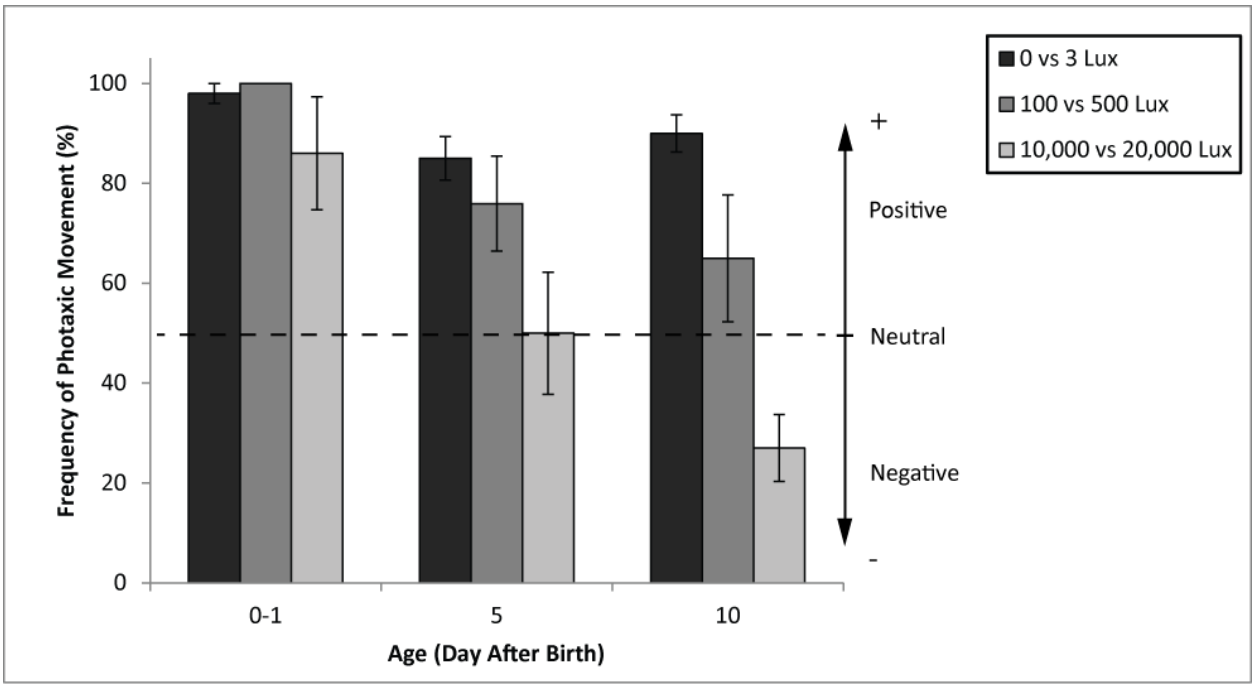

Figure 1.5: Ontogenetic shifts of phototaxis behavior shown by the frequencies of directional movements in binary phototaxis experiments. Column values are mean±s.e.m.; dash line indicates the expected frequency of no directional bias predicted by the null hypothesis. See text for statistical results.

1.3.3 Ontogenetic variation of aerial escape and accidental fall behaviors

We recorded the behavioral responses to 91 simulated attacks in 7 individuals of 0 DAH, and 50 attacks in 7 individuals in each of 5 DAH group and 10 DAH group. Voluntary drop is only found in the 0-DAH group (17.8±3.7 %, mean frequency ± s.e.m.). For accidental fall experiments, we conducted 59 runs for 0 DAH group, 30 runs for 5 DAH group and 32 runs for 10 DAH group. Similar to the results from our voluntary drop experiments, the accidental fall due to slippery surface was only recorded in the 0-DAH group (average frequency, 55.9±6.7%) but not in two older groups (Figure 1.8).

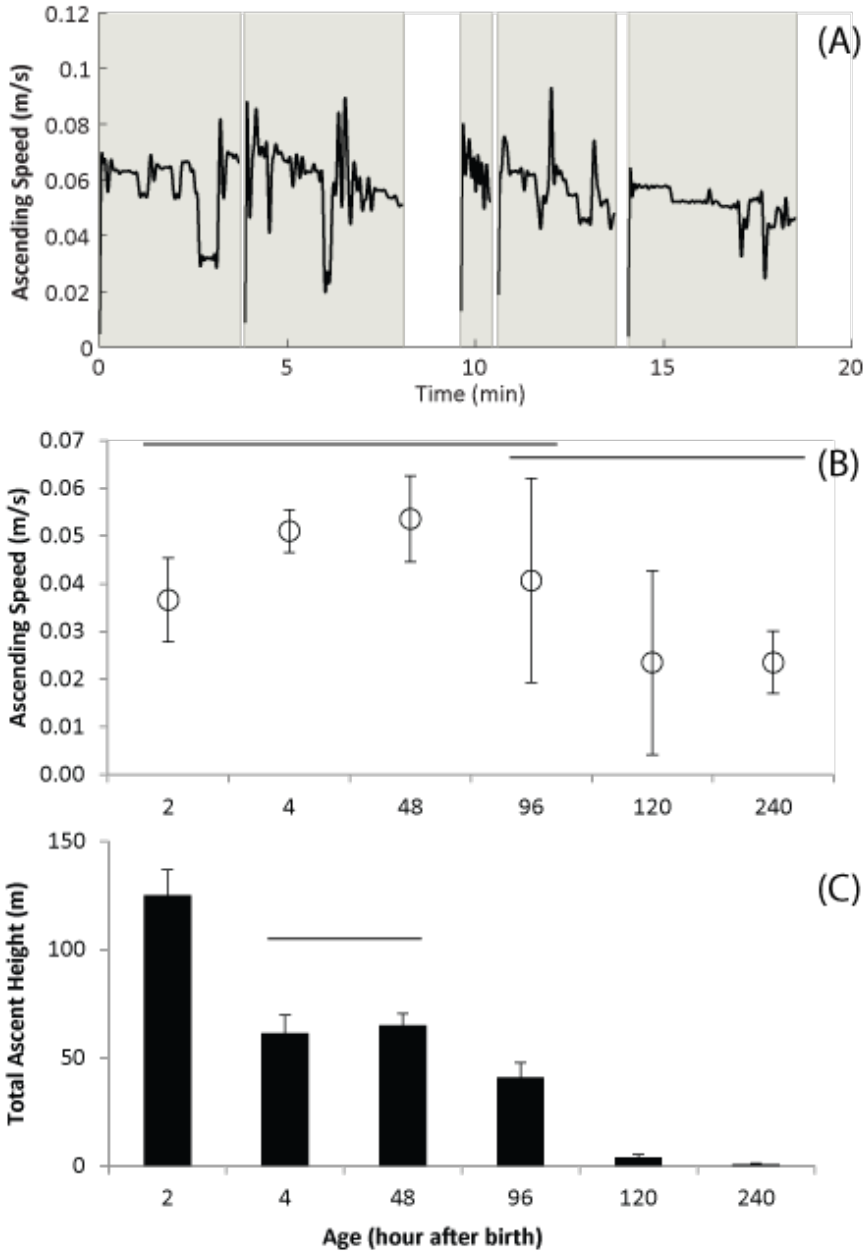

Figure 1.6: (A) A example plot of the ascending speed as a function of time during the first 20 minutes of running in a 4-hour-old individual. Shaded sections indicate active ascending. (B) Ascending speed in different age groups. Values are mean±s.e.m. (C) Total climbed heights within 1 hour in different age groups. Values are mean±s.e.m. (Horizontal lines indicate the lack of significant difference among the measured means from the marked groups.)

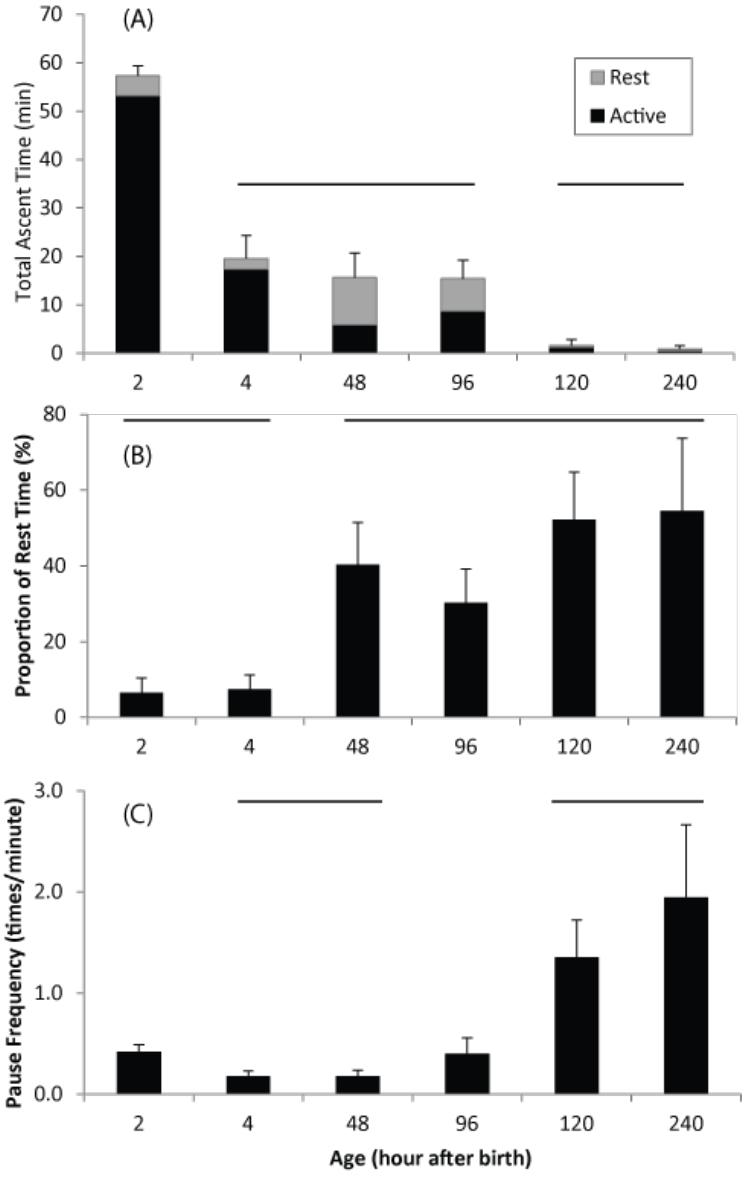

Figure 1.7: Ontogenetic shift in temporal patterns of ascending movement. (A) Comparison of climbing endurance between different age groups. Columns are average climbing time (mean±s.e.m.) measured in different age groups, with the proportions of time spent in ascending and in rest filled by black and gray, respectively. (B) Proportion of total rest time within 1 hour. Values are mean±s.em. (C) Frequencies of pauses in climbing motion. Values are mean±s.em. Horizontal lines indicate lacks of significant difference among the measures from the marked groups.

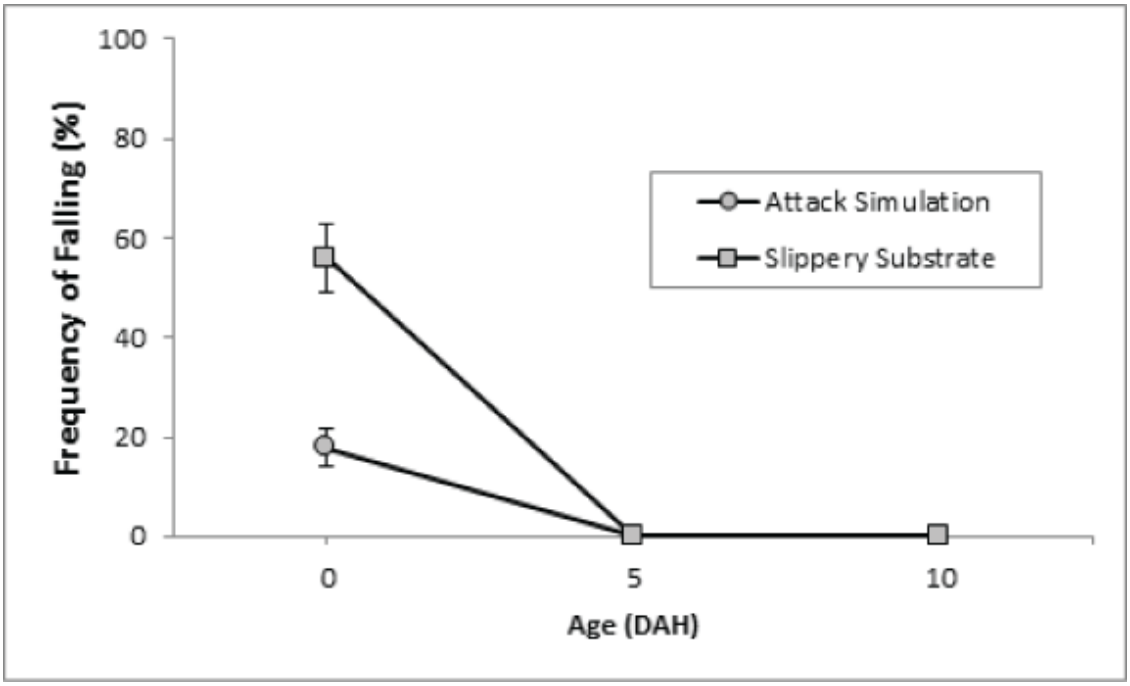

Figure 1.8: Ontogenetic change of drop frequencies under simulated attacks and of running through slippery surfaces. Values are frequency mean±s.e.m.

1.4 Discussion

Our results demonstrated several taxic behaviors and one airborne defensive behavior that are temporally correlated with the hyperactive dispersing phase in larval *E. tiaratum*, and which developed immediately after hatching. Our goal is to have a multi-dimensional understanding of the ontogenetic shifts in behavioral niche during the early life history of *E. tiaratum*.

1.4.1 Larval dispersal towards tree canopies

Our results strongly support that larval *E. tiaratum* use light gradient and gravity as cues in directed movement. First, larval *E. tiaratum* in all tested ages showed consistent behavioral responses when exposed to light gradients under low, median and high brightness conditions. Also, directed movement with the perception of gravitational field alone was recorded in larval *E. tiaratum* of all tested ages. Significant negative gravitaxis was found in all ages, but the overall ascent frequency decreases with increasing age. Moreover, our results showed integrated uses of light and gravity signals in larval *E. tiaratum*. Positive gravitaxis was only found under complete darkness, while negative gravitaxis was shown under all light conditions, including low light (5 Lux). Such light-sensitive gravitaxic behavior indicates that newly hatched *E. tiaratum* avoid negative gravitactic dispersal under complete darkness, which may potentially enhance the survivorship and energy conservation in the wild. Previous studies [1, 139] also suggested that the integrated use of environmental cues in directional movement may depend on specific environmental contexts in different taxa. Furthermore, our results showed a decline in frequencies of phototactic and negative gravitactic behaviors through ontogeny, as well as an ontogenetic shift in the choice of favored light environment in larval *E. tiaratum*. Such pattern supports the prediction that the youngest larvae are behaviorally the most capable of directed dispersal, and it implies a shift in preferred microhabitats on host trees through ontogeny. Based on our new evidence, we further predict that a continuous transition in habitat is correlated with the shift in taxic behaviors: the newly hatched *E. tiaratum* larvae follow light gradients and travel along vegetative bodies until reaching the open canopies, only then settling into favorable microhabitats where they gradually develop into a more camouflaged phase with a preference for less exposed microhabitats, e.g. more shaded midstories. Given that the biology of *E. tiaratum* under natural condition is understudied, it remains unclear whether there is a shift in dietary use of the host through ontogeny [57]. More details may be revealed in future studies that investigate how these taxic behaviors are correlated with the daily rhythm of activities under daily cycles of environmental cues, e.g. lighting and temperature. Also, tracking the pathway of freely dispersing larval *E. tiaratum* under natural conditions may provide more information about the tactical uses of environmental cues.

Taxic behaviors facilitate food searches in insects [9]. Highly directional taxic behaviors

in larval *E. tiaratum* clearly assist their locating tree canopies and likely assist their search for suitable food plants. Given the spatial complexity of forests, various environmental cues may be used as navigation references. For example, arboreal ants may use memorized canopy patterns for navigation during daily foraging trips [58], and path integration of skylight and terrestrial landmarks are used in social hymenopterans [132]. Although we didn't test whether other environmental signals, e.g. chemical signals, canopy pattern, etc., can be utilized by larval *E. tiaratum*, it is unlikely for them to adopt very sophisticated navigation strategies, given their ephemeral need of arboreal dispersal and different scale of transport compared with foraging hymenopterans.

1.4.2 Ontogeny of dispersal

We have shown that the greatest dispersal capability is developed immediately after hatching in *E. tiaratum*, and such capability rapidly declines approximately during the first 3 days after hatching. Efficient movement may be favored by natural selection given that larval dispersal is energetically costly and limited by the available energy from embryonic storage, and that the dispersal can be slowed by navigating among vegetation structures and disrupted by potential predation and climatic disturbances [80, 118]. Besides the endurance of climbing, the temporal patterns of rest and pauses differ significantly between the freshly hatched larvae (2–4 DAH) and the older groups. Such variation may reflect not only changes in physiological capability but also differences in locomotor strategies, which may be explained as life history tradeoffs. The rapidly moving ant-mimicking larvae use startle display as active defense during highly exposed diurnal traveling, while the older nymphs adopt temporally disrupted intermittent movement, with frequent pauses and rest phases, as a behavioral camouflage along with morphological mimicry of dry leaves or lichen [54]. We were only able to investigate a limited number of parameters of the dispersal locomotion in larval *E. tiaratum*, and, due to a wide variety of biotic and abiotic factors may limit the dispersal activities in insects [94], future work may investigate the behavioral interaction among dispersing larval *E. tiaratum* and other sympatric organisms, and quantify their dispersal effectiveness in the native habitats for a further understanding.

1.4.3 Aerial escape

The voluntary drop employed by newly hatched *E. tiaratum* is a defensive or protective response to potential predation or substrate perturbation. Given their extensive daytime exposure during canopy dispersal, such sensitively triggered airborne escape may be an effective anti-predatory mechanism. On the other hand, older nymphs of a different behavioral niche intentionally avoid dropping themselves. Such a shift in defensive strategy may be complemented by coloration camouflage and startle displays [18] under predatory pressure. More importantly, our results indicate voluntary drop may frequently be adopted under natural

conditions as a behavioral initiative of aerial performances, e.g. aerial righting and directed aerial descent. Our lab experiments were only conducted under an idealized environment and simplified perturbation. Future work may identify and quantify the environmental perturbation and predatory attacks in natural habitats, and further examine the utilities of various behaviors in response to different conditions.

1.4.4 Ecological and evolutionary significance

Our results provide one specific example for understanding the process of directed movement between terrestrial and arboreal habitats. In newly hatched larval *E. tiaratum*, several temporally correlated traits during the dispersal phase potentially indicate selective advantages. Future studies should quantitatively investigate the combined influence of these traits on dispersal success and survivorship. The most active dispersal phase of the life cycle of *E. tiaratum*, especially considering females, is the newly hatched initial phase. Foraging ants are known to transport eggs, thus contributing to dispersal, and the hatchlings may find themselves in an unfavorable habitat. Future work should include quantitative assessments of the integrated influence of these traits on dispersal success and survivorship. Comparison among phasmid species that have ant-mimicking larvae, e.g. *Phyllium sp.*, may help identify the key ecological components in the evolution of this phenotype. Furthermore, comparing different oviposition styles, dietary specificity [62, 12], host plant abundance and spatial heterogeneity of habitats between species may yield insights on how different dispersal strategies benefit species-specific life history.

Lastly, our study provides a multi-dimensional view for understanding the ontogenetic variation of locomotor tactics in relation to niche shifts. Voluntary drop behavior, shown as a defensive reaction here, can lead to other airborne behaviors at forest canopies. . Given the demand of dispersal towards canopies, directed aerial descent, which allows the insects to return to tree trunks with a shorter height loss, would potentially ease the process of reallocating resources and help avoiding predation from the understories. How such defensive response is ecologically related with wingless aerial locomotion may be further investigated by comparing the behavioral initiatives of gliding among other arboreal arthropods [37].

Chapter 2

The visual ecology of directed aerial descent in a larval stick insect (*Extatosoma tiaratum*)

Visual signals are used as locomotor references by many animals. Both the visual environment and the visual capacities of the organism determine the qualities of perceived visual signals. Dynamically changing visual signals perceived in locomotion may be used to guide and correct the movement. Here we investigated the visual stimuli used as locomotor references during directed aerial descent in a larval stick insect, *Extatosoma tiaratum*. The directed aerial descent movement is characterized by steep trajectories performed among vegetative structures in forest, and effective use of visual cues may enhance the efficiency of such performance. Under controlled lab conditions, we examined glide performance within a wide variety of visual environments. Larval *E. tiaratum* were able to discriminate and respond to different contrast patterns. Our results suggest the use of vertically constant contrast edges. Specifically, they are sensitive to vertically aligned contrast edges, with a preference to surfaces with low reflectance. The utility of contrast as visual cues was further shown to be dependent on both the heterogeneity of the visual environment and the quality of perceived signals. The strategic use of visual cues found in larval *E. tiaratum* may enhance their directed aerial descent performance in native habitats. Our study contributes to an understanding of the function and adaptive significance of controlled aerial behaviors in canopy invertebrates.

2.1 Introduction

Diverse visual signals are used by insects in locomotion. First, with compound eyes, spatial variation of visual signals can be perceived using the angular differential between neighboring ommatidia. This allows detection of object sizes and shapes, as well as texture and reflective properties of different surfaces [90]. The discountinuity of perceived signals forms contrasts, e.g., near pattern profiles and object edges, which can be useful spatial references. For instance, the chromatic contrast pattern is used in edges and texture detection in honeybees [77, 66]. Second, the spatiotemporal variation of perceived visual signals generates optic flow, which may be commonly used by insects in locomotion. Translator optic flow field provides not only referential information about the insects' instantaneous self–motion but also reliable estimation of the 3D layout of the surrounding environment [73]. The use of optic flow in flight has been shown in numerous taxa [38, 6, 55]. Also, distance discrimination can be further enhanced by binocular stereopsis of a pair of eyes [111]. Besides integrative use of different signals, insects can behaviorally enhance signal quality and acuity. For example, locusts and mantis use body oscillation, the peering motion, for distance discrimination based on movement parallax [129, 115, 71]. Furthermore, the quality of visual signal perception highly depends on the visual capacity of insects. According to Weber's Law, the acuity of signal discrimination correlates with the magnitude of signals, i.e., stronger signal can provide a greater stimulus. For this reason, natural selection may favor mechanisms that enhance the signal strength in performances depending on signal use. For instance, spatial and spatiotemporal parameters offered by floral structures are tuned to pollinators' visual capacities and visually guided behaviors [30].

Visual signals are highly involved in controlled aerial behaviors. Most prior studies have focused on the functional roles of visual signals in flight control [51, 120, 121]. On the other hand, less is known about the use of visual signals in directed aerial descent (DAD). DAD performance enables lateral travel in descent for returning to tree trunks, which is of great fitness significance, e.g., in the context of escape and dispersal. It has been documented in many arboreal invertebrate lineages as a result of numerous times of independent evolution, indicating the common demand of such a behavior in arboreal habitats [36]. In a macroevolutionary perspective, such gliding with steep trajectories has also been considered as a stage which preceded the evolution of flight [143]. Compared to free flight with great 3D maneuverability, DAD motion is more dominated by vertically downward translation, even though maneuvering can be performed with asymmetric leg movements through all stages of trajectories [144]. Aerial targeting in DAD requires directional judgment based on an instantaneously changing visual environment, such that the insect can perform fast maneuvering accordingly. Therefore, DAD performance may potentially use and interact with the visual environment at forest canopies.

Forest canopies has complicated visual signals. First, it is highly heterogeneous, given spatially varying brightness and contrast patterns formed by vegetative structures (citations),

and can be of use by aforementioned mechanisms. The targeting of DAD performance in *Cephalotes* ants was found to be associated with the reflectance properties of tree trunks. Secondly, the interaction between descent motion and visual environment may characterize the visual ecology of DAD. With respect to falling insects, the visual environment is instantaneously moving upward and refreshed, potentially causing a noisy visual field, especially in the vertical direction. For this reason, vertically invariant signals may be of particular use for the targeting. For example, arbor trunks and vertically hung liana can potentially be reliable cues for targeting. Furthermore, the visual environment on canopies changes across different heights, because both the composition of vegetative structures and the light environment [44] vary between different forest levels. Overall, a wide variety of signals can be used as visual cues in DAD, and the strategies can be specific to both taxa and habitat.

Here we studied the visual ecology of DAD in the newly hatched larvae of stick insect *E. tiaratum* under controlled lab conditions. This species is an arboreal form native to coastal rainforests of Eastern Australia [16]. Young insects hatch from eggs dropped to the forest floor and disperse diurnally towards tree canopies. This hyperactive stage, also characterized by ant–mimicking, may last 3 to 5 days [22, 23, 24]. Our preliminary studies showed that DAD may start through an aerial phase initiated by active aerial escape or by disturbances. Given the life history demand of ascending to the canopies, falling to lower heights may significantly affect survivorship of newly hatched individuals, e.g., it increases the energetic cost and exposure of travelling before reaching a suitable habitat. For this reason, accurate targeting that enhances the efficiency of returning to vegetative structures may be favored by natural selection. Since larval *E. tiaratum* potentially disperse from the forest floor to the canopies, they are active across a greater height range in the forest, particularly within the understories, when compared with other insect species inhabiting canopies. We examined the use of visual cues in DAD of larval *E. tiaratum*. Following the preliminary results on the use of visual contrasts as references, we further tested their DAD performances under a variety of contrast patterns. We aim to address the major visual component used as directional reference in DAD, and answer whether the use of such visual cues may enhance DAD performance in native habitats.

2.2 Materials and Methods

E. tiaratum eggs from our lab colony were incubated under constant temperature (25°C) and humidity (50–70%). We used 0–1 day old first instars in all experiments. Newly hatched larvae were collected within the first 24 hours and were transferred to clear plastic cups (355–470 ml) with lids. Constant humidity was maintained in the plastic cups by periodical water spray, and all cups were kept in an environmentally controlled room with constant temperature ($\geq$ 25°C) and 12–hour light–dark cycles. Experimental insects were transported and kept in the same type of cups with constant humidity maintained by wet paper towel.

2.2.1 Experimental setup and protocols

Environmental temperature ranges 26–30°C in all experimental spaces. Environmental luminance was measured with a lightmeter (Extech–401025). According to results on gliding trajectories, 0–1 day old first instar *E. tiaratum* (25±2 mg, body mass) released 40 cm from visual target descend 1.7±0.4 m before landing. To ensure sufficient space for experimental insects to finish maneuvering and landing, the point of release was at least 3 m above ground.

We used two major setups for different experiments. First, we used a suspended flat screen for decorating visual patterns (Setup No.1). We first set up a screen (3.5 m, height; 1.5 m, width) in the central green house of Plant Lab, University of Washington. Additional lighting was used to maintain a minimum of 1000 Lux environmental brightness, similar to minimal daylight brightness [67]. A TEFLON–coated funnel with the nozzle facing downward (3 cm, nozzle diameter) was positioned 3 to 3.5 m above the ground and 40 cm away from a screen of visual targets. In experiments, insects were dropped through the funnel via triggering the flip of a TEFLON–coated vial on top of a pole (Figure 3.1). A replicate setup of similar dimensions and the same environmental brightness was built in the Animal Flight Laboratory, University of California at Berkeley. This setup was used for studying DAD directionality in front of simple grayscale and chromatic targets. We also constructed a cylindrical enclosure (3.5 m, height; 80 cm, inner diameter) at Animal Flight Laboratory (Setup No.2). We installed 6 to 8 floodlight bulbs (GE–PAR38–29529) directly above the space for sufficient environmental brightness (a gradient of 5000 Lux to 1000 Lux, from top to bottom). In experiments, we stood on a ladder and dropped insects in haphazard initial orientations through a TEFLON–coated funnel, which was mounted atop the enclosure at its central axis (Figure 3.1). Gliding and landing performances were observed by experimental personnel and recorded by a high–definition video camera (50 fps, SONY XR160) mounted directly above the arena. In digital videos, the landing points were extracted based on a single landmark at the longitudinal center of the insect body using commercial software (Pro-Analyst, Xcitex Inc.) and analyzed using custom–written scripts in MatLab [82]. Circular distribution of landing points recorded with setup No.2 was analyzed using CircStat package with R [101], which calculates the mean direction θ and concentration κ using maximum likelihood methods.

The reflectance profiles of the used materials were measured with a spectrophotometer (USB2000, Ocean Optics) (Figure 2.9). The contrast between two neighbor surfaces was calculated as

$$C = \frac{L_1 - L_2}{L_1 + L_2}, \tag{2.1}$$

where L_1 and L_2 are the average reflectance within the significant wavelength range. There are no prior results on spectral sensitivity of *E. tiaratum*. In the following experiments, we averaged reflectance over 300–550 nm, which covers the visible spectrum of most invertebrates, particularly of orthopteran insects [95, 15].

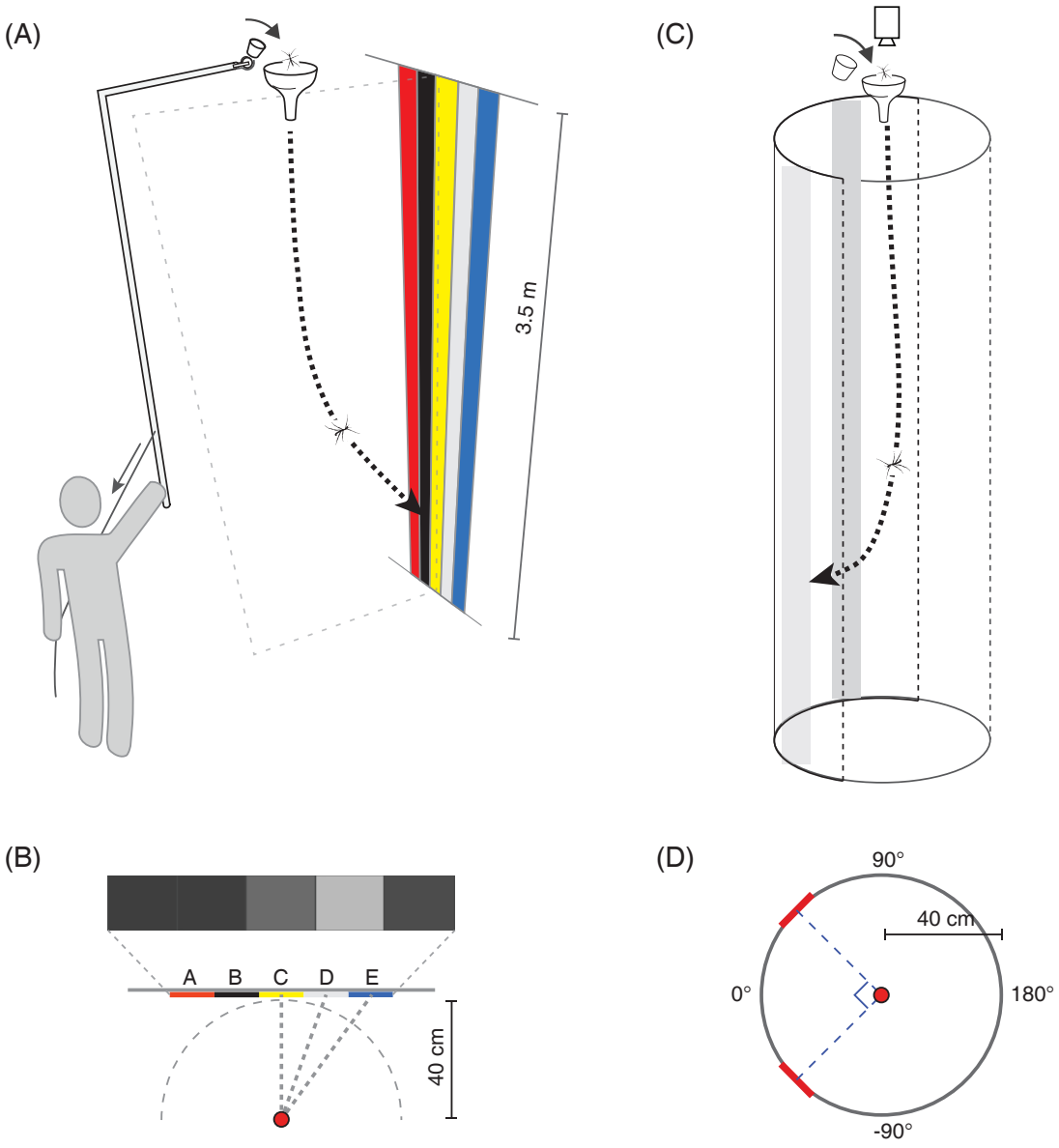

Figure 2.1: Experimental setups. (A) Setup No.1, demonstrated with one trial with color sheets. (B) Setup No.1 in top view. Bars show the average reflectance over 300–550 nm with grayscale. Letters denote five positions from left to right. A red dot denotes release point. (C) Setup No.2 in semisectional view, demonstrated with paired vertical stripes. (D) Top view of Setup No.2. Red bars denote the position of paired vertical stripes in visual contrast experiment.

2.2.2 Visual contrast

We first studied DAD directionality when exposed to simple contrast patterns formed by a narrow vertical stripe in a background of different reflectance. For simplicity and clarity, we used black and white felt materials. Installed in Setup No.1, the potential visual target was one vertical stripe (15 cm, width) in front of a background (200 cm, width). Simple contrast patterns ("black in white" and "white in black") were used (Figure 2.2-A). We dropped 6 individuals, each 10–12 times, in each setup. The preference of landing location were recorded as the color landed on each time.

Because contrast edges are potentially used for discrimination of object profiles, we further tested if the reduction in continuity of contrast edges affect landing behavior. We used three modified version of what was used in the previous experiments under Setup No.2. The first one was built with continuous contrast edges but alternating contrast patterns (CT1, Figure 2.2-B). The second and third were "black in white" and "white in black" types of contrast with discontinuous edges (CT2 and CT3, Figure 2.2-B). Each setup was tested in 6 individuals, each dropped 5–7 times.

We also tested whether the sharpness of a contrast edge is used as visual reference by larval *E. tiaratum*. The contrast patterns were generated using MatLab and printed by commercial printer (Staples Inc.). The reflectance profile $y(x)$ of each stripe was generated as

$$y(x) = \begin{cases} (erf((x+\delta)e) - 1)/2 & x < 0 \\ (erf((x+\delta)e) - 1)/2 & x \geq 0 \end{cases},$$

where

$$erf(x) = \frac{2}{\sqrt{\pi}} \int_0^x e^{-t^2} dt$$

is an error function, 2δ is band width (15cm), and e is the sharpness coefficient. Here we used 2 different sharpness values (0 and 0.5) and 2 contrast types ("black in white" and "white in black") (Figure 2.3). In Setup No.2, we suspended paired stripes of different edge sharpness 90°apart from each other (Figure 3.1-D). Two stripes of the identical sharpness were used as the controls, and we tested 3 sets of controls. The protocol of dropping and filming was the same as aforementioned. We tested each setup using 5 individuals, each dropped 5–6 times. Our null hypothesis assumes insects land in random directions with no preference for the sharpness of potential target, which predicts statistically non–significant differences between landing frequencies on both stripes of different contrast edge sharpness. The null frequency thus equals to the angular coverary of the potential target relative to the whole vision field. For a 15cm wide target that has a horizontal distance 40cm from the release point, the null frequency is about 0.06. The recorded landing frequencies associated with each stripe were compared among individuals using One–Way Repeated Measures ANOVA, and then the overall frequencies associated with each stripe was compared to the null frequencies (1:1) using the G–test with Williams correction [117].

2.2.3 Complex patterns

We studied how larval *E. tiaratum* respond to more complex patterns by adopting a similar approach used by Yanoviak and Dudley [141]. We first used four felt sheets (15 cm, width) representing a grayscale gradient (black, dark gray, gray and white), suspended in parallel in setup No.1, with a dark green background screen 1 m behind the screen plane. The juxtaposition of sheets formed a screen 60 cm in width (Figure 3.1 A) With 7 possible combinations of sheet position (Table 2.3), we recorded DAD landing in 5 individuals, each dropped 4–5 times in each of 7 trials. We ensured a minimum of 60 successful landing events for each trial. We also replicated the experiment with 6 color sheets (red, black, white, yellow, green, blue; 15 cm, width) with 14 combinations, which were also adopted from that used by Yanoviak and Dudley [141] (Table 2.4). For reasons of logistical limitations, blue and green sheets were not used together in any trial. A group of 6 individuals was used in the experiment within 2 days. Each individual was dropped 7–10 times in each of 14 trials, and each trial had 45–63 landing records. The landing point in each drop was recorded as the color of corresponding sheet, or as a 'miss' if the insect failed to land on the screen.

For all trials, we used a G–test with William's correction to compare landing frequencies on each sheet to null frequencies, which were calculated based on its relative distance from the drop point [141]. Based on observation of trajectories, the null landing points approximated a hyperbolic conic section for a cone with apex about 0.7 m below the drop point and with a slope of 20°. We compared the mean proportion landing on each sheet with a one–way ANOVA. Proportional data were arcsine square–root transformed before analysis and statistical significance of the ANOVA results was determined with Bonferroni–adjusted α of 0.025. For trials with color sheets, the proportion used to calculate null frequencies for G-test were: 0.172 (landing on sheet position A or E in Figure 3.1-B), 0.214 (landing on sheet position B or D in Figure 3.1-B) and 0.229 (landing on sheet position C in Figure 3.1-B). For trials with grayscale sheets, the proportion used to calculate null frequencies for G-test were: 0.233 (landing on a lateral sheet) and 0.267 (landing on a central sheet).

Because preliminary results indicated a potential association between the visual pattern formed by sheets and the landing preference of larval *E. tiaratum*, we further examined how the contrast pattern formed by sheets of the same trial may have influenced their directional choice. We proposed three hypotheses to potentially explain the variation of landing frequencies in both aforementioned experiments. (H_1) Landing preference is associated with the reflectance properties of sheet materials, which predicts that frequency of landing is either correlated with the magnitude of reflectance or with the reflectance profile characteristic to a particularly sheet, as suggested in prior study [141]. The null hypothesis predicts non–significant differences of landing frequencies between different sheets. We used linear regression model to test the correlation between landing frequencies and brightness, and used One–Way ANOVA to test whether landing preference is associated with the particular reflectance range of each sheet. (H_2) Landing preference is correlated with the contrast or

contrast magnitude formed between neighbor sheets, which predicts that neighbor sheets forming greater contrast have greater landing frequencies. Here, we calculated both the contrast between each pair (C of 2.1), and the average contrast formed by each sheet with its two neighbor sheets, or one neighbor sheet and background sheet if the sheet is at margin: $C_2 = (C_L + C_R)/2$, where C_L and C_R are contrast formed on left and right side, respectively. We used linear regression models in R to examine the potential correlation between C and the landing frequencies on both sheets of the same pair, and used the same method to examine the correlation between C_2 and landing frequency on each sheet. The same tests were conducted for the magnitude of both contrasts ($|C|$ and $|C_2|$). (H_3) Landing preference is correlated with the contrast or the magnitude of contrast formed by a target sheet against all other sheets, which predicts greater landing frequencies on those sheets that form greater contrast against the average of all other sheets. Here the contrast between individual sheets and all other sheets in the same trial was calculated as $C_3 = (L_i - \bar{L_x})/(L_i + \bar{L_x})$, where $\bar{L_x}$ is the average reflectance of all other sheets. We used a similar protocol as in testing H_2 to address the potential correlation.

2.2.4 Spatial frequency of contrast

With Setup No.2, we created a series of visual environments of different spatial frequencies of contrast and different overall reflectance. The insects were dropped from the center top, after which they were exposed to the artificial visual environment. As in the simple contrast experiments, we used materials of black and white. The overall reflectance was adjusted by changing the proportion of white and black surfaces. We used 3 different "average reflectance" values: 10%, 50% and 90%, corresponding to 1:9, 1:1, and 9:1 of black:white area ratio. The spatial frequency of contrast was adjusted by changing the number of vertical stripes attached on the arena wall. We used 3 different numbers (2, 8 and 32) of black stripes, defined as "patchiness". The stripe width was determined as $W = d\pi(1 - R)/N$, where d is inner diameter of arena (80 cm), R is average reflectance value and N is patchiness. Spatial frequency of contrast edges was calculated as $f_C = 1/\Delta\phi$, where $\Delta\phi$ denotes the angular period between two contrast edges (Table 2.1). In each trial, we recorded 6–8 drops from each of 5 individuals. Using digital video, we recorded the landing location as "black", "white", "floor", or "edge", where "edge" means landing on contrast edges. We used One–Way repeated–measures ANOVA to compare the variation of landing frequencies between individuals. Using G–tests with William's correction, we compared the proportion of landing on black and white against a null hypothesis based on random drifting, in which case the proportion of landing on each color is expected to be the same as the relative proportions of area (Table 2.1).

Trial	N_B	W_B(cm)	$\Delta\phi_B(^\circ)$	f_C(cyc/rad)
P2-R10	2	127	182	0.02
P2-R50	2	70	100	0.03
P2-R90	2	14	20	0.16
P8-R10	8	32	46	0.07
P8-R50	8	17	24	0.13
P8-R90	8	4	6	0.55
P32-R10	32	8	11	0.27
P32-R50	32	4	6	0.55
P32-R90	32	1	1	2.19

Table 2.1: Visual environment design in heterogeneity experiment, shown with the variables of black stripes. N_B, number of stripes in the enclosure; W_B, stripe width; $\Delta\phi_B$, angular period; f_C, spatial frequency.

2.3 Results

2.3.1 Visual contrast

For testing the role of simple contrast patterns, we recorded 131 successful landings from 173 drops in 12 individuals, with the frequency of landing on screen significantly greater than expected by null (75.7%; G–test, P<0.0001). With "black in white" contrast, 91.4% of the glides landed on the central black stripe (G_{adj} =125.6, d.f.=2, p<0.0001). While with "white in black" contrast, only 53.0% landed on the central white stripe (G_{adj} =50.7, d.f.=2, p<0.0001) (Figure 2.2-C). Despite the variation in frequency of landing, both frequencies of landing on narrow stripe were both significantly different from that expected by chance.

In experiments testing the effect of contrast edge continuity, only with "black in white" type of discontinuous edges (CT2) the frequency of landing in the potential target area, the region of narrow stripe, was significantly different from that expected by the null case. Landing occurred on the black stripe region in 18 of 30 drops (60%) (G_{adj}=61.4, d.f.=1, P<0.0001). Landing behavior under other 2 setups (CT1 and CT3) were not significantly different from null (Figure 2.2-C).

In experiment testing effect of the sharpness of contrast edges, we recorded 255 successful landings on the arena wall out of 284 drops. Landing only occurred at the half arena where contrast patterns were present. The majority (>95%) of landing points formed two clusters associated with two stripes. The mean direction of von Mises distribution of each was close to that of the contrast edge ($\Delta\theta$ <10°). Also, non–significant differences of landing frequencies was found in all control experiments with stripes of the same sharpness. With two stripes with edges of different contrast sharpness, more than a half of landing occurred

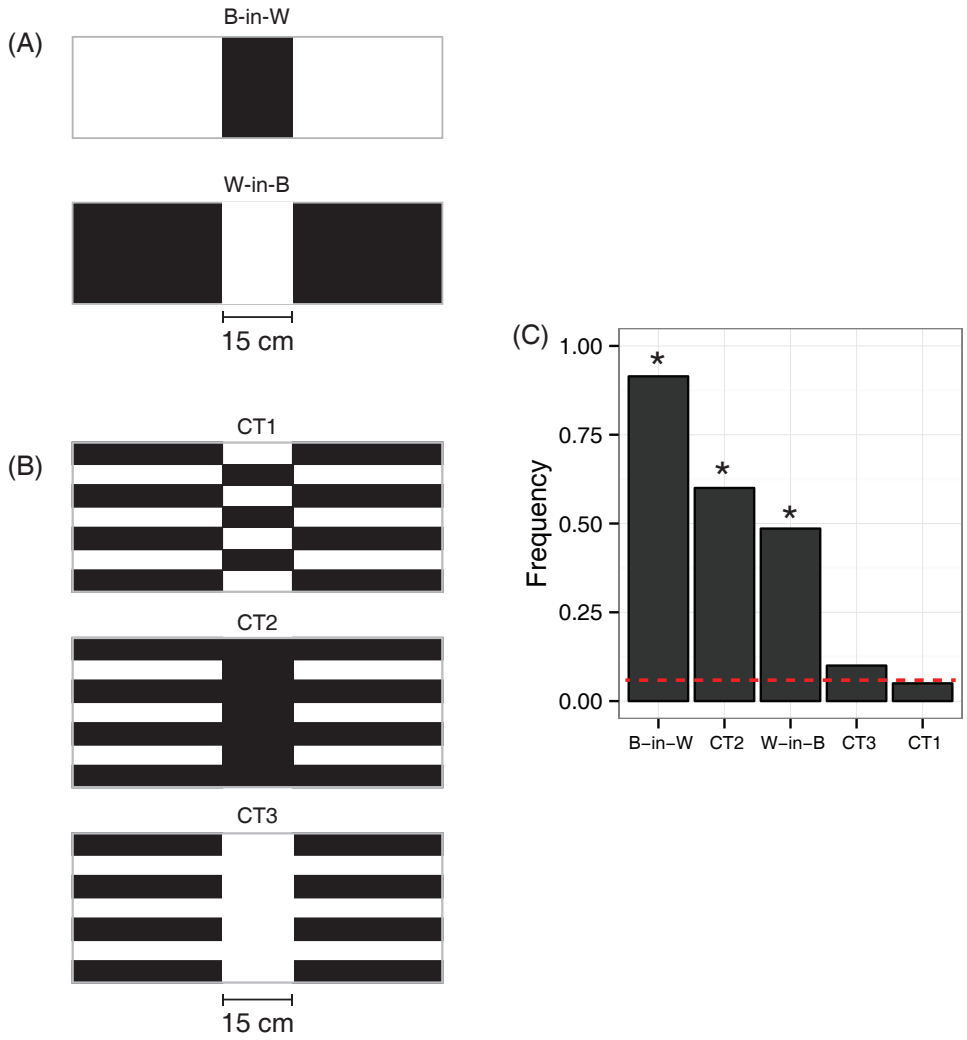

Figure 2.2: Visual contrast patterns and results. (A) Design of simple contrast patterns, showing the central section. "B–in–W" and "W–in–B" represent "black in white" and "white in black", respectively. (B) Design of simple contrast patterns with discontinuous edges. (C) Landing frequencies in visual contrast experiments. Red dash line denotes the null frequency 0.06. Asterix symbols indicate landing frequencies significantly greater than the null, all P-values <0.0001.

near the sharper one, significantly different from what expected by null (Table 2.2). Also, the landing points near sharp contrast stripes are more concentrated, shown by a greater value of concentration parameter κ (68.1) than that of blurred side (13.6) (Figure 2.3).

Experiment	N	Frequency	G_{adj}	P
CS1	84	68%	10.89	<0.0001
CS2	36	83%	17.23	<0.0001
Control-1	54	57%	1.18	0.28
Control-2	51	44%	0.17	0.68
Control-3	30	53%	0.13	0.72

Table 2.2: Details of results on the effect of contrast sharpness. N, number of landing. Frequency, the frequency of landing near the stripe with sharper contrast edge. G_{adj} and P-value are from G–test with William's correction.

2.3.2 Complex patterns

In experiments of DAD landing on patterns formed by grayscale sheets, 136 of 140 drops (97%) successfully landed on screen, significantly different from that expected from the null hypothesis of random drifting (G_{adj} =179, d.f.=1, P<0.0001). Also, in 5 of 7 trials, landing frequency on individual sheets differed significantly from that expected by chance (G–test, P<0.0001; Figure 2.10). High landing frequencies (>30%) occurred on black and dark gray sheets in 5 and 4 trials, respectively. The most frequent landing occurred on sheets which formed strong contrast with neighboring sheets or background. The distribution of overall landing frequencies on each sheet also showed black and dark gray sheets as the most attractive (Figure 2.4-A). Generalized linear regression analyses did not support the correlation between landing frequency and the contrast formed by sheet pairs (P=0.18), but landing frequency was significantly correlated with the negative correlation between contrast formed by each sheet with neighboring sheets or background (C_2, P<0.01) and the contrast against background average (C_3, P<0.05)(Figure 2.5). Landing frequency showed significant variation among sheets of different reflectance profile (One–Way ANOVA, P<0.05).

In experiment of DAD landing on patterns formed by color sheets, we recorded a total 1103 drops with only 39 (3.5%) missing the screen. The landing frequencies on each sheet differed significantly from that expected by chance in 12 of 14 trails (G_{adj} >12.58, d.f.=4, P<0.025; Figure 2.11). Overall, the average landing frequencies on black and white sheets were significantly higher than those on blue and green sheets, with the frequencies associated with red and yellow sheets at the intermediate level (Figure 2.4-B). Further analyses with generalized linear models suggest landing frequency is positively correlated with the magnitude of contrast formed by each sheet with its neighboring sheets or background

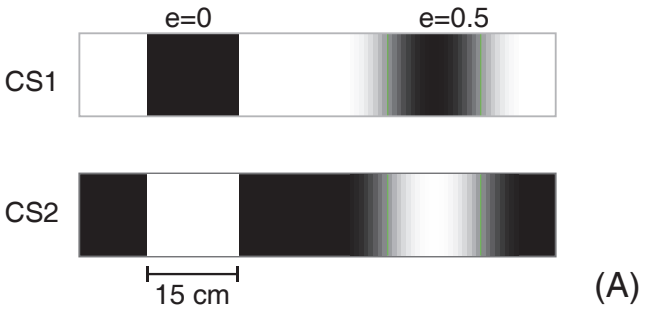

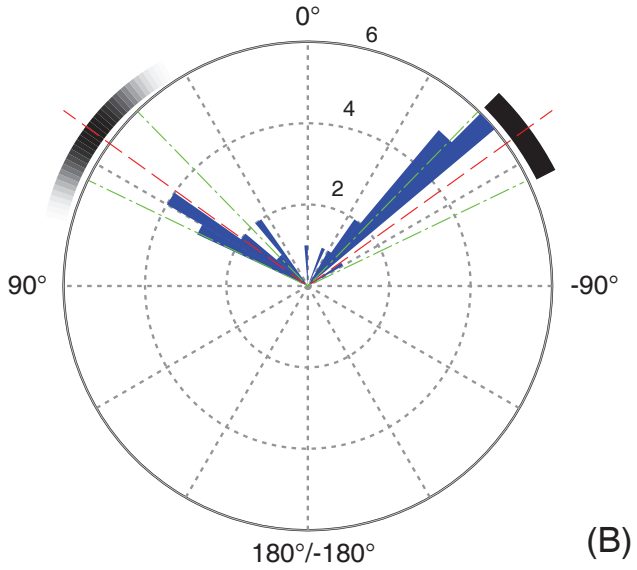

Figure 2.3: (A) Stripe patterns of various sharpness. Only representative sections are shown. (B) Angular distribution of landing points from one trial of pattern CS1.

($|C_2|$) (P<0.05), but is not correlated with either contrast formed by sheet pairs (C_1) or by individual sheets against all others (C_3) (Figure 2.6).

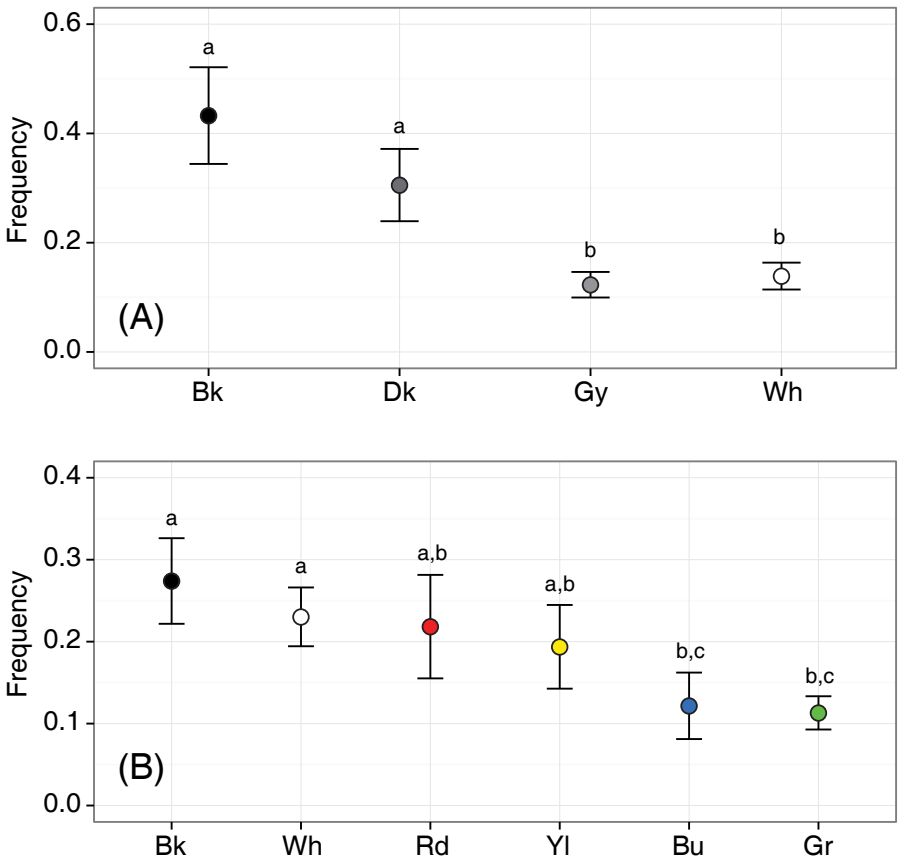

Figure 2.4: (A)Frequencies of landing on each stripe in grayscale experiments. (B) Frequencies of landing on each color stripe. Values are mean±s.e.m. The same letters indicate lack of difference between means.

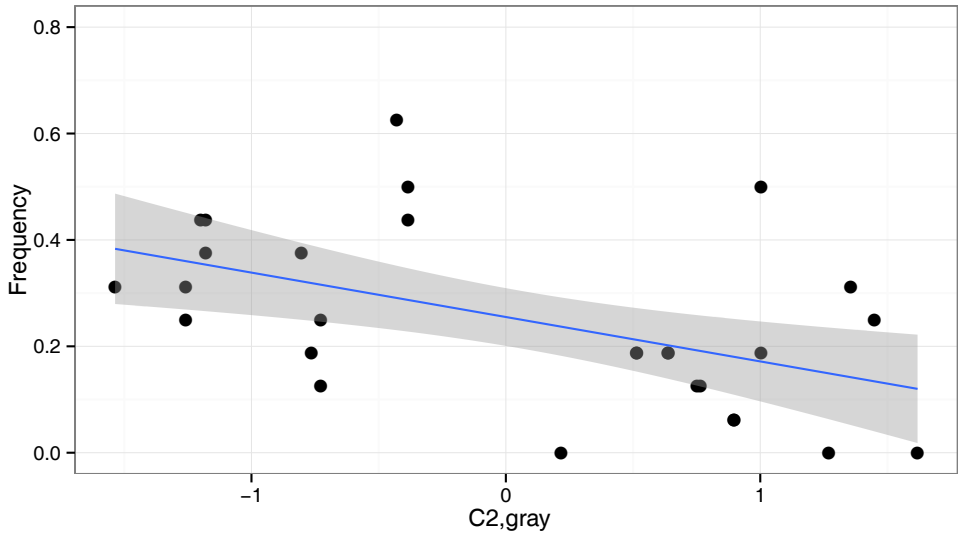

Figure 2.5: The relationship between landing frequency on different grayscale sheets and the contrast of individual sheets against neighboring sheets or background (C_2). Regression line shade denotes 95% CI. There was a significant negative effect of C_2 on landing frequency (R^2=0.251, $F_{1,26}$=8.71, P<0.01).

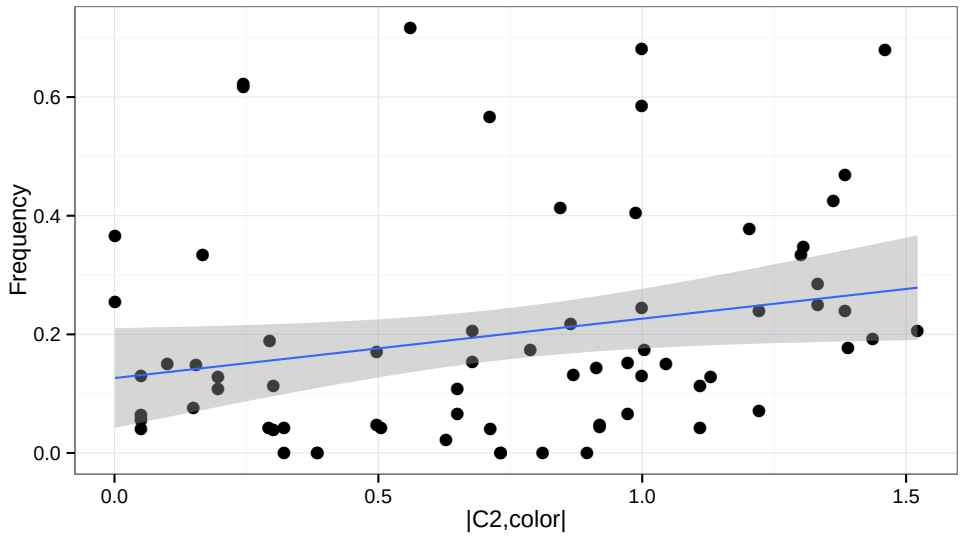

Figure 2.6: The relationship between landing frequency on different color sheets and the magnitude of contrast formed by individual sheets against neighboring sheets or background (C_2). Regression line shade denotes 95% CI. There was a significant positive effect of $|C_2|$ on landing frequency (R^2=0.05, $F_{1,68}$=4.01, P<0.05).

2.3.3 Spatial frequency of contrast

We recorded 324 DAD performances, 60 (19%) of which landed on the arena floor. Of the landing that occurred on the arena wall, the majority was clearly on either black or white, and only 10 landings occurred at the border between black and white sheets. The landing frequencies on black and white from 3 trials (P2–R10, P2–R90 and P2–R50) were significantly different from null expectations (Figure 2.7). In P2–R10 and P2–R90, both with 2 narrow stripes in the background of opposite color, the landing frequencies were significantly greater on the narrower stripes compared to null frequencies. In P8–R50 with equal proportions of black and white, the landing frequency was biased towards black. The frequency of landing on floor differs among trials (Figure 2.8). Lastly, the landing frequencies were found to be random in 5 trials with high spatial frequencies (P8–R10, P8–R90, P32–R10, P32–R50, and P8–R90).

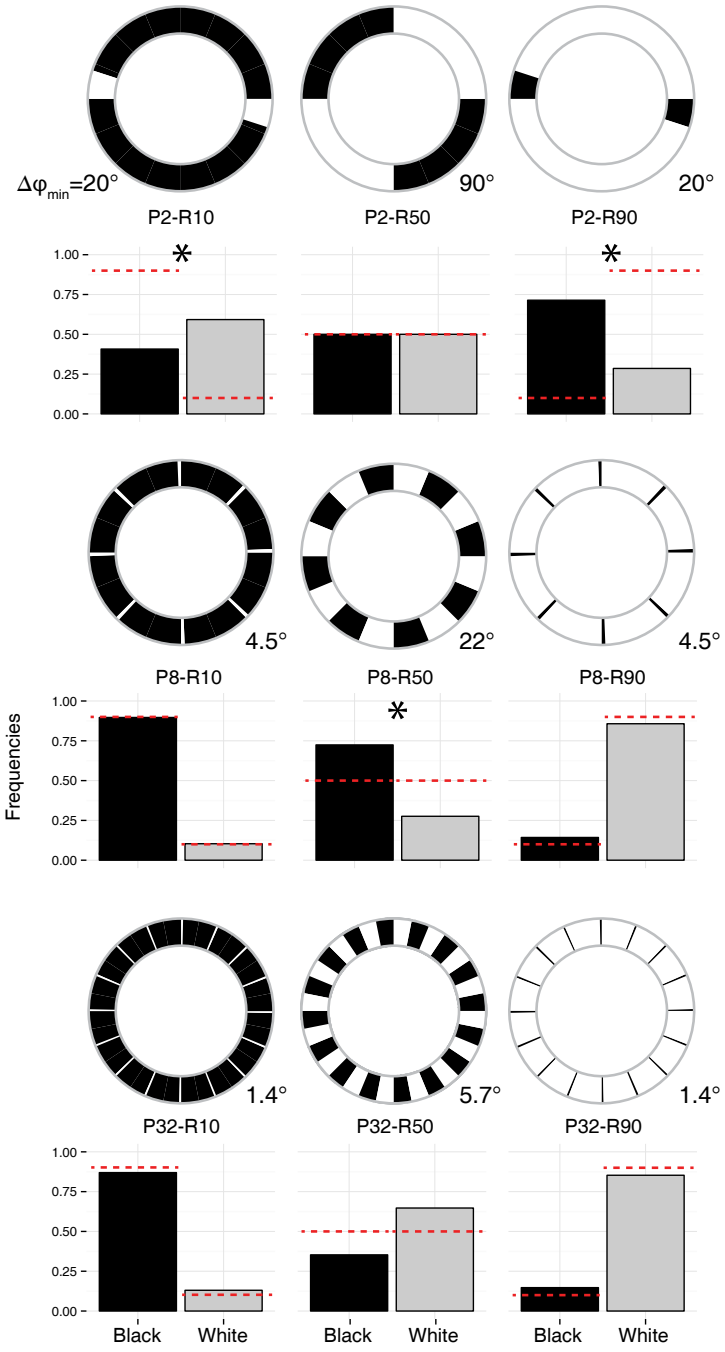
Δφmin=20°
90°
20°
P2-R10
P2-R50
P2-R90
4.5°
22°
4.5°
P8-R10
P8-R50
P8-R90
Frequencies
1.4°
5.7°
1.4°
P32-R10
P32-R50
P32-R90
1.00
0.75
0.50
0.25
0.00
Black
White

Figure 2.7 ***(preceding page)*****:** Landing frequencies, accompanied with schematic cartoon of the visual environment in top view. $\Delta\phi_{min}$, minimum angular period of contrast pattern. Dash lines indicate the frequencies expected under null hypotheses. Asterix symbols denote frequencies significantly different from that expected by null. P2–R10, $G_{adj} = 38.7, P < 0.0001$; P2–R50, $G_{adj} = 0, P = 1$; P2–R90, $G_{adj} = 44.2, P < 0.0001$; P8–R10, $G_{adj} = 0, P = 0.95$; P8–R50, $G_{adj} = 5.94, P < 0.05$;P8–R90, $G_{adj} = 0.25, P = 0.62$; P32–R10, $G_{adj} = 0.21, P = 0.64$; P2–R50, $G_{adj} = 1.45, P = 0.23$; P2–R90, $G_{adj} = 0.73, P = 0.40$.

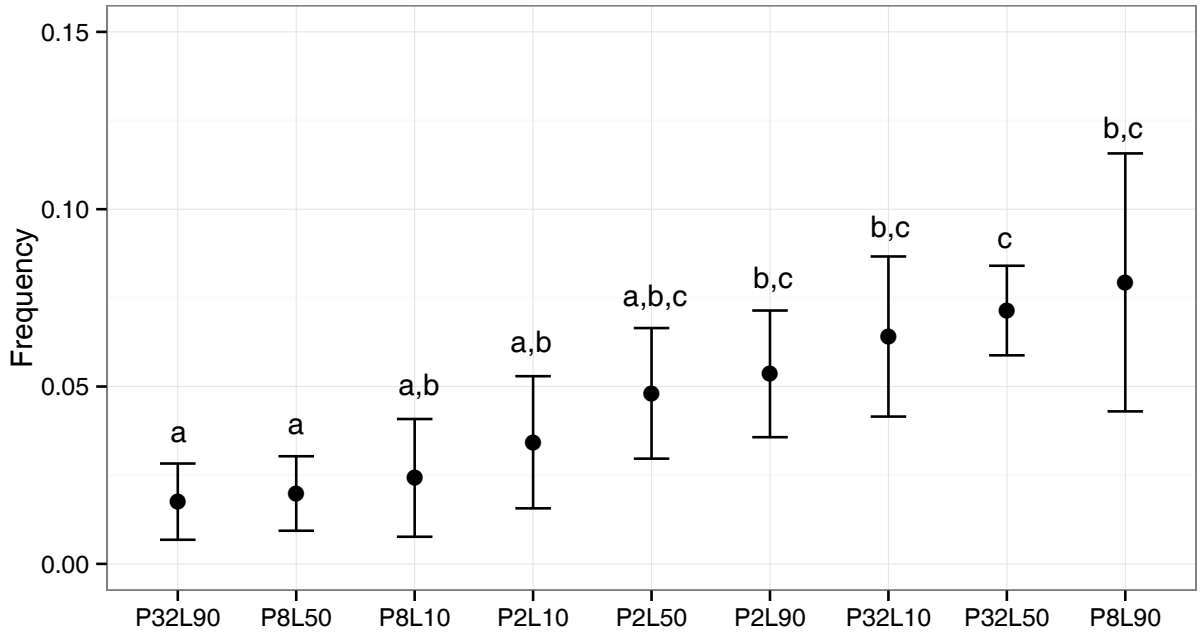

Figure 2.8: The frequency of landing on floor. Values are mean±s.e.m. The same letters indicate lack of difference between means.

2.4 Discussion

In this study we found visual contrast used as visual cues in DAD of larval *E. tiaratum*. Under controlled lab conditions, specimens were able to responded to variations of contrast pattern with different landing behaviors. Specifically, they are sensitive to vertically aligned contrast edges, with a preference to surface with low reflectance. The utility of contrast as visual cues was further shown to be dependent on both the heterogeneity of the entire visual environment and the quality of perceived signals during DAD performance.

2.4.1 The role of visual contrast

In experiments of simple contrast formed by a single vertical stripe against a background of the opposite color, we found DAD landing was associated with the narrow objects in the visual field. Particularly, surfaces with low reflectance, represented by black here, were more attractive than more reflective one (white). Also, we found reduction in continuity of such vertical contrast edges significantly weakened the insects' tendency of landing in the same region. Furthermore, the sharpness of contrast edge significantly influenced the directional choice of where to land. Greater proportion and more concentrated distribution of landing points were found to be positively correlated with contrast sharpness, indicating the strength of contrast signal was used by larval *E. tiaratum* as a directional reference.

In experiments of DAD with complex patterns formed by grayscale sheets, our results showed greater landing frequency was associated with the surfaces of the lowest average reflectance (black and dark gray), suggesting a preference of gliding towards darker objects when exposed to this particularly setup. Also, the landing frequency is negatively correlated with local contrast, indicating that greater negative contrast, which can be formed by dark objects against a brighter background, is more attractive. On the other hand, the results from experiments with complex patterns of color sheets suggest selection of chromatic signals is involved in aerial targeting. The landing frequencies were not significantly different between black, white, yellow and red, which was likely due to the strong contrast formed between these sheets with neighboring sheets. Also, this potentially confirms the lack of sensitivity beyond wavelengths of 600 nm, e.g., orange and red color, in larval *E. tiaratum* as in most other insects [15]. Although no data are available on spectral sensitivity of stick insect eyes, some studies showed locusts and crickets have a spectral sensitivity peak at about 550 nm, beyond which the sensitivity is reduced to nearly zero [78, 95]. Moreover, blue and green sheets were found to be the least attractive target among all others, strongly suggesting that selection against surfaces characterized by spectral profiles similar to these two colors. Under this setup, we showed that a greater landing frequency is correlated with greater local contrast formed between individual sheets against the neighboring or background sheets, which corresponds with the results from other experiments. However, other than an overall preference to dark sheets in grayscale pattern experiment, the landing frequency on white

sheet was not significantly different from that of black sheet, and this change may be possibly associated with different landing strategies corresponding with different heterogeneity of visual fields. Overall, our results showed that larva *E. tiaratum* use different strategies from those of *Cephalotes* ant workers [141].

Our experiment with different spatial frequencies of contrast demonstrated the limitation of targeting acuity and the dependence of overall visual field in DAD of larval *E. tiaratum*. First, random landing was found in 5 trials with low spatial frequencies of contrast ($\leq 5.7°$). This may be due to the limit of visual acuity intrinsic to the visual system, not only because the spatial frequency of visual stimuli is inversely proportional to the sampling frequency of optic apparatus, but also because the increase in spatial frequency of contrast leads to reduction of perceived contrast signal due to optical cut–off effect [75]. For these reasons, in a visual field filled with narrow stripes (e.g., P8–R10, P8–R90, P32–R10 and P32–R90), the spatial frequency of two contrast edges associated with individual stripes can be ineffective. Also, in a visual environment of dense and uniform contrast pattern (e.g. in P32–R50), the sampling frequency is further increased through aerial maneuvering, which may easily go beyond the maximum detectable by eyes of larval *E. tiaratum*. The limit of aerial maneuverability may further increases the acuity of landing on narrow stripes within our setup. Second, comparing results from the other 4 trials (P2–series and P8–R50) further suggests the dependence of visual field heterogeneity in targeting. Larval *E. tiaratum* showed significantly greater preference to the narrower object in visual field from both P2–R10 and P2–R90, which is similar to the results from simple contrast experiments. On the other hand, comparing results between P2–R50 and P8–R50, the latter, which provides greater spatial frequency of contrast and thus greater variation of reflectance in a smaller spatial scale, may have provided sufficient visual signals for maneuvering and landing. In contrast, in P2–R50, which has two large areas in uniform color associated with each contrast edge, the similar landing frequencies on black and white was likely due to the lack of signals for directional bias when gliding towards the contrast edges.

2.4.2 Adaptive significance

Overall, our results suggest larval *E. tiaratum* can discriminate and use variations of contrast pattern from the visual environment for aerial targeting, and their behavioral strategies potentially enhance DAD performance in their native habitat. First, the preference of narrow vertical objects is most likely associated with targeting arbor or liana structures, which are in contrast with foliage and sky at the canopy level. Also, the use of contrast sharpness potentially enhances the efficiency and certainty of landing on the nearest target with less aerial travel distance. Furthermore, selection for continuity of contrast edge also enhances the certainty of landing on trunks or liana. As the appearance of tree trunk profiles can be very irregular with varying light, shadow, color, texture, and epiphytic plants, targeting a vertically continuous target can lead to great certainty of landing success. These utilities of

contrast may also be adopted by canopy ants in descent given the visual contrast formed between tree trunks and surrounding foliage [141]. The avoidance of blue and green color may help landing on stems other than foliage of complex spatial structure. The preference to low reflectance surfaces is likely an adaptive strategy for DAD performed in understory and sub–canopy environments, where potential targets are in contrast with a brighter background [44]. Lastly, our finding suggests the heterogeneity and complexity of visual environment can limit the targeting acuity of DAD performance.

As larval *E. tiaratum* were randomly dropped, aerial righting and stabilizing may cost substantial height before they start visually mediated maneuvering. Our observation on trajectory dynamics suggest they could still be in accelerating phase at 2 m below release point, which may have also affected the acuity of landing with about 40 cm available for horizontal travel. As we only used artificial material and lighting sources here, future sampling of reflectance properties from vegetative structures and the spatial brightness at different forest heights at the native habitat of *E. tiaratum* would further clarify which are the useful components from the visual environment. Our study was also constrained by available space. Measuring the spectral sensitivity of *E. tiaratum* eyes in the future can also help more accurately assessing their contrast perception. As larval *E. tiaratum* don't have developed ocelli, it's unlikely they use polarized light in orientation [47]. However, besides direct use of contrast, other mechanisms of distance discrimination, e.g., binocular stereopsis, may also be used by larval *E. tiaratum*.

2.A Reflectance properties of experimental materials

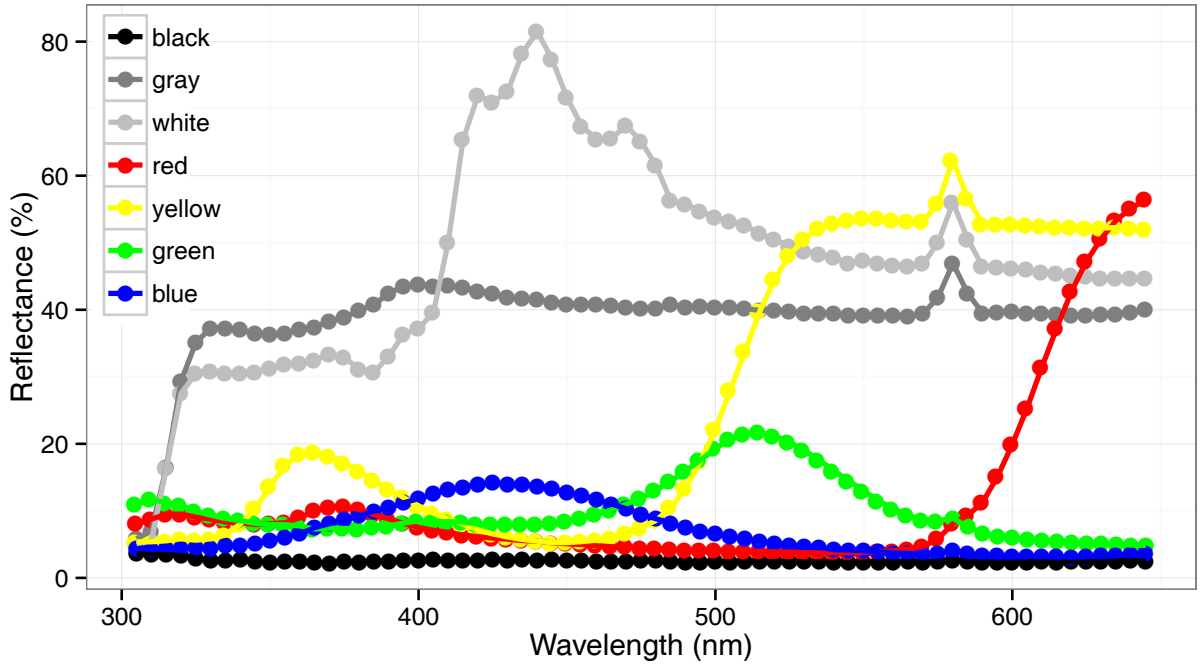

Figure 2.9: Reflectance profiles for each of the seven felt sheets. SE values are not visible here.

2.B Detailed results of sheet array experiment

	Position			
Run	A/B	B/C	C/D	D/E
1	Bk	Dk	Gy	Wh
2	Wh	Bk	Dk	Gy
3	Gy	Wh	Bk	Dk
4	Dk	Gy	Wh	Bk
5	Dk	Wh	Gy	Bk
6	Wh	Dk	Gy	Bk
7	Bk	Wh	Dk	Gy

Table 2.3: Arrangement of grayscale sheets.

	Position				
Run	A	B	C	D	E
1	Bk	Yl	Bu	Rd	Wh
2	Yl	Bk	Bu	Wh	Rd
3	Bu	Bk	Wh	Yl	Rd
4	Bu	Wh	Bk	Rd	Yl
5	Wh	Yl	Bu	Rd	Bk
6	Wh	Yl	Rd	Bu	Bk
7	Rd	Bk	Yl	Wh	Bu
8	Bk	Yl	Gr	Wh	Rd
9	Yl	Bk	Gr	Rd	Wh
10	Gr	Bk	Wh	Yl	Rd
11	Gr	Wh	Bk	Rd	Yl
12	Wh	Yl	Gr	Rd	Bk
13	Wh	Yl	Rd	Gr	Bk
14	Rd	Bk	Yl	Wh	Gr

Table 2.4: Arrangement of grayscale sheets.

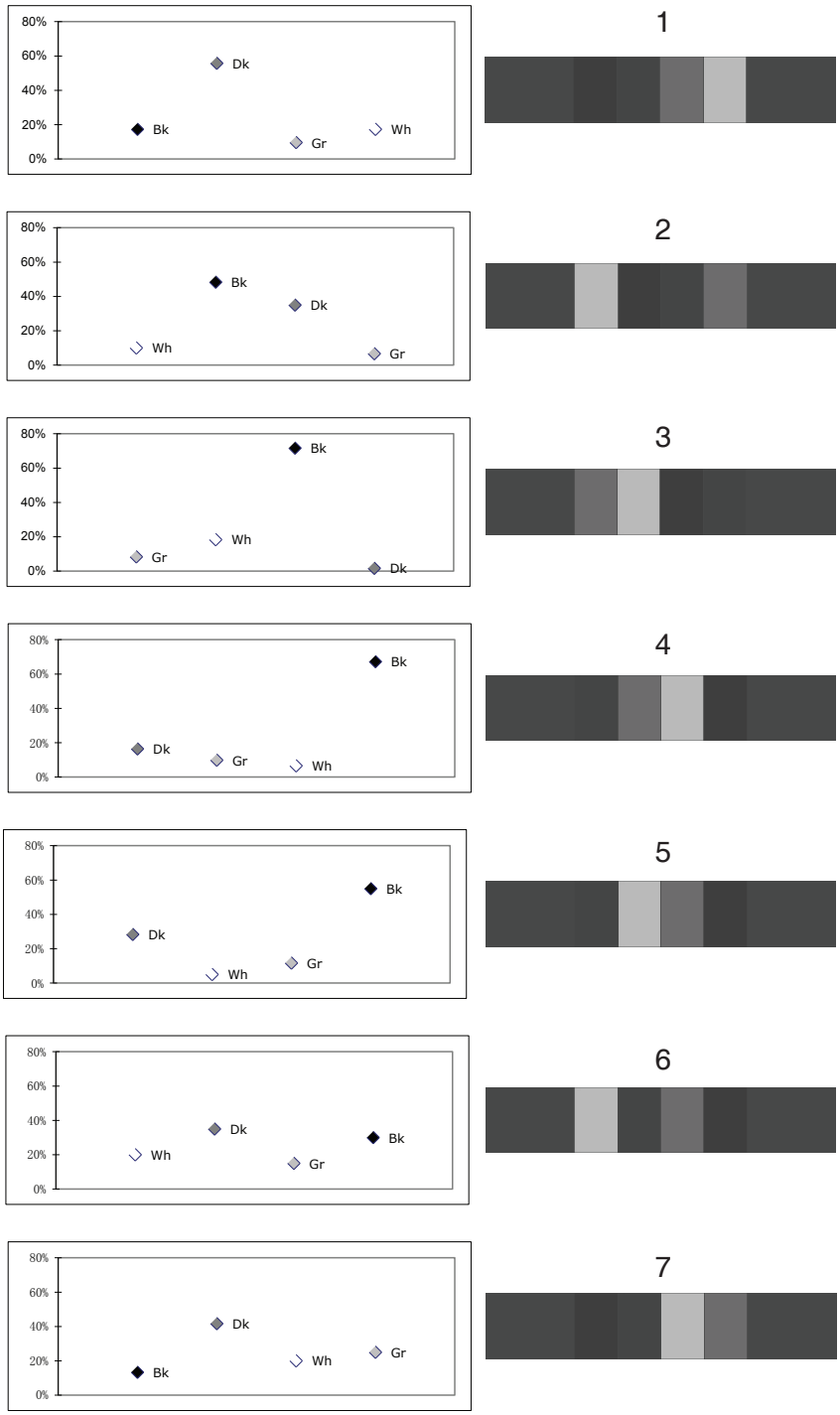

Figure 2.10: Landing frequencies in each trial in experiments of complex pattern formed by grayscale sheets.

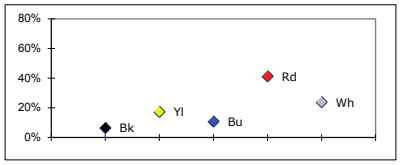
80%
60%
40%
20%
0%
Bk
Yl
Bu
Rd
Wh

1

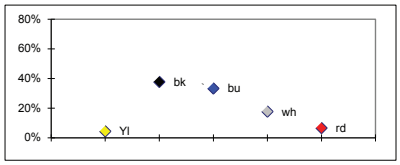
80%
60%
40%
20%
0%
Yl
bk
bu
wh
rd

2

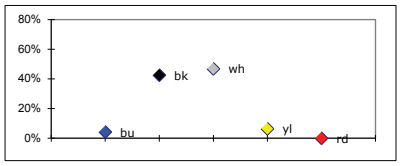
80%
60%
40%
20%
0%
bu
bk
wh
yl
rd

3

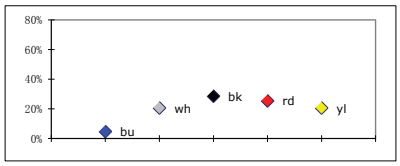
80%
60%
40%
20%
0%
bu
wh
bk
rd
yl

4

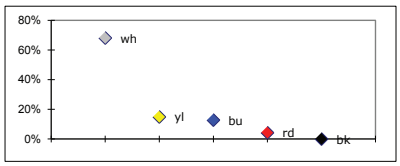
80%
60%
40%
20%
0%
wh
yl
bu
rd
bk

5

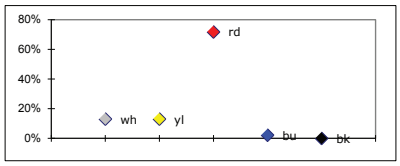
80%
60%
40%
20%
0%
rd
wh
yl
bu
bk

6

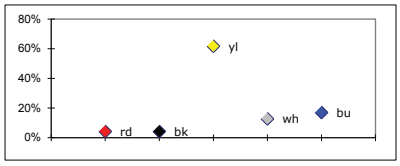
80%
60%
40%
20%
0%
yl
rd
bk
wh
bu

7

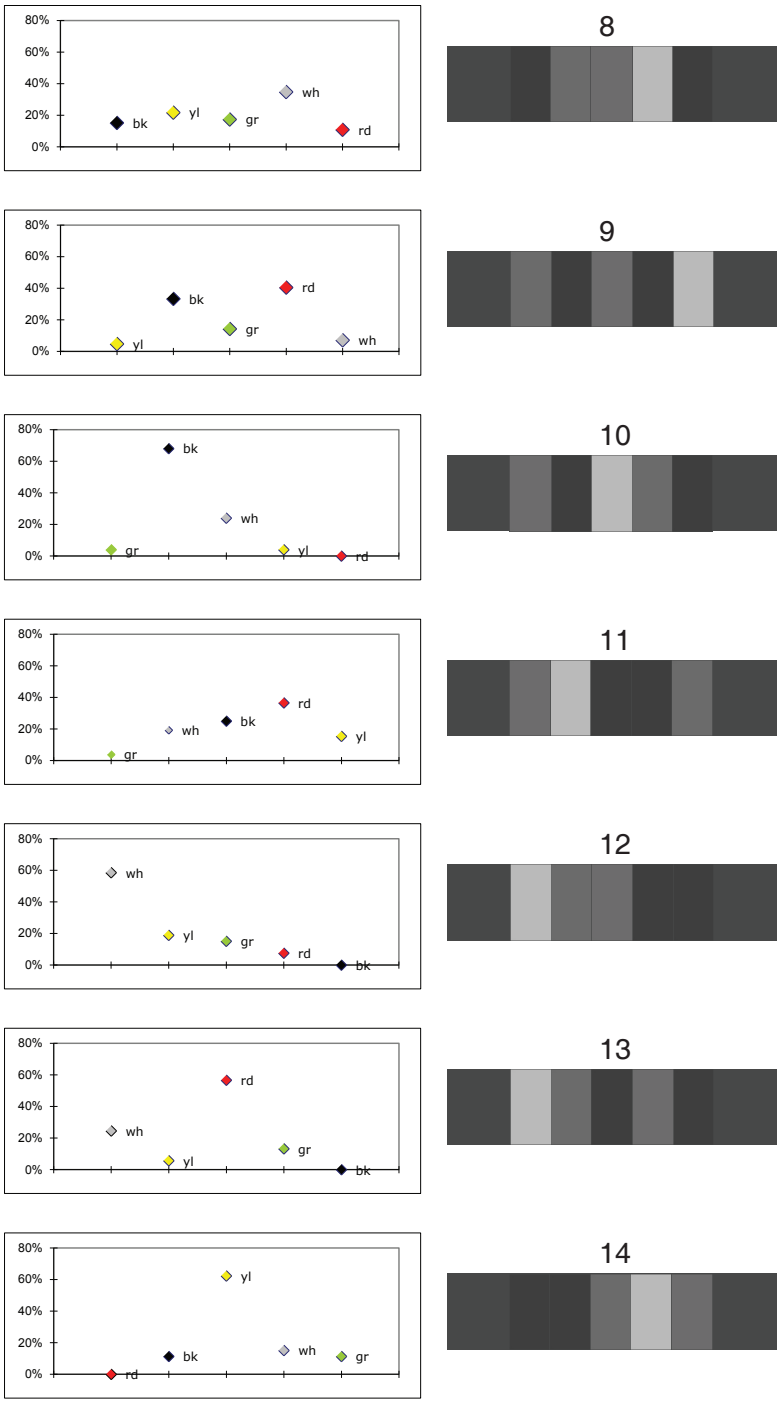

Figure 2.11: Landing frequencies in each trial in experiments of complex pattern formed by color sheets.

Chapter 3

The biomechanics of aerial righting maneuvers in a larval stick insect (*Extatosoma tiaratum*)

The aerial capabilities of wingless invertebrates subjected to unsteady and perturbed conditions are largely unexplored. We studied the aerial righting maneuvers of first instar larval stick insects *Extatosoma tiaratum* introduced to unintentional drops and catapulted ascent. Three–dimensional high–speed filming and detailed motion reconstruction were applied to describe the whole–insect dynamics as well as the movements of all six legs. To recover body orientation, all experimental insects responded with a righting reflex to initiate rapid rotation by aerodynamic torque. The major rotation and subsequent deceleration phases were achieved through stereotypic posture control accompanied with small–scale asymmetric leg movements. Further analyses suggested leg movements were organized as strokes with intermittent directional changes, which corresponded with the dynamics of whole–insect rotation. Since the legs together provide not only a substantial area of aerodynamic surfaces but also significant inertia, the aerodynamic function of leg movements was associated with inertial effects. Our results demonstrate hierarchical leg movement control involved in aerial righting maneuvers, and provide useful information for understanding the ecology and evolution of controlled aerial behaviors in invertebrates.

3.1 Introduction

Midair recovery of body orientation is an adaptation for animals that live in elevated habitats or that perform controlled aerial behaviors. After active takeoffs or accidental drops from

heights, the rapid adjustment of body orientation allows animals to be prepared for landing, gliding or other aerial performances [64]. Moreover, the use of aerial righting maneuvers may be associated with a wide variety of unsteady and perturbed conditions in nature. Given the selective advantage of this ability, aerial righting is considered a basic skill in animal aerial locomotion, and its evolution presumably preceded other types of maneuvers during the evolution of flight [36, 37].

Animals show diverse mechanisms of aerial righting maneuvers. The righting dynamics can vary with the size and shape of the body and appendages, as well as the implemented control strategies. Specifically, both inertial and aerodynamic effects can be utilized for effective torque generation applied about the animal's center of mass. Empirical studies suggested that both effects scale with body size. In flying animals, wings are the primary apparatus involved in active righting maneuvers. Birds and bats can use wings as the primary control apparatus for body reorientation in takeoffs and flight [130, 61]. Although relatively understudied, winged insects can also use asymmetric wing movement for recovering body orientation after perturbation [107]. On the other hand, many wingless animals can also perform midair righting. Wingless vertebrates right by rotating body parts, e.g., torso, legs or tails, in which case the conservation law of angular momentum explains the mechanism [65, 40, 48, 63].

However, the mechanism of aerial righting in wingless invertebrates is largely unexplored. The potential variety is primarily related with the morphological diversity, as well as different ecological contexts where body reorientation is on demand, such as parachuting and directed aerial descent in arboreal environments [142, 143], and aerial escape and dispersal [106, 8]. Also, in small–sized invertebrates, e.g., body size of the majority of insects are under 5 cm [85], aerodynamics likely plays a predominant role in their righting, given the greater aerodynamic forces compared to body inertia towards smaller scales. Two recent studies have demonstrated the use of aerodynamic torques engaged with controlled leg postures during righting in wingless insects [105, 64].

How aerial righting maneuvers could have provided functional opportunities for appendages during the early evolution of complex kinematics, e.g., wing strokes, remains unclear, yet this is fundamental to understanding the evolution of flight and other controlled aerial behaviors. A detailed investigation on the control and utilities of potentially novel behaviors is therefore necessary to provide data of relevance for development of hypotheses of behavioral adaptation. Understanding mechanistic feasibilities may aid in inferring the coupling between incipient morphology and kinematics within a functional context. Although proto–wing morphology and kinematic data are inaccessible of the earliest winged insects, which likely had body sizes in the range of 2 to 4 cm [49, 136, 74], our questions may be addressed by studying functional equivalents, e.g., legs, in extant taxa that exhibit such a behavioral scenario at a similar scale.

The potential mechanisms by which legs facilitate reorientation during righting maneuvers depend on both morphology and kinematics. Intentional control of postures and move-

ments can affect the whole–insect dynamics with both aerodynamics and inertial effects. First, movement of legs can generate aerodynamic force, the torque of which may affect the whole–insect rotation, depending on the flow state around the insect. Second, rapid turning can generate inertia torque (depending on mass and angular acceleration). The inertial effect has been found in wing flapping [45, 46]. Having six legs provides necessary space for combining these effects so they can act collectively to the whole–insect. For example, pitching torque generation due to fore–aft control, and bilaterally asymmetric control potentially affects both yaw and roll. In addition, changes in the spatial configuration of legs can shift the center of mass (COM) as well as the moment of inertia (MOI). In a context relevant to evolution of controlled aerial behaviors, asymmetric movement control can be used for directional control at equilibrium aerial trajectories [144], but whether asymmetric leg movements is also involved in righting maneuvers is unknown.

Aerial righting maneuvers under natural conditions are likely to occur often in transient movements, involving unsteadiness of both translational and rotational components. For example, righting from an upside-down fall is a process with rapid angular acceleration and angular deceleration coupled with translational acceleration. On the other hand, righting during other types of perturbation can be coupled with both acceleration and deceleration of translation. The central question is whether an organism can respond to the varieties of perturbation, and adjust whole–insect dynamics under specific conditions. A biologically relevant task is to recover to a right–side–up orientation with respect to gravity, to prepare for descent. Insects are potentially capable of responding rapidly to rotation and air flow. Earlier studies suggested that insect legs have a variety of reflex mechanisms to trigger rapid responses after the loss of contact [99, 32, 10, 134].

Here we studied righting maneuvers in first instar larvae of stick insect *E. tiaratum*. Newly hatched individuals actively disperse in arboreal environments and likely engage in aerial escape in response to perturbation (unpublished data). Studies on directed aerial descent behavior in these larvae also suggested the necessity of aerial righting maneuvers after voluntary takeoff, accidental drops and midair perturbation under natural conditions (unpublished data). We captured three-dimensional kinematics of whole–insect and legs, and used model-assisted analyses to address the orientation recovery and associated leg movements under unsteady and perturbed conditions. Furthermore, to understand the organization and functionality of leg movements, we analyzed the correlational pattern, and estimated aerodynamic and inertial effects.

3.2 Materials and Methods

3.2.1 Insect preparation and morphometrics

Eggs of *E. tiaratum* were incubated under constant temperature (25°C) and humidity (70%). Newly hatched larvae were collected within the first 24 hours and were transferred to clear plastic cups (355–470 ml) with lids. Constant humidity was maintained in the plastic cups by daily water spray, and all cups were kept in an environmentally controlled room with constant temperature (25°C) and 12–hour light–dark cycles. Only healthy, active and intact first instars within their first 2 days after hatch were used in our experiments. Experimental insects were transported and kept in the same plastic cups served with water during experiments.

We divided the body into multiple sections by the major relevant joints (coxa–femur, femur-tibia, and first abdominal joint) involved in the righting motion, and sampled mass, width and length of each section, including 1) head with three thoracic segments, 2) abdominal segments, 3) femur of each leg, and 4) tibia and tarsus of each leg. The mass of each body segment from deep frozen specimens (N = 25) was measured with an electronic balance (R200D, SATORIUS). COM of each segment, cut from frozen specimens, was determined by placing the segment on a horizontal pin, and the position of COM is measured in ImageJ. (mass loss <6% after cutting) In total, 15 joint landmarks were used to represent the insects body as 8 linked sections (Figure 3.2). The projected plan area, length and width of each segment were quantified based on high-definition digital images taken from anesthetized individuals (N = 10) laid on a flat surface.

3.2.2 Experimental setup and protocols

Aerial righting performance was filmed by two synchronized high-speed cameras (1280 × 1024, 500 Hz, HiSpec, FasTec Imaging). A film section (40 cm, height) was set in front of a white background and provided with sufficient lighting. Camera spatial resolution > 2 pixel/mm.

To eliminate the effect of initial perturbation in accidental falls, we designed a device which vacuum-tethers an upside-down insect by its mesosternum at a fixed angle with a capillary tube connected with a pressure source. Insects were released by releasing the pressure in capillary tube (Figure 3.1). With this setup and protocol, we used anesthetized insects (N = 10) as control, each was treated with a 3-minute exposure of gas CO2 prior to release. All experimental trials were calibrated with freely dropped deadweight.

To simulate an unstable initial condition, we launched experimental insects in right–side–up orientation. A TEFLON-coated plate (3 cm, diameter) was fastened upon a spring-powered launcher with manual trigger (Figure 3.1-C). The launcher was positioned vertically, and releases experimental insects at 2.4 ± 0.02 m/s (maximum acceleration about 600 m/s^2).

In experiments, insects were first transferred to the plate, and the plate was launched when the insect traveled near the center of the plate.

Motion reconstruction was completed with commercial software (ProAnalyst, Xcitec Inc.). Most morphological landmarks (Figure 3.1) were manually tracked. Digitization error was first minimized by using a single person for digitizing and by proof-reading for all frames. To assess the effect of digitizing error, a single trial was digitized 5 times. The standard deviation of each landmark from these five trials was $< 0.01\%$ in all coordinates. We used a quintic spline function to fit the positional data of each landmark, and the averaged root mean square (RMS) error [128] of positional data was about 0.86% in x-coordinate, 0.89% in y-coordinate and 0.18% in z-coordinate. 3D calibration was completed with 160 digitized landmarks on two angled (120°) plane, and the calibration of camera position has mean error < 0.1 cm.

3.2.3 Kinematics and aerodynamics

We used the term "body" to represent the body section excluding all legs (i.e., head, thorax and abdomen combined; denoted by b), in contrast to "whole–insect", which represents the collection of all segments (denoted by B). Motion analyses were conducted using custom–written scripts in MatLab [82], and statistical analyses were performed with custom–written codes in R [101].

3.2.3.1 Whole–insect kinematics

The insect body is modelled as a system of linked rigid bodies, the mass of each of which is concentrated at one point. The body–fixed frame is centered at the midpoint between two mid–coxae. It is defined by an X_b axis parallel to the longitudinal axis through the head and all thoracic segments pointing to the posterior end, an Z_b axis that is dorsally oriented and an Y_b axis that is the cross product X_b of and Z_b (Figure 3.2). Conversion among coordinate frames follows Murray et al. [89]. The translation of body–fixed frame was calculated with respect to the spatial coordinates as

$$v_b = -\dot{R}_b {R_b}^T p_b + \dot{p}_b = \left[v_{b,x}, v_{b,y}, v_{b,z}\right]^T, \tag{3.1}$$

where v_b is body translation, R_b and p_b are rotational matrix and position of body frame in spatial coordinates, respectively. Also, the angular velocities of each rotation about three principal axes were calculated based on the derivative of rotation matrices

$$\omega_b = (\dot{R}_b {R_b}^T)^\vee = \left[\omega_{b,x}, \omega_{b,y}, \omega_{b,z}\right]^T. \tag{3.2}$$

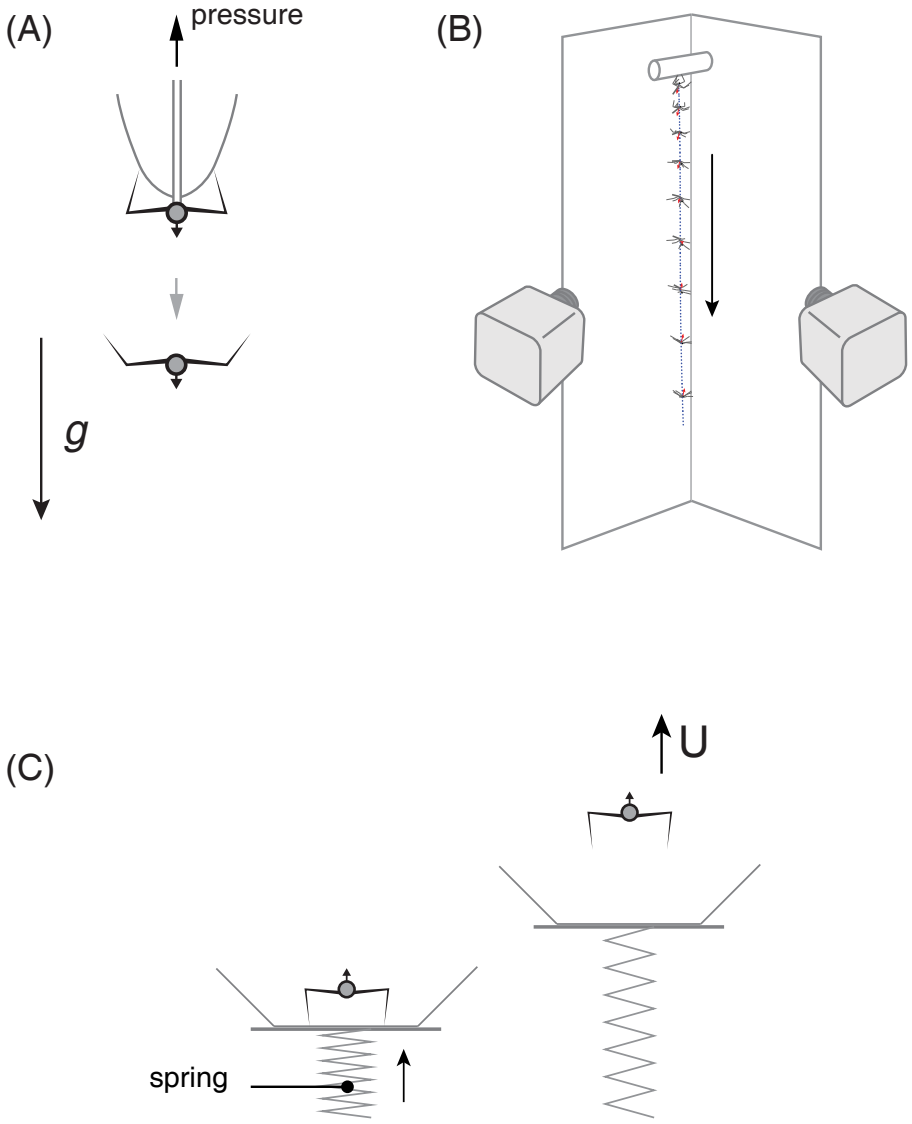

Figure 3.1: (A) Release insects in upside–down orientation from a capillary tube connected to a vacuum source. (B) Camera configuration for filming righting maneuvers. (C) Setup configuration for insect catapulting.

Together, homogeneous transform of spatial frame to body–fixed frame is

$$H_{b-S} = \begin{bmatrix} R_b & p_b \\ 0 & 1 \end{bmatrix}. \tag{3.3}$$

The instantaneous position of whole–insect COM in spatial frame is calculated as

$$p_B = m_B^{-1} \sum_{i=1}^{13} m_i p_{m,i}, \tag{3.4}$$

where m_B is total mass, m_i and $p_{m,i}$ are mass and longitudinal COM position of each body section (3.1), respectively. Likewise, position of COM with respect to body–fixed frame is $p_{B-b} = R_b p_{COM}^T + p_b$. COM–fixed frame has all axes parallel to those of body–fixed frame, written as

$$H_{B-S} = \begin{bmatrix} R_B & p_B \\ 0 & 1 \end{bmatrix}. \tag{3.5}$$

Furthermore, the body orientation relative to gravity and horizon are biologically relevant to our questions. We defined body orientation with respect to gravity as the angel between unit vectors z_b and z_S, $\beta_Z = cos^{-1}(z_b \cdot z_S / |z_b| \cdot |z_S|)$. For example, the insect is "perfectly" upside-down when β_Z is 180°; during righting initiated in upside–down orientation, β_Z decreases towards 0°. Similarly, body orientation with respect to horizon β_{XY} is the angle between y_b and the y_S.

3.2.3.2 Whole–insect dynamics

As a system of linked rigid bodies subject to gravity and interacting with ambient air flow, the complete dynamics can be described by the Newton-Euler equation of motion

$$\begin{bmatrix} m_B I & 0 \\ 0 & T_B \end{bmatrix} \begin{bmatrix} \dot{v_B} \\ \dot{\omega_B} \end{bmatrix} + \begin{bmatrix} \omega_b \times m_b v_b \\ \omega_b \times T_b \omega_b \end{bmatrix} = F_b = \begin{bmatrix} f_l \\ \tau_l \end{bmatrix} + \begin{bmatrix} f_b \\ \tau_b \end{bmatrix} + \begin{bmatrix} f_g \\ 0 \end{bmatrix}, \tag{3.6}$$

where m_B is total mass, I is identity matrix, $_B$ is the matrix of whole–insect moment of inertia about COM, and v_B and ω_B are translational and rotational velocities of body COM, respectively. Also, f_l and f_b are aerodynamic forces acting on legs and body, respectively; and τ_l and τ_b are aerodynamic torques acting on legs and body, respectively.

We estimated the overall aerodynamic torque acting on the whole–insect by tracing temporal changes in the sum of angular momentum. The total angular momentum is calculated as

$$L_B = \sum_{i=1}^{13} r_i \times m_i v_i, \tag{3.7}$$

where m_i is point mass of each body section, r_i is the vector from body COM to section COM, $v_i = \omega_i \times r_i$ is linear velocity of section COM with respect to COM–fixed frame.

We estimated instantaneous aerodynamic torque as the time derivative of the total angular momentum :

$$\tau_{ext} = \tau_l + \tau_b = \frac{dL_B}{dt}. \tag{3.8}$$

3.2.3.3 Leg kinematics

We simplified the structure of legs by dividing each leg into two sections: section 1 covers coxa to tibia–femur joint, and section 2 covers tibia–femur joint to the distal end of the last tarsal segment (3.2). Since the thoracic-coxal joint enables 3 degrees of freedom of the coplanar segments, and the bending of tibia-femur joint, a total of 4 degrees of freedom is associated with each leg [29]. A coxa–fixed coordinate frame is set at each coxa with three axes parallel to those of the body frame, and two segment–fixed frames are set at the distal end of leg section 1 and section 2, respectively. Local X axes of segment–fixed frames are parallel with the longitudinal axes, and Z axes are coplaner with Z_b.

We omitted the rotation about X axis of segment–fixed frames. Position of each leg is described by sweep angle ϕ, deviation angle ψ and rotation angle λ, which are Euler angles corresponding to the rotations of X_l of section1–fixed frame from a lateral position paralleled Y_b (Figure 3.2). As self–rotation is omitted, $\lambda = 0$. Leg's angular position with respect to coxa–fixed frame is

$$\theta_{l-c} = \left[\psi, \phi, 0\right]^T \tag{3.9}$$

and angular velocity of a leg with respect its local coxa frame is described as

$$\omega_{l-c} = \left[\dot{\psi}, \dot{\phi}, 0\right]^T. \tag{3.10}$$

In addition, the angle between leg section 1 and section 2 is γ.

Asymmetry indices were used to describe bilateral asymmetry of leg movements, including stroke phase (0% to 100%), angular position, angular velocity and angular acceleration within each pair. Each angular term has two components, in sweep and elevation directions. Instantaneous stroke phase asymmetry index (PAI) is calculated as

$$PAI_t = \frac{P_L - P_R}{|P_L + P_R|}, \tag{3.11}$$

where P_L and P_R are stroke phase of a given leg and a given time. Other asymmetry indices for angular position (OAI), angular velocity (VAI) and angular acceleration (AAI) were calcualted in the same format.

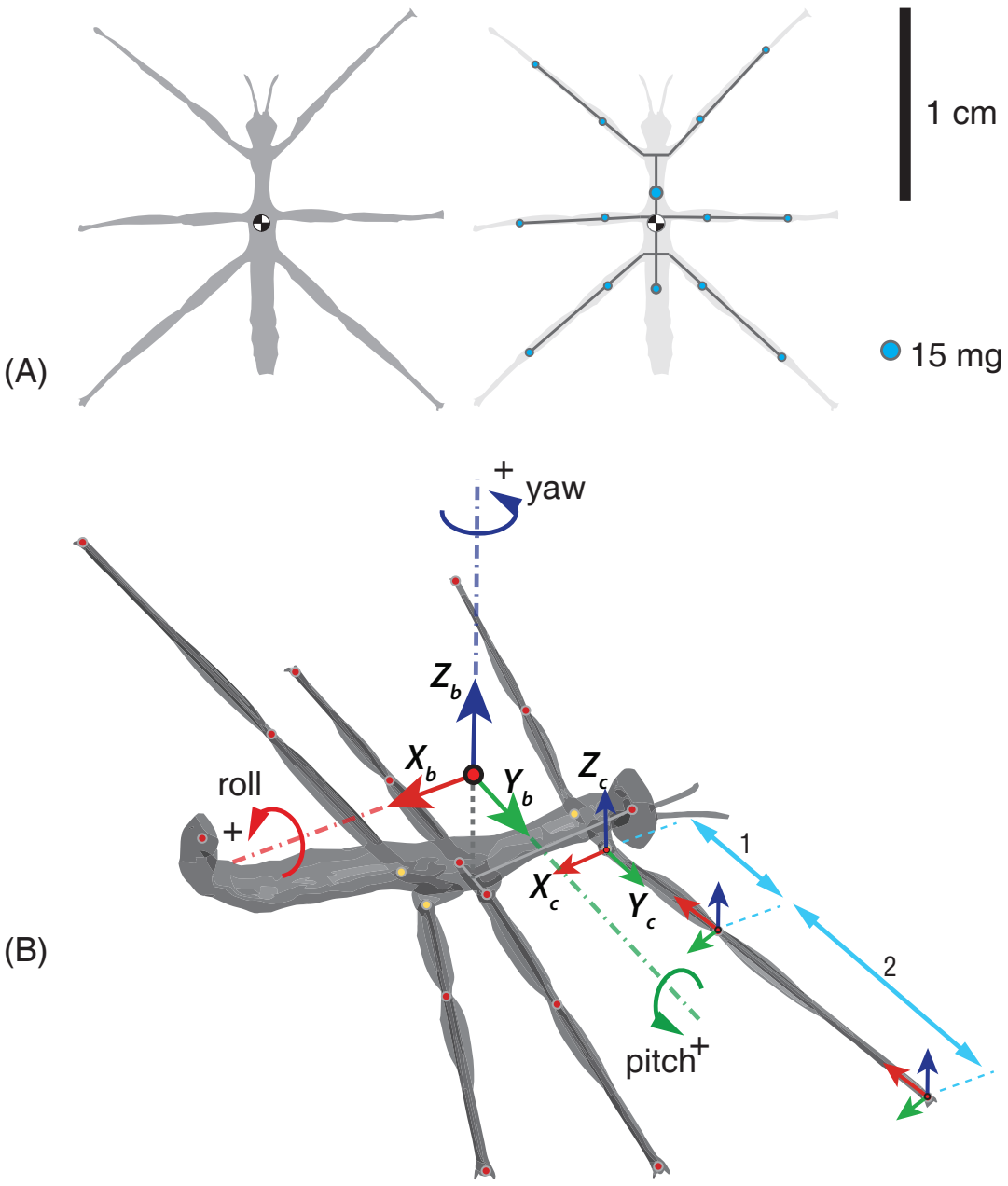

Figure 3.2: (A) Left: planform profile in top view. Right: insect body modeled as a system of linked point mass. (B) Configuration of body–fixed coordinate frame, elevated in Z direction for clarity. Coxa– and leg–fixed fames are marked on right front leg.

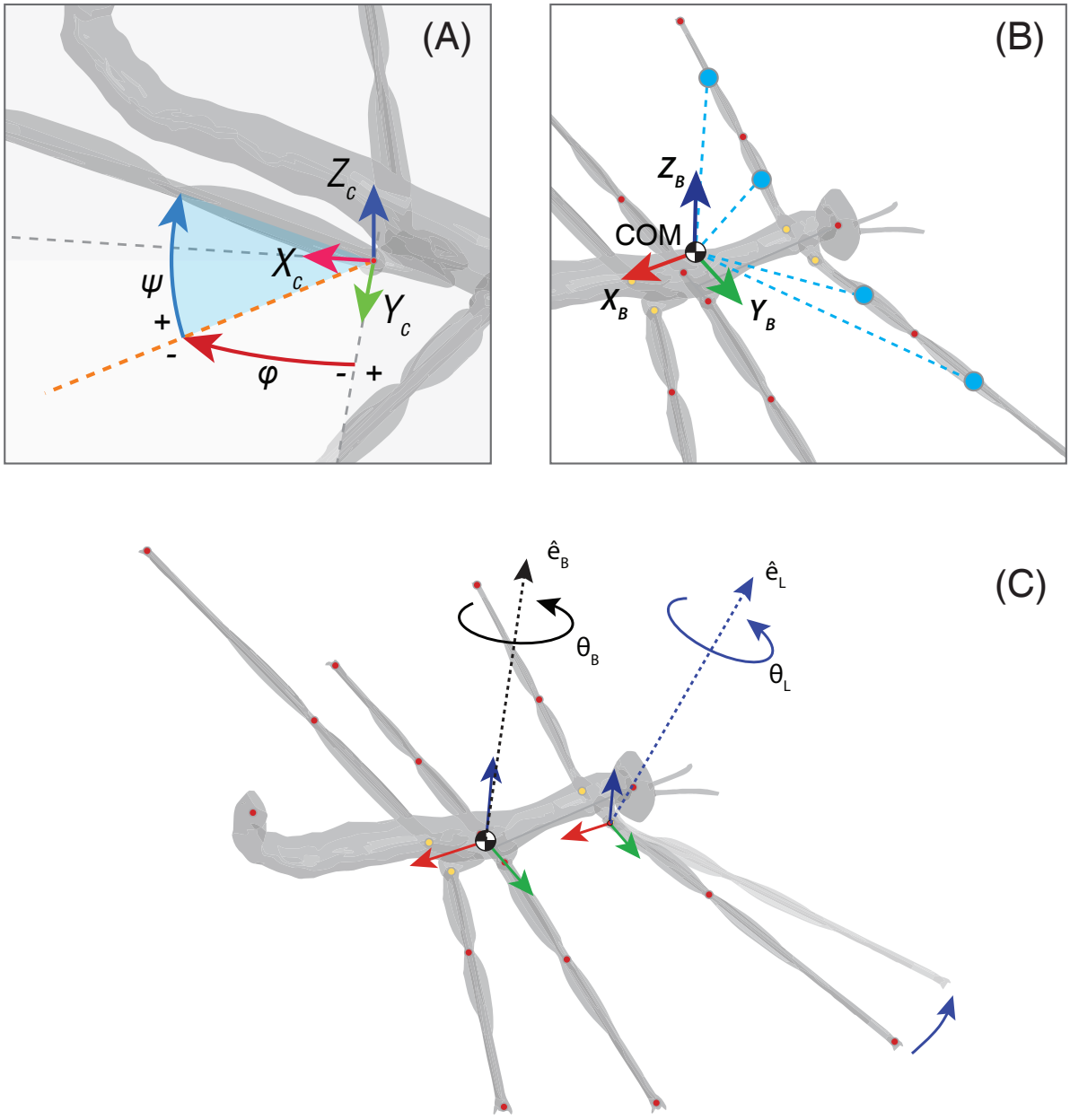

Figure 3.3: (A)Sweep and elevation angles of leg, shown with right hind leg. (B)Configuration of COM–fixed frame, with point mass associated with forelegs highlighted. (C)Axis-angle representation of body rotation about COM, and of leg rotation about local coordinates centered at coxa joint.

3.2.3.4 Stroke movements

For clarity in directionality and magnitude of highly variable leg movements with respect to coxa–fixed frames, aforementioned angular position representation was converted into "axis-angle" form: $\left(\hat{e}, \boldsymbol{\omega}_l\right)$, where $\hat{e} = \left[\hat{\omega_x}, \hat{\omega_y}, \hat{\omega_z}\right]^T$ is the unit vector of rotation axes (rotations normalized by resultant magnitude), and $\boldsymbol{\omega}_l$ is the magnitude of rotation speed (Figure 3.3). This format also allows us to represent body rotation as three normalized simultaneous rotations (roll, pitch and yaw) and the magnitude rotation speed.

The changes in direction of leg swing can be identified by local curvatures along its path. The path of a leg frame can be mapped to a spherical coordinates frame centered at the associated coxa. Path curvature is calculated as $k = d\boldsymbol{V}/dt$, where $\boldsymbol{V} = \left[\dot{\psi} \quad \dot{\phi}\right]$ is the velocity vector, and t is time. According to the right–hand rule, here the curvature is equivalent to the shift in rotation axis through time, the time derivatives of $\hat{e}$, and thus $k = d\hat{e}/dt$.

Primary analyses indicated the majority of leg movement about associated coxa is characterized by smooth swing–alike movement with little change in direction, separated by short intervals with rapid changes in direction (Figure 3.8).

According to results of sensitivity test, 85% of the intervals have small (< 2500 deg/s) changes in direction (Figure 3.8). The peaks of k, associated with sharp turnings, was used to determine the temporal conjunctions between smooth intervals (Figure 3.7). These smooth intervals between sharp turnings were defined as "strokes", following its original definition "a single unbroken movement" and "a controlled swing" [86].

Kinematic variables for describing individual strokes include: amplitude θ_s and period $\boldsymbol{T}_s$ are the angular distance and temporal distance between starting point t_{s0} and ending point t_{s1}, respectively; mean angular velocity $\bar{\omega}_s = \left[\bar{\phi}, \bar{\psi}\right]$ mean angular speed $\boldsymbol{\omega} = \theta_s/\boldsymbol{T}_s$. A stroke plane is one that contains a stroke in corresponding coxa–fixed frame. Prior to further analyses, multivariate linear models and analyses of variance were first conducted to check the pattern of variation between leg groups, in which the grouping factors of legs are "side" (left and right) and "pairs" (fore-, mid- and hind-legs).

3.2.3.5 Strokes in relation to whole–insect dynamics

Prior to further analyses, we first tested if mean posture of each leg is affected by body rotation and translation. We tested correlation between mean stroke posture (sweep and elevation angle components) and the whole–insect rotation and translation, including both directional components and magnitude, using linear regression models.

The directionality of strokes was analyzed with respect to instantaneous whole–insect translation and rotation, as well as the flow local to each leg. To express whole–insect kinematics in coxa–fixed frame,

$$v_{b-c} = v_b, \tag{3.12}$$

$$\omega_{b-c} = R_{bc} \cdot \omega_b, \tag{3.13}$$

The resultant vector of these two:

$$V_{b-c} = v_{b-c} + \omega_{b-c}. \tag{3.14}$$

The intersection angles between strokes and above components: θ_{ST}, θ_{SR} and θ_{SV} are stroke plane angle with respect to whole–insect translation, rotation and resultant motion, respectively. Each term ranges between 0°and 180°(Figure 3.4). We used time–averaged values of kinematic variables over the duration of each stroke. To reduce the dimension of analyses, all following statistics were applied to each leg pair (fore-, mid- and hind-legs) separately. First, we applied linear regression models to find the correlations between kinematic variables of strokes and those of whole-insect kinematics. Tested body kinematics variables include the directional vectors and magnitude of principal rotations (roll, pitch and yaw), translation (axial, lateral and dorsalventral) and time derivatives of each component, a total of 16 variables, all with respect to local coordinate frame centered at whole-insect COM. Second, we used ANOVA and ANCOVA models to test the significance of variance associated with the different pairs of legs. Third, we applied MANOVA to identify the variance and interactions among stroke kinematics between leg pairs and between legs of different position with respect to axes of roll and yaw (Figure 3.12, Figure 3.13).

3.2.3.6 Inertial effects

We calculated inertia torques based on instantaneous angular acceleration of all leg segments with respect to COM (Figure 3.3). With respect to COM–fixed frame, the inertia torque associated acceleration of a body section i is $\tau_i = r_i \times m_i v_{iB}$, where r is the moment arm from body section COM to whole–insect COM and v is linear acceleration. The total inertial torque is the sum of all segmental inertial torque

$$\tau_{inr} = \sum\nolimits_{i=1}^{13} \tau_i. \tag{3.15}$$

Inertia power is calculated as

$$P_{\tau,inr} = \tau_{inr} \cdot \omega_B. \tag{3.16}$$

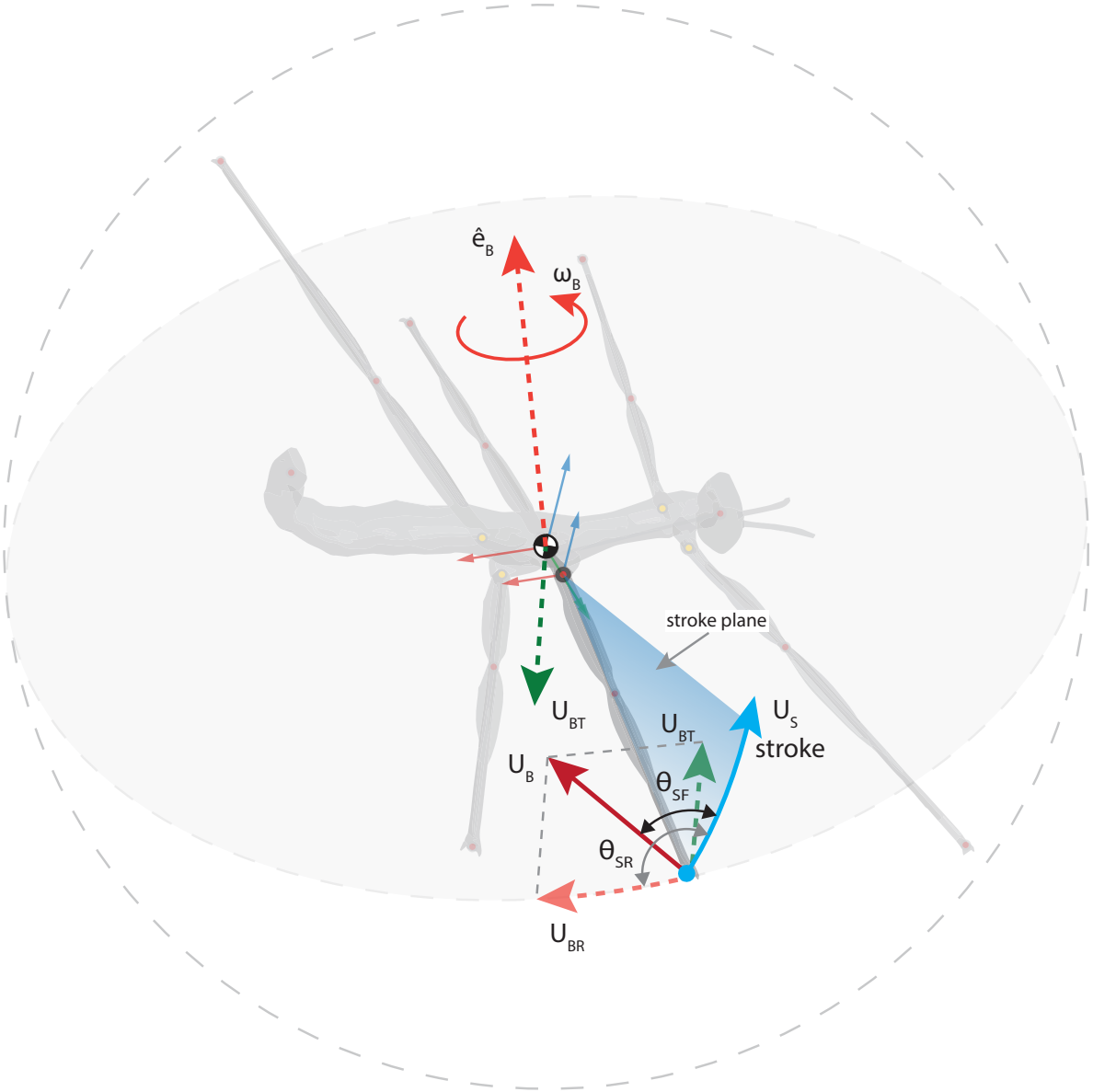

Figure 3.4: Configuration of leg stroke in relation to translation, rotation and resultant motion of whole–insect COM. U_{BT}, COM translation; U_{BR}, whole–insect rotation; U_S, stroke velocity.

3.3 Results

The following results are based on 20 righting trials from upside–down descent and 20 in catapulted ascent. Values are presented as mean ± s.d. unless stated otherwise. The legs together hold about 40% of the total mass and about 60% of the total planform area (Table 3.1).

	m (mg)	$COMx$(%)	L (mm)	W (mm)	A (mm^2)
head-thorax III	9.17 ± 1.07	35 ± 2	9.1 ± 0.66	1.66 ± 0.06	15.14 ± 1.62
abdomen	5.76 ± 0.46	55 ± 2	7.95 ± 0.43	1.44 ± 0.07	11.41 ± 0.48
section 1, F	0.45 ± 0.04	53 ± 4	5.1 ± 0.23	0.53 ± 0.03	2.7 ± 0.27
section 2, F	0.36 ± 0.05	48 ± 3	7.5 ± 0.36	0.36 ± 0.02	2.71 ± 0.25
section 1, M	0.56 ± 0.05	50 ± 3	4.45 ± 0.15	0.69 ± 0.04	3.08 ± 0.27
section 2, M	0.44 ± 0.05	47 ± 4	6.32 ± 0.36	0.44 ± 0.03	2.76 ± 0.33
section 1, H	0.77 ± 0.12	48 ± 4	5.39 ± 0.23	0.72 ± 0.05	3.91 ± 0.43
section 2, H	0.74 ± 0.1	44 ± 3	8.63 ± 0.41	0.5 ± 0.05	4.36 ± 0.56

Table 3.1: Morphometrics of body parts (N = 10). $COMx$, center of mass with respect to the longitudinal axis from the near end or anterior end. F, M, and H correspond to fore–, mid– and hind–legs, respectively.

3.3.1 Whole–insect kinematics

The righting success was 100% in all 40 trials. In upside–down descent, the translation of insect COM resembles that of a free drop, in which the vertical component dominants. Major righting rotation occurred 0.25 ± 0.08 seconds after release, with maximum speed 1560 ± 220 deg/s. The completion of righting ($\beta_Z < 10^\circ$) occurred 0.3 ± 0.07 seconds after release and 30.9 ± 6.4 cm below the release point. The major rotations were followed by stabilizing phases, during which the insect underwent angular deceleration. Initiation of negative pitch (nose–down) was typically seen during the late stabilizing phase (Figure 3.2). The insects remained in vertically downward acceleration at the completion of righting. In catapulted ascent, the insects exhibited parabola–alike trajectories with ascending and descending phases. Major righting rotation occurred immediately after launch, with the maximum rotation speed 1760 ± 370 deg/s. The stabilizing phases typically started prior to the parabola apex, and ended in descent (Figure 3.3). Parabola apex was reached at 0.12 ± 0.02 seconds after launch, and was 33.2 ± 7.5 cm above the point of release. The righting rotation under both cases did not follow any single rotation axis of the body–fixed frame but rather in combinations of all three principal rotations. Shift of rotation axis was seen during the stabilizing phases.

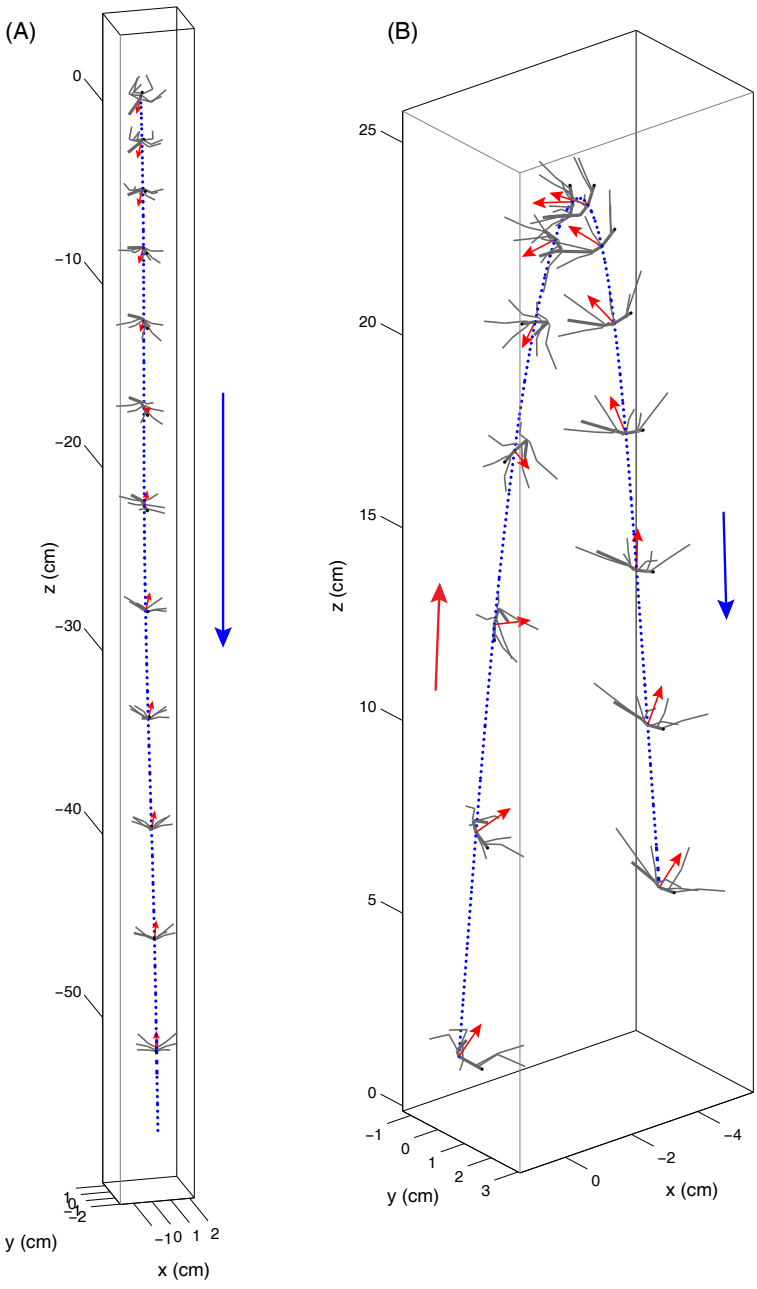

Figure 3.1: Righting trajectories in spatial frame. (A) Righting trajectory from a fixed–position release. (B) Righting trajectory from a catapulted ascent. Red arrows indicate the dorsal direction of body–fixed frame. Dash lines show trajectory of COM.

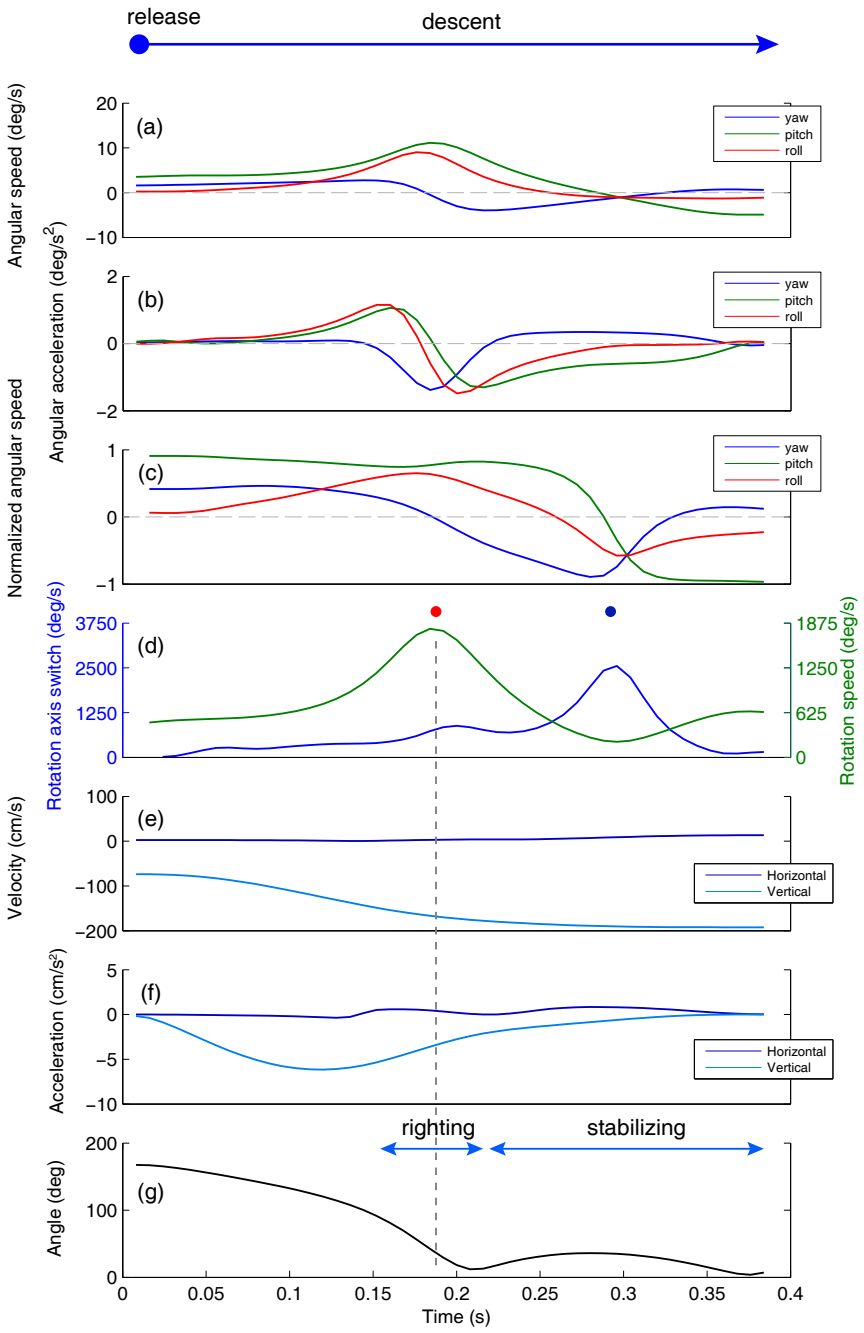
release
descent
Angular speed (deg/s)
(a)
yaw
pitch
roll
Angular acceleration (deg/s^2)
(b)
Normalized angular speed
(c)
Rotation axis switch (deg/s)
(d)
Rotation speed (deg/s)
Velocity (cm/s)
(e)
Horizontal
Vertical
Acceleration (cm/s^2)
(f)
righting
stabilizing
Angle (deg)
(g)
Time (s)

Figure 3.2 ***(preceding page)*****:** Whole–insect dynamics in righting initiated with upside–down fall. (a) Principal rotations of body–fixed frame. (b) Angular acceleration of principal rotations. (c) Normalized principal rotations. (d) Dynamics of rotation axis shift and rotation speed. Red and blue dots indicate a major rotation and an active shift of rotational axis, respectively. (e) Translational velocity of whole–insect COM. (f) Translational acceleration of whole–insect COM. (g) Body orientation angle with respect to gravity, β_Z.

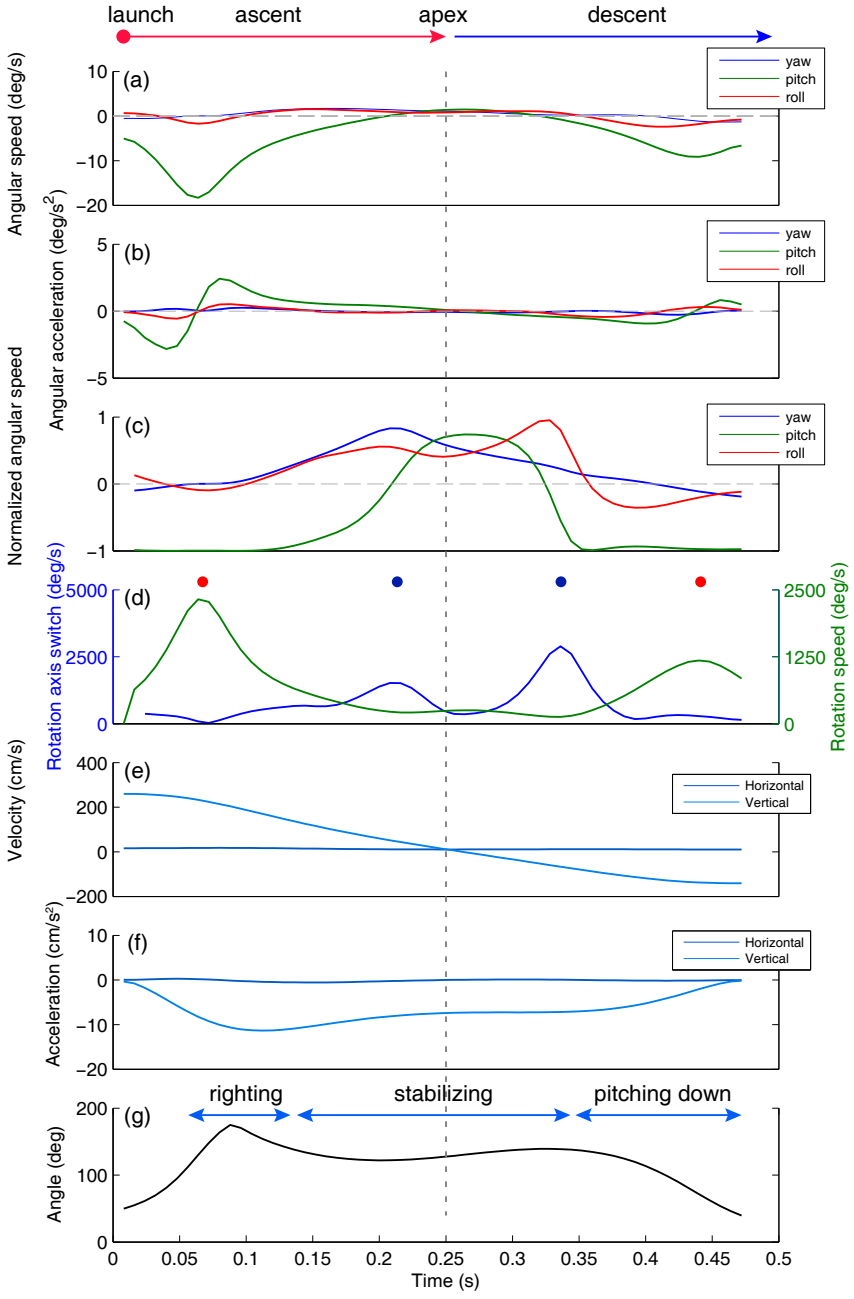
launch
ascent
apex
descent
(a)
yaw
pitch
roll
Angular speed (deg/s)
(b)
Angular acceleration (deg/s^2)
(c)
Normalized angular speed
(d)
Rotation axis switch (deg/s)
Rotation speed (deg/s)
(e)
Horizontal
Vertical
Velocity (cm/s)
(f)
Acceleration (cm/s^2)
righting
stabilizing
pitching down
(g)
Angle (deg)
Time (s)

Figure 3.3 ***(preceding page)*:** Whole–insect dynamics in righting initiated with catapulted ascent. (a) Principal rotations of body–fixed frame. (b) Angular acceleration of principal rotations. (c) Normalized principal rotations. (d) Dynamics of rotation axis shift and rotation speed. Red and blue dots indicate a major rotation and an active shift of rotational axis, respectively. (e) Translational velocity of whole–insect COM. (f) Translational acceleration of whole–insect COM. (g) Body orientation angle with respect to gravity, β_Z.

3.3.2 General postural control

In both upside–down descent and catapulted ascent, the major righting rotations were initiated with a rapid dorsiflexion of all legs. The dorsiflexion phase was completed rapidly (angular speed: fore–legs, 365–875 deg/s; mid–legs, 402–780 deg/s; hind–legs, 313–1110 deg/s). It took 0.12±0.03 seconds for all leg pairs to reach the extreme posture after the loss of contact. This stereotypic posture makes a shuttlecock–like body shape (Table 3.2). Afterwards, legs recover from the extreme posture through plantarflexion at a slower speed (angular speed: fore–legs, 151–353 deg/s; mid–legs, 304–380 deg/s; hind–legs, 118–168 deg/s). Compared with the recovered posture, the stereotypical posture associated with major righting rotation causes about 2 mm dorsalward shift of whole–insect COM (Figure 3.4-B). Also, the extreme posture causes about 20% reduction of MOI in yaw and about 10% increase in pitch (Figure 3.4-C). Despite the changes in average posture from early to late phases of righting, all asymmetry indices change in alternating patterns (Figure 3.6). During righting initiated with upside–down descent, local flow speed increases from 0 m/s to about 2 m/s. Shifting of flow in each principal direction happens during major righting rotation (Figure 3.5). Reynolds number reaches 100 after righting, if based on width of section 1, and reaches 50, if based on width of section 2.

	"P"		"R"	
	ϕ	ψ	ϕ	ψ
F	9.8 ± 6.5	0.08 ± 8.5	21.7 ± 1.3	34.4 ± 1.7
M	-6.4 ± 4.1	0.61 ± 5.0	8.4 ± 1.3	25.9 ± 1.0
H	-22.8 ± 9.3	25.8 ± 10.1	10.1 ± 1.5	65.4 ± 2.1

Table 3.2: Sterotypical leg postures associated with righting rotation ("R") and post–righting stabilization ("P"). Values are mean ± s.d. N = 10.

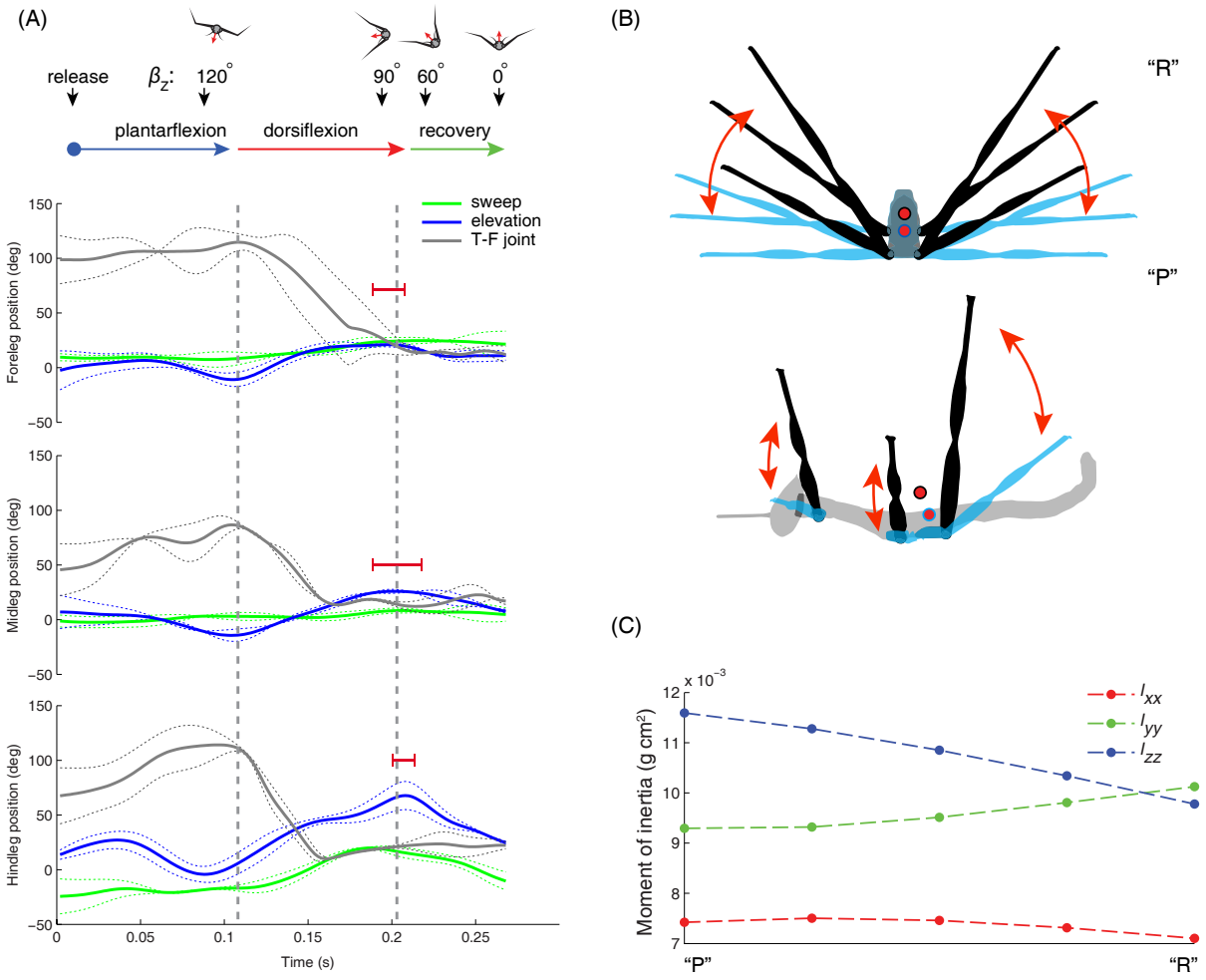

Figure 3.4: General postural control for major righting rotation. (A) Temporal dynamics of postural control in one trial. Red bars indicate extreme dorsiflexion posture within 10% range. (B) Contrasting extreme dorsiflexion (black) and average recovered posture (blue), in both axial and lateral views. Red dots indicate estimated location of COM of each posture. (C) The relationship between MOI of three principal rotations and two postures in (B).

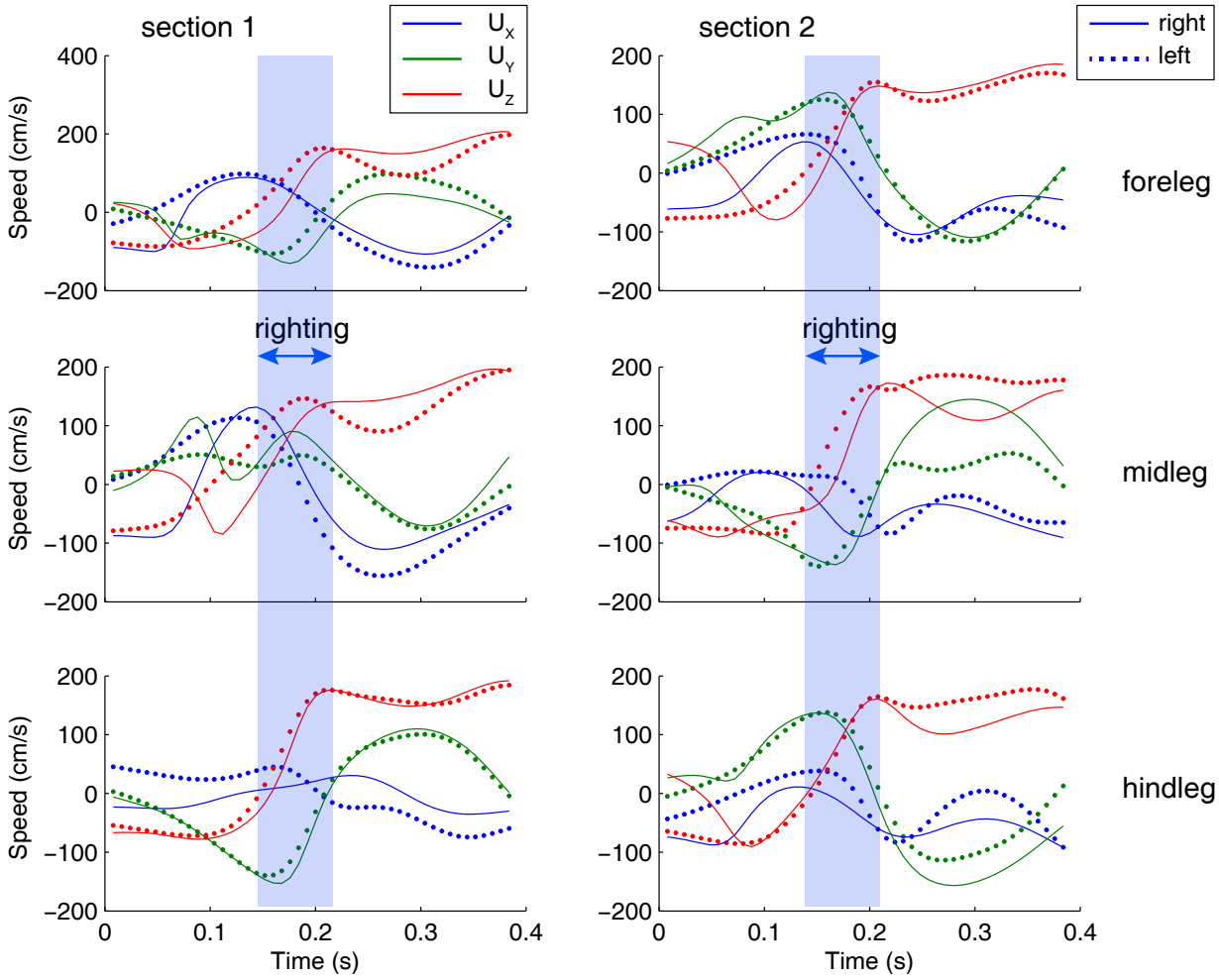

Figure 3.5: Rapid changes of flow speed local to each leg section during righting, based on the same trial in Figure 3.2. U_x, U_y and U_z correspond to flow components parallel to x, y, and z axes of local coordinates fixed to each leg section (Figure 3.2)

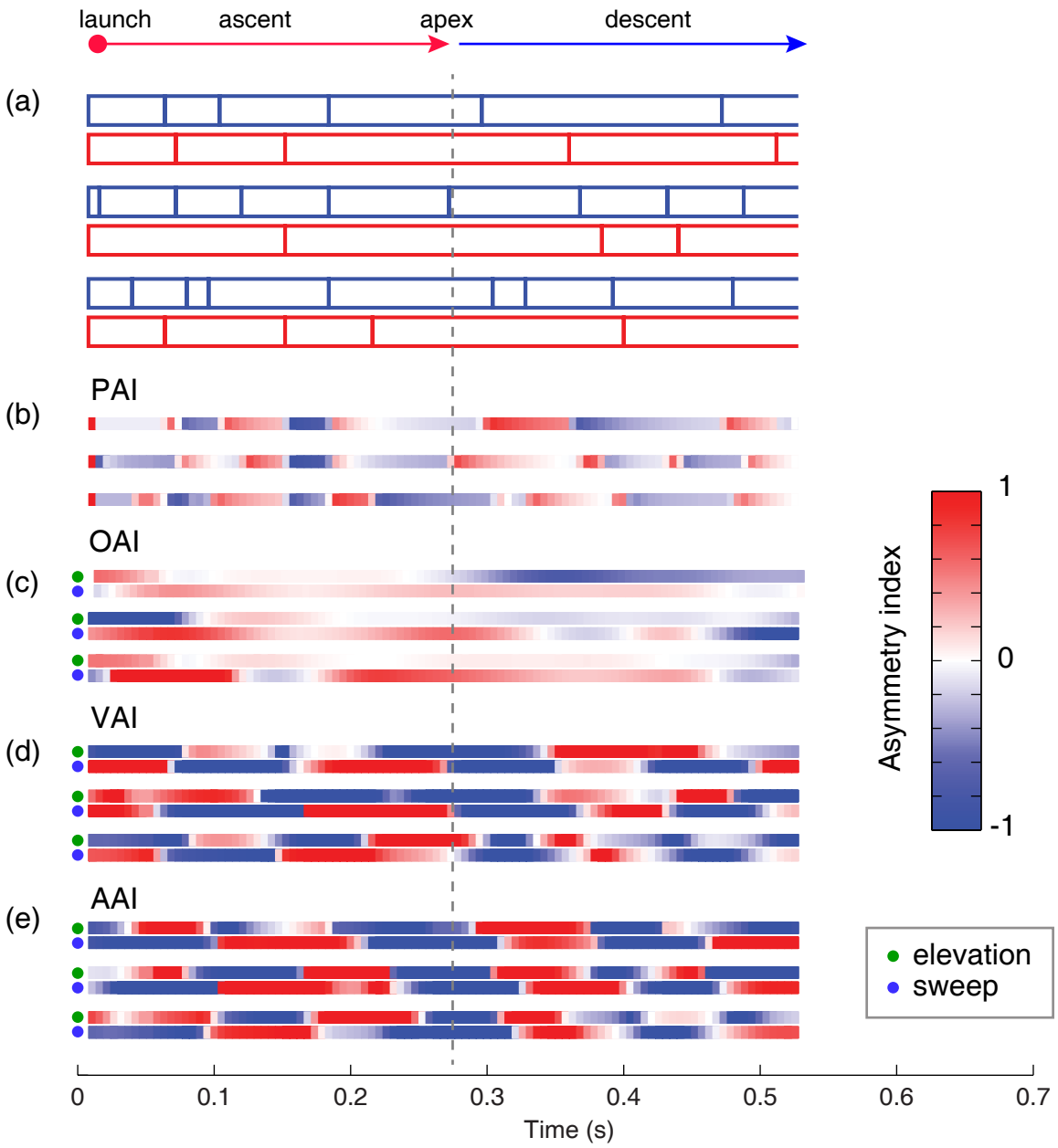

Figure 3.6: Temporal dynamics of asymmetric leg movement in a catapulted ascent, demonstrated using one trial. Top to bottom in each subplot are each pair of fore-, mid- and hind-legs. (a)Stroke period of each leg. (b)Phase asymmetry index. (c)Angular position asymmetry index. (d)Angular velocity asymmetry index. (e)Angular acceleration asymmetry index.

3.3.3 Basic stroke kinematics

Here we particularly analyzed strokes in the stabilizing phase. First, stroke period is in similar ranges among all three leg pairs. Hind legs have larger maximum of stroke amplitude (Figure 3.9). Stroke period is positively correlated with amplitude in all leg pairs, and the average stroke velocity of hind–legs is significantly larger than that of fore– and mid–legs (Fore–leg, 76±6.0 deg/s; mid–leg, 77±7.8 deg/s; hind–leg, 137±11 deg/s; Figure 3.9). Also, all legs were capable of moving in different directions. (Figure 3.10).

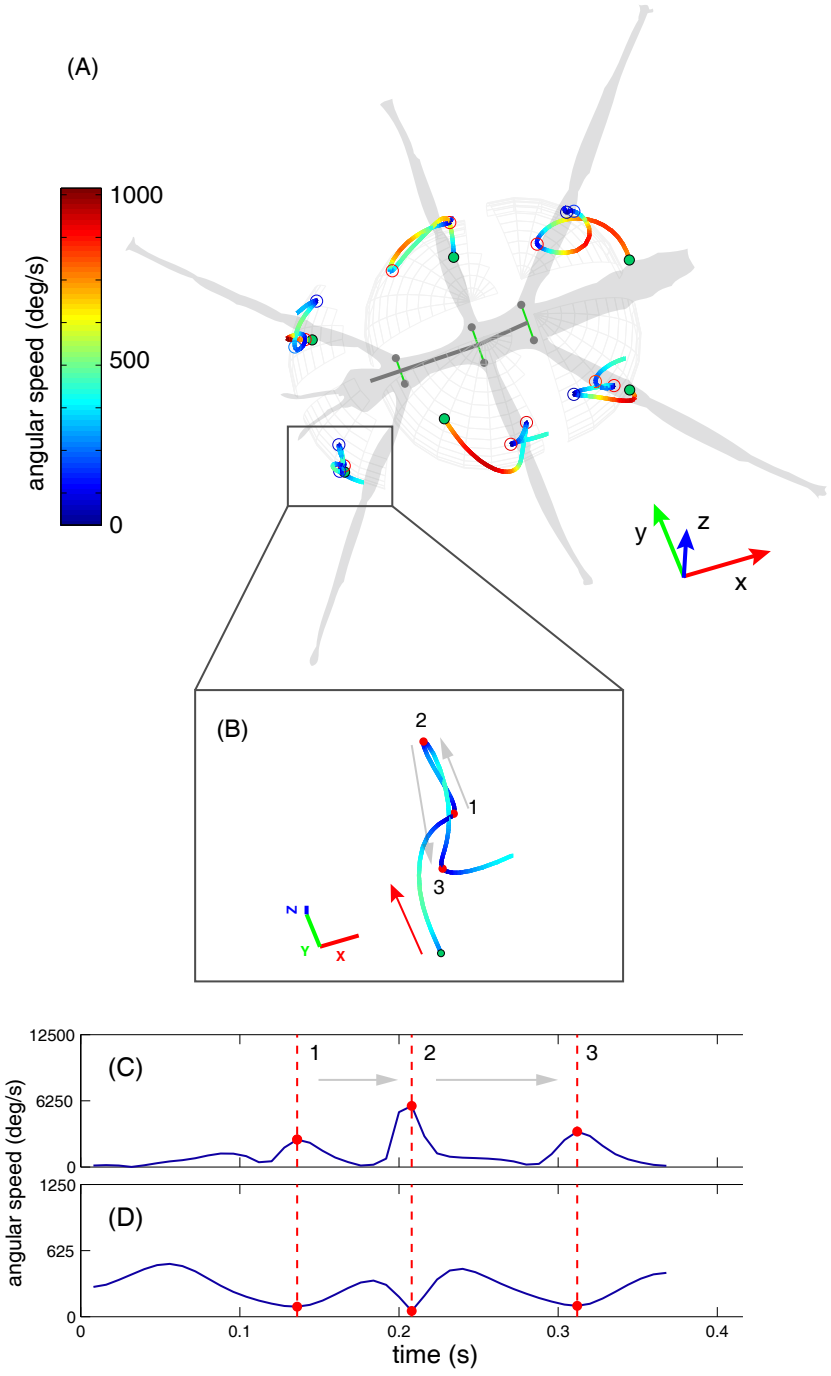
(A)
angular speed (deg/s)
1000
500
0
y
z
x
(B)
1
2
3
N
Y
X
12500
6250
0
(C)
1
2
3
1250
625
0
(D)
angular speed (deg/s)
0
0.1
0.2
0.3
0.4
time (s)

Figure 3.7 ***(preceding page)*****:** Stroke identification based on temporal shifts of rotation axis, demonstrated using one trial. (A) Here shows the path of rotation of left fore–leg from one trial. (B) Details of left fore–leg trajectory. Red dots indicate sharp turnings. (C) Peaks of rotation axis change $d\hat{e}/dt$ indicate sharp turnings, highlighted by red dots. (D) Leg rotation. Numbers correspond to sharp turnings in (B).

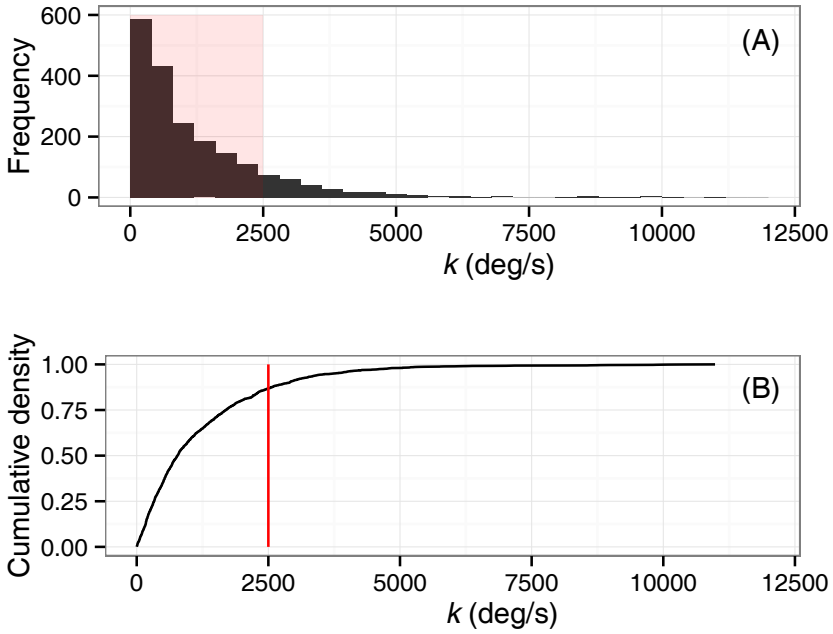

Figure 3.8: Distribution of leg rotation axis shift rate (k). (A) Distribution of k, 85% of the total intervals highlighted in red shade. (B) Cumulative density of k.

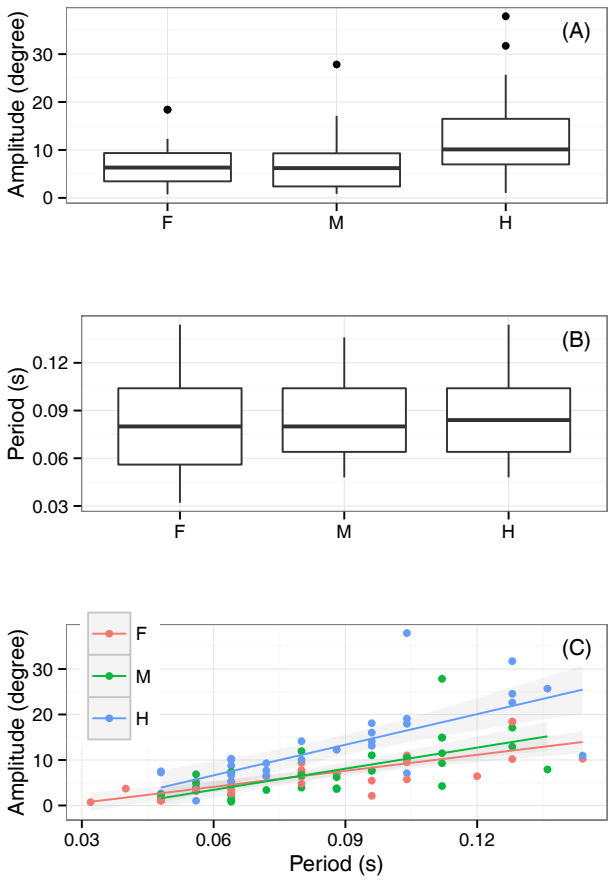

Figure 3.9: (A) Variation of stroke amplitude of each leg pair. (B) Variation of stroke period of each leg pair. (C) The relationship between stroke amplitude and stroke period, with linear regression lines shaded by 95% C.I. P<0.0001 for all leg pairs. N = 40 trials.

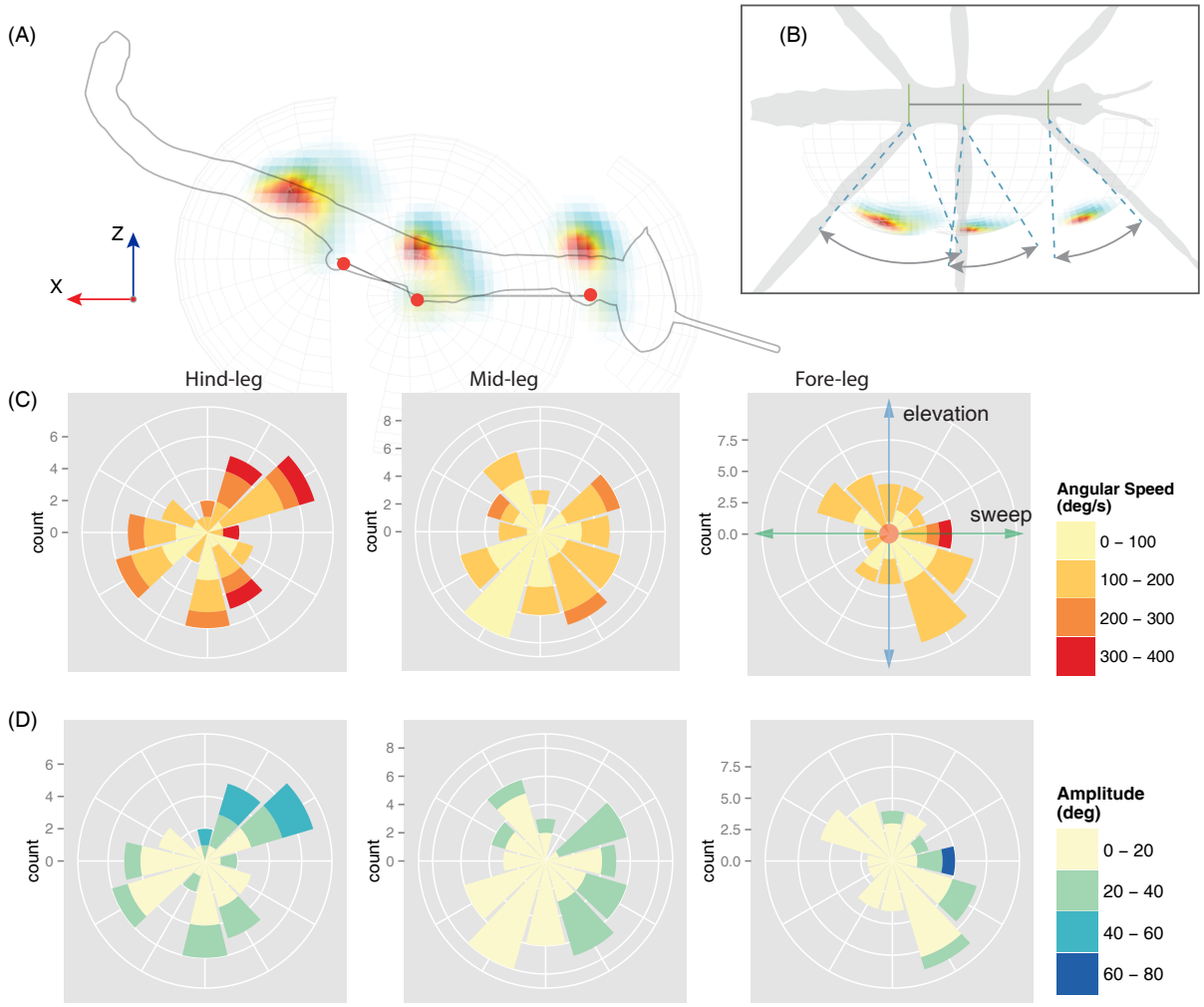

Figure 3.10: Directionality of strokes, based on 6 trials from 3 individuals. (A) Probability density mapping of leg position during stabilizing phase in lateral view. (B) Probability density mapping in top view. Coordinate axes are parallel to those of body–fixed frame. (C) Frequency distribution of stroke speed. (D) Frequency distribution of stroke amplitude.

3.3.4 Stroke and whole–insect dynamics

First, stroke kinematics is highly correlated with certain components of whole–insect dynamics. The distributions of stroke plane angles with respect to whole–insect rotation, translation and resultant velocity did not support complete compliance ($11^\circ < \theta_{SR} < 128^\circ; 13^\circ < \theta_{SR} < 141^\circ; 8^\circ < \theta_{SR} < 143^\circ$). Generally, strokes with greater amplitude and speed are more codirectional with body–frame rotation, and strokes with smaller amplitude tend to move in the opposite direction of body-frame rotation (Figure 3.11). It was also found that stoke activities are correlated with body orientation. Stroke amplitude is positively correlated with the time derivative of body orientation with respect to horizon ($d\beta_{XY}/dt; P < 0.05$).

Second, stroke activities is correlated with the leg's position in yaw and roll. Stroke amplitude and stroke plane angle θ_{SR} differ with respect to the leg's position in yaw (θ_{SR} to position in yaw, P<0.001, ANOVA; Θ to position in yaw, P<0.05, ANOVA). Also, both stroke period and stoke amplitude were found to be positively correlated with yaw speed if the leg is at 'backward' side during yaw (Figure 3.12). The leg's position in combined rotation of yaw and roll also influences stroke kinematics. The largest amplitude and strongest coordination among leg pairs were seen in legs of both 'foreward' and 'downward' sides (Figure 3.13). Also, the variance of stroke plane angle θ_{SR} is significantly associated with the interaction of leg's positions in roll and yaw (P<0.05, MANOVA).

	Stroke			Whole–insect			
	T	Θ	θ	rotation	normalized rotation	translation	orientation
T		+	+ θ_{SR}	ns	+ ω_Z ;	+ dU_{Bx}/dt	ns
Θ	+		$-\theta_{SR}$	+ ω_Y;	+ ω_Y; - ω_Z	ns	+ $d\beta_{XY}/dt$
θ_S	ns	ns		ns	ns	ns	ns
θ_{ST}	ns	ns		ns	ns	- U_{Bz}	ns
θ_{SR}	+	-		ns	ns	ns	ns

Table 3.3: Correlational relationship between stroke kinematics and whole–insect dynamics variables. "+" and "-" denote significant positive and negative correlations, respectively (P<0.05); "ns" denotes non–significant correlation.

(A)

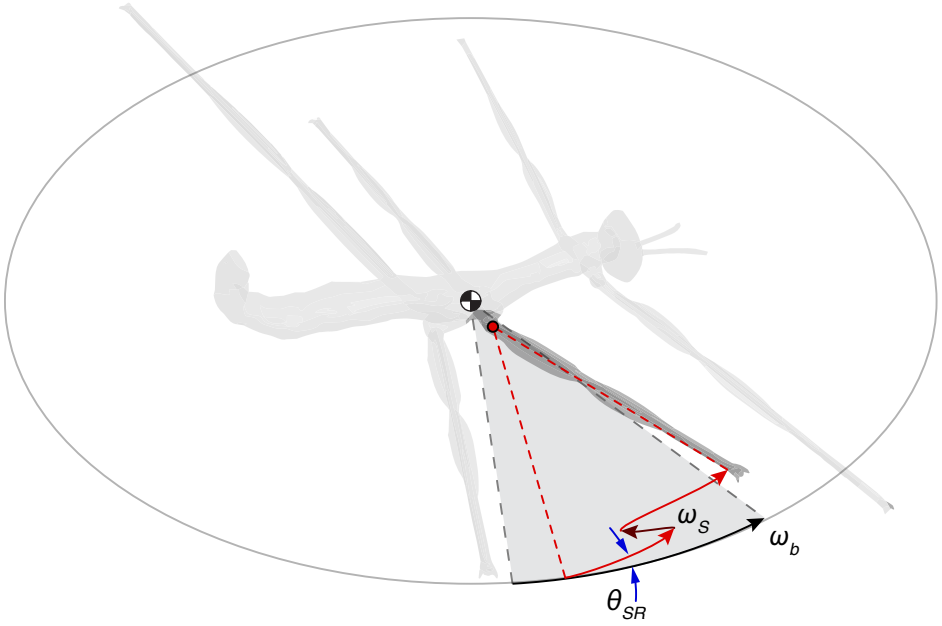
ω_s
ω_b
θ_{SR}

(B)

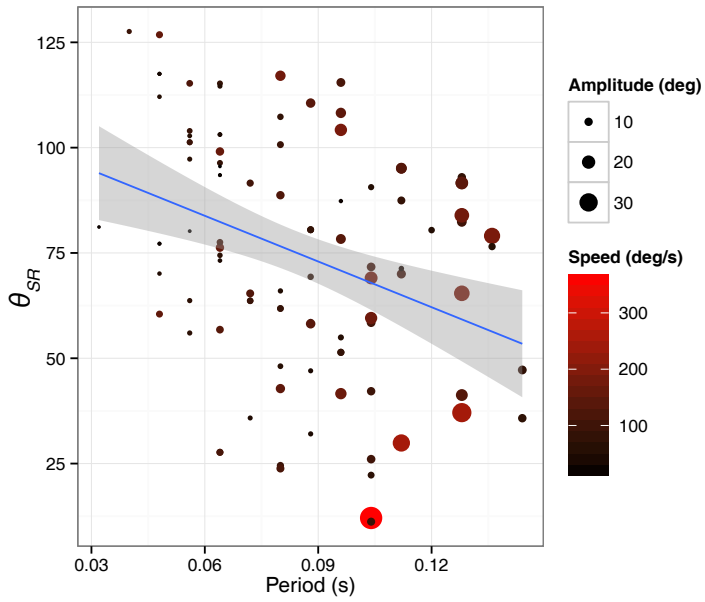
125
100
75
50
25
θ_{SR}
0.03
0.06
0.09
0.12
Period (s)
Amplitude (deg)
10
20
30
Speed (deg/s)
300
200
100

Figure 3.11 ***(preceding page)*****:** General pattern of stroke direction control. (A) Stroke plane angle with respect to whole–insect rotation. Schematic stroke path demonstrates strokes with larger amplitude codirectional to whole–insect rotation, and reversed strokes with smaller amplitude. (B) The relationship between stroke plane angle with respect to whole–insect rotation θ_{SR} and stroke kinematics. Points are average values of each parameter during the period of a single stroke. Slope line based on generalized linear regression model, R=0.12, P<0.00001. N = 40 trials.

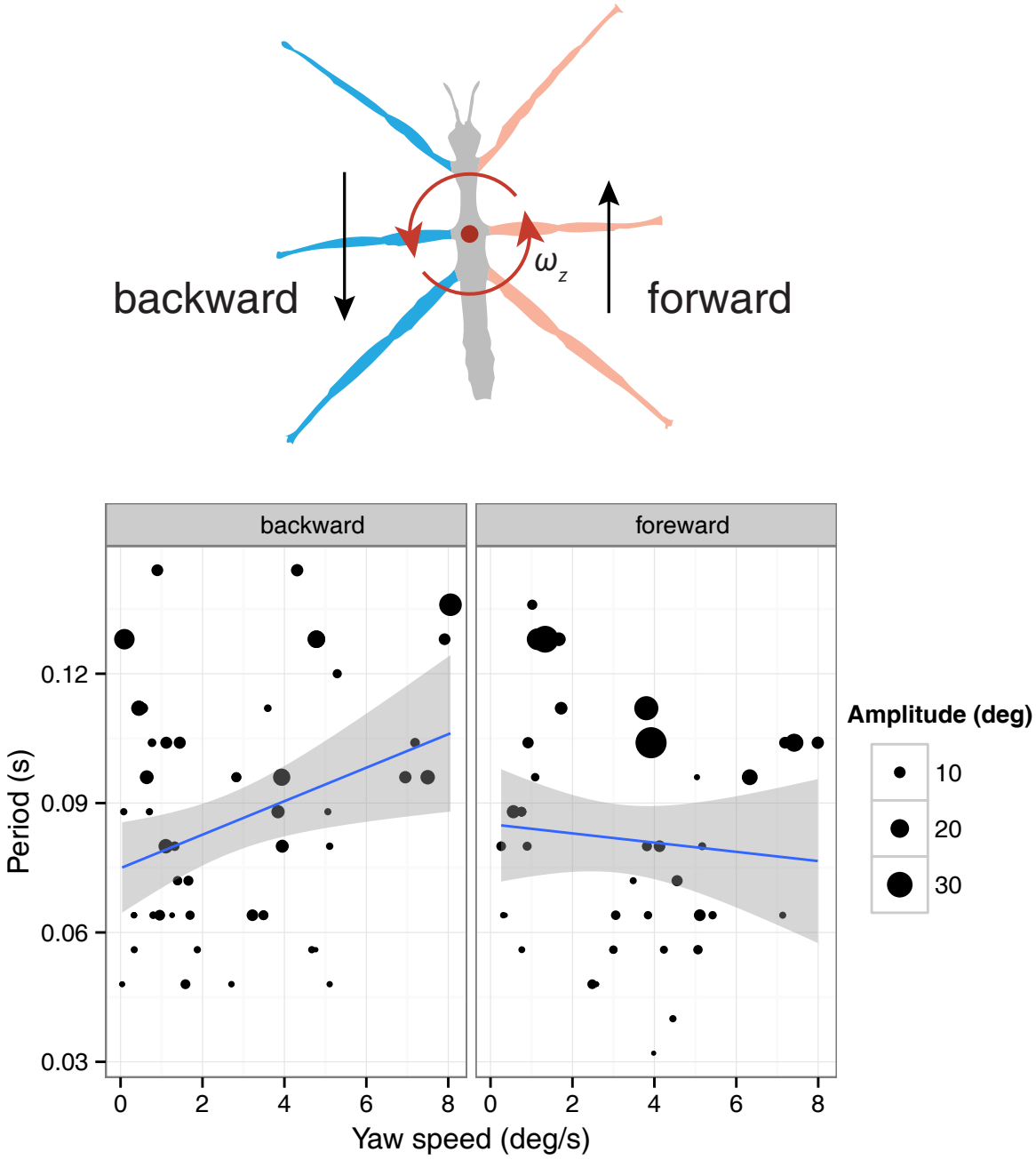

Figure 3.12: Bilaterally asymmetric stroke kinematics associated with legs' position in yaw. Stroke period and amplitude are positively correlated with yaw speed at the 'backward' side based on a linear regression model, $P<0.05$, but are not correlated at the 'forward' side. $N = 40$ trials.

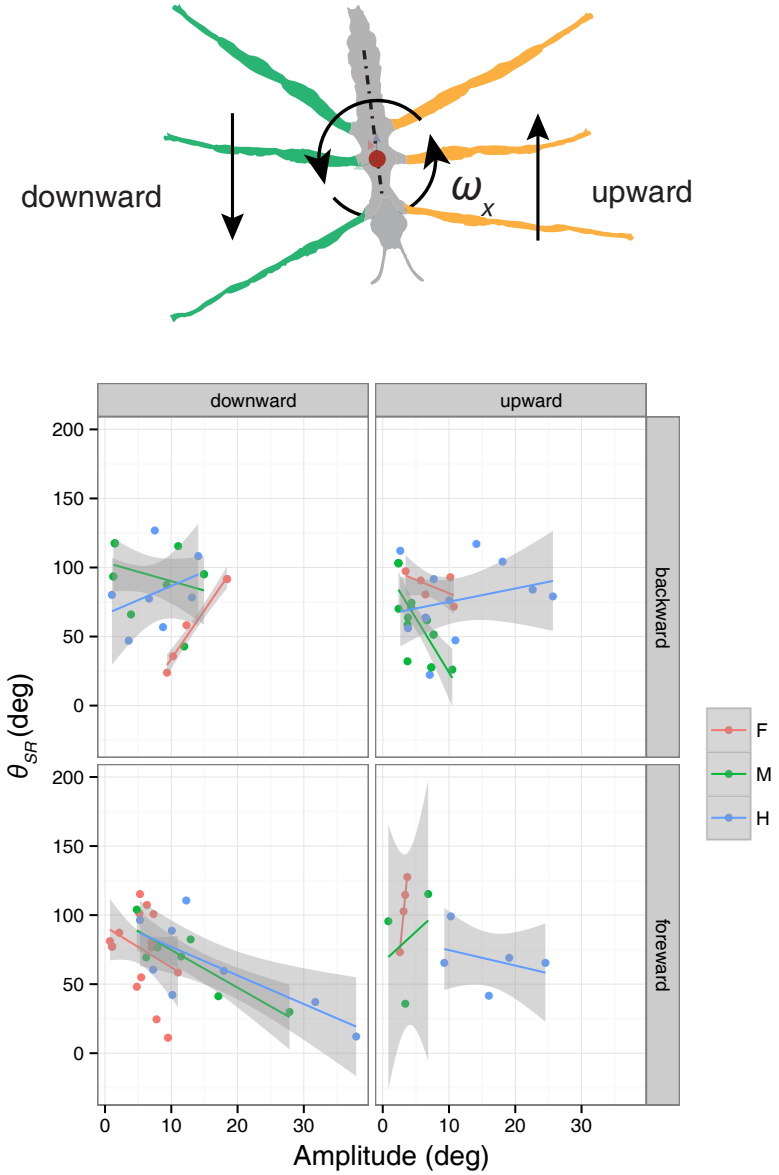

Figure 3.13: Variation of stroke kinematics due to legs' position in both roll and yaw. Trendlines are based on linear regression models. Shaded areas represent 95% CI.

3.3.5 Aerodynamic and inertial effects

The estimated aerodynamic torques peak during the major righting rotation. Inertial torques estimated based on leg movements is proportional to the angular acceleration terms. Average inertial power is positively correlated with the speed of principal rotations, and there is no correlation between average aerodynamic power and the speed of principal rotations (Figure 3.14-A). Also, each leg pair contributes to total inertial power differently (Figure 3.14-B).

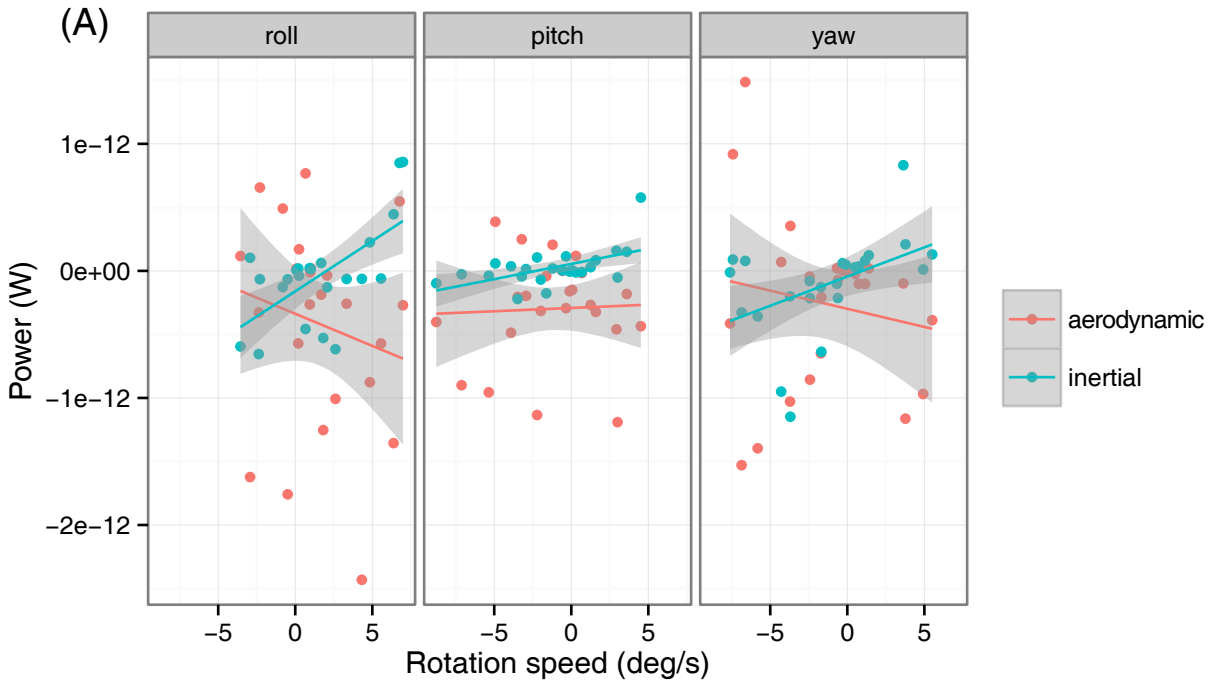
(A)
roll
pitch
yaw
1e−12
0e+00
−1e−12
−2e−12
Power (W)
−5
0
5
Rotation speed (deg/s)
aerodynamic
inertial

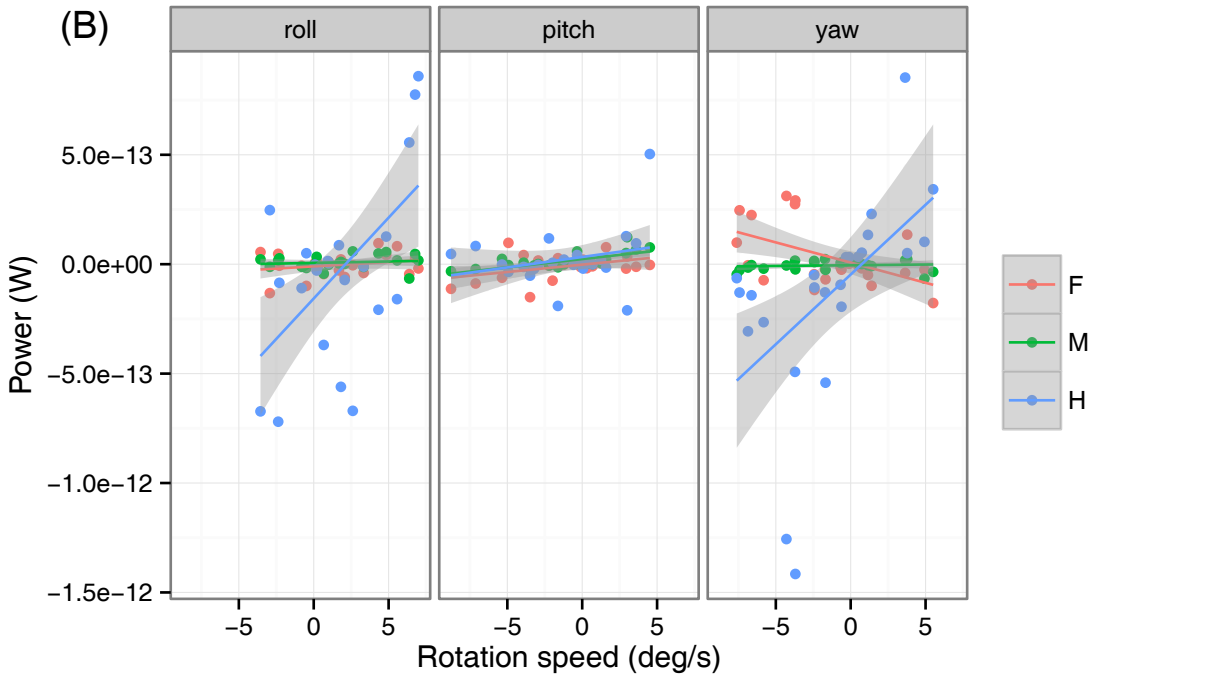
(B)
roll
pitch
yaw
5.0e−13
0.0e+00
−5.0e−13
−1.0e−12
−1.5e−12
Power (W)
−5
0
5
Rotation speed (deg/s)
F
M
H

Figure 3.14 ***(preceding page)*:** (A)The relationship between aerodynamic power, inertia power and principal rotations. No significant correlation between aerodynamic power and rotation speeds. Inertial power is significantly correlated with the speed of each principal rotation ($P<0.05$ for yaw; $P<0.001$ for pitch and roll). (B)Contribution of inertia power by leg pairs. The correlation between inertial power and rotation speed is significant for: hind–legs in roll, $P<0.01$; fore–legs ($P<0.05$) and mid–legs ($P<0.01$)in pitch; fore–legs ($P<0.05$) and hind–legs ($P<0.01$) in yaw. Each point represent mean values sampled from a 0.16 second snippet during stabilizing phase after major righting rotation.

3.4 Discussion

In this work we described details of whole–insect dynamics and controlled leg movements during aerial righting maneuvers in the first instar larval *E. tiaratum*. Particularly, we decomposed complex leg movements into strokes and analyzed the correlation between strokes and whole–insect dynamics. The aerodynamic and inertial effects associated with leg movements were also assessed.

3.4.1 Body orientation control

Under controlled lab conditions, experimental insects exhibited robust capability for rapid reorientation after release or launch. All righting processes were initiated with an angular acceleration phase in which the insects underwent rotations of large amplitude. The major rotations were followed by stabilizing phases in which the insects underwent angular deceleration and eventually began maneuvers for controlled descent. Notably, insects did not follow any single rotation axis but rather a variety of combinations, which may be due to relatively small anterior–posterior asymmetries of aerodynamic surfaces, and the fact that MOI about roll and pitch axes are in the same order of magnitude. For these reasons, the direction of major rotations may involve unpredictability, causing combinations of roll, yaw and pitch. In all cases, insects controlled the transition from major righting rotation to subsequent phases, e.g., negative pitch (nose–down) in descent. The strong desire for returning to a prone posture is an important behavioral trait for midair performances, as seen in many other taxa [64]. As discussed in the introduction, intentional control of body shape is an essential component of righting performance, and variations in behavior may result in different performances even with similar morphologies. As active aerial travel may be involved in the dispersal stage of newly hatched larval *E. tiaratum*, their righting may be under substantial selective pressure for efficiency, e.g. minimizing time cost and height loss, in contrast to voluntary dropping behaviors found in later developmental stages or in other species (unpublished data).

3.4.2 Pattern and functionality of controlled leg movements

First, our results indicate active control of leg posture and movements throughout all phases of righting. The general postural control suggests the utilization of aerodynamic torque for major righting rotation. We observed both reflexes of plantarflexion immediately after contact loss, and subsequent dorsiflexion through which larval *E. tiaratum* achieve a shuttlecock–like body shape. This stereotypic posture is characterized by the asymmetry of surface area about rotation axes through COM, and can create torque for both roll and pitch when flow intersects the insects from a dorsal direction, e.g., in either upside–down descent or right–side–up ascent. Although aerial righting is largely unexplored in arthro-

pods, engaging such a posture through reflexes may be common in other taxa [99, 32, 105]. Furthermore, the recovery from stereotypic posture with plantarflexion happened in stabilizing phases of righting, during which the insects used vertically upcoming flow to decelerate body rotation. The engagement of different postures at different phases of righting implies strategies for stability control with respect ambient flow. Given the insect body is also in descent, the righting performance, e.g., height loss by righting completion, can be sensitive to subtle differences in postural control (unpublished data). Investigating the role of sensory inputs in future studies may also help understanding the control strategies and robustness of the performance.

Secondly, despite the general postural control sampled by averaging from left and right legs, our results revealed asymmetric movements of legs during righting. Based on leg behaviors during stabilizing phases, unbroken swing movements were rapid, with periodical changes in direction and speed, best decomposed as strokes. The differences in stroke amplitude between hind–legs and other pairs are potentially due to differences in coxa–trochanter joint design. Strokes were found to be highly correlated with the instantaneous rotation of whole–insect: faster strokes with larger amplitude are more codirectional with whole–insect rotation, and smaller strokes moving in reverse directions. Although detailed aerodynamics local to each leg awaits further description and analyses, this correlation pattern primarily suggests the utilities of drag for angular deceleration. The instantaneous and coordinated control of stroke movements suggests rich sensory inputs are potentially involved, e.g., musculature stress sensor for aerodynamic pressure local to each leg, gyroscopic and gravisensor for detecting the rotation of whole–insect. Besides the general pattern of counter–torque generation, we found asymmetric control of strokes are specifically correlated with the legs' position in both roll and yaw, the dynamics of which determines flow asymmetry experienced by left and right legs. It is known that arthropods use asymmetric leg movements for many activities, e.g., terrestrial transport and predation [70]. Our results suggested a new type of behavior that involves instantaneous interaction with flow. Stereotypic posture control and small–scale strokes may reflect hierarchical control underlying the performance.

Thirdly, our assessment on aerodynamic and inertial effects of leg strokes provided a first step towards understanding its functional significance. Estimated inertial power is positively correlated with the speed of all principal rotations, which is in accord with the directionality of strokes. Since faster strokes are more codirectional with the whole–insect rotation, the subsequent turning points involve sharp changes in direction and thus induce inertial counter–torques at the coxa joint. Even though the estimation of total inertial torque was at the same order or magnitude as aerodynamic torque experienced by the whole–insect, it was unlikely to observe obvious effect to whole–insect orientation due to structural and aerodynamic damping. We also observed different contribution of inertial power between leg pairs, which is caused by the relative position and movement pattern.

Future investigation may specifically address the aerodynamic interactions between stroke movements and local flow. Also, recording the muscle activities and joint stiffness can provide

more accurate estimate of inertial effects as well as damping effects associated with both types of counter–torques [56]. An improved mechanical model may evaluate the cyclicity of strokes with respect to whole–insect movements for a more generalized understanding of the underlying control strategies.

3.4.3 Ecological and evolutionary implications

Our results suggest highly coordinated asymmetric leg movements are involved in aerial righting maneuvers. Future sampling in other taxa of different morphologies and sizes may help addressing the generality of such behaviors, as well as the coupling between morphology, e.g., appendicular and body design, and kinematics in righting maneuvers. Also, characterizing the ontogenetic variation of both righting performance and leg kinematics can help understanding how morphology, kinematics and performance scale with body size. As similar small–scale leg movements have been observed in directed aerial descent (unpublished data), studying its function at different stages of aerial descent helps to understand its underpinning within a ecogical context.

Furthermore, our results imply the importance of the coupling between morphology and kinematics in studies of aerial maneuverability in arthropods. Although the mechanical feasibility of small–scale asymmetric leg movements was demonstrated using an specific example, it suggests selection for kinematics exists in such a fundamental scenario was a necessary stage in flight evolution [37]. Besides aforementioned sampling from a wide variety of leg morphologies, it is also informative to apply this to other appendages and functional analogous in aerial movements, e.g., proto–wings. It is important for future studies to incorporate small–scale kinematics in addressing stability and maneuverability of particular body shape or posture configuration in aerial locomotion in basic and non–equilibrium performances such as aerial righting. Combining empirical data, e.g., scaling of kinematic parameters, and measurements from physical or theoretical models may help testing hypotheses regarding the selection for morphology and kinematics of proto–wings at the early stages of flight evolution [36].

Chapter 4

Biomechanics of flight reduction along ecological gradients in a stick insect (*Asceles tanarata*)

The evolutionary transition between winged and wingless morphologies in insects is not well studied. Such a transition is associated with gradients of ecological factors in nature. Progressive wing size reduction along an altitudinal gradient is found in three populations of a stick insect (*Asceles tanarata*) native to Malay Peninsula. We investigated how wing and body morphology change along the altitudinal gradient, and further studied the biomechanics of flight associated with each morphology. Our results indicate the reduction of flight apparatus leads to changes in wing design and wing kinematics. Reduced flapping flight performances resemble parachuting and gliding. Due to both altered kinematics and flight trajectories different from conventionally recognized flapping flight, the aerodynamics of wing flapping is characterized by large advance ratio and reduced half–stroke asymmetries. Although the reduction in flight performance is closely correlated with the reduction of wing size, wing aerodynamics shows more complex pattern along the performance gradient. Furthermore, both body and leg kinematics exhibit re–organization in flight performance of size–reduced wings. This study demonstrated details of the evolution of flight reduction, from flapping flight to parachuting, in one lineage, and the results suggest the selection gradient for flight performance, including various degrees of controlled descent, is associated with the ecological gradients in this case.

4.1 Introduction

Insect flight evolved from a single common ancestor, and has since undergone repeated losses [35, 109]. The evolutionary transition between wingless and winged morphologies is presumably mediated by ones of intermediate sizes. To understand the process of such transition, it is possible to integrate ecology, performance capacity and functional morphology to interpret the ecological role and evolution of the designs [127].

First, during evolutionary transition of relative wing size, the relationship between wing kinematics and relative wing size is unclear. Flight in extant insects are highly derived. Most functional studies to date have only focused on the wing stroke movements of fully developed wings. Previous assessments on the functionality of incipient wing morphology relied mostly on model–based experiments, lacking reference of the scaling relationship between relative wing size and kinematics ([43, 49, 68]). Although kinematics of the historical transitional forms is inaccessible, we may be able to address the coupling between wing stroke kinematics and relative wing size, as well as the aerodynamic consequences, by investigating intermediate forms found in extant lineages. One example is size–reduction of wings associated in specific ecological conditions, e.g. island and montane environments [87, 110].

The process of wing reduction requires accommodation at the whole–organism level. The flight apparatus in insects, primarily comprised of wings, flight–related thoracic structures and flight musculature, is subject to the consequence of energy allocation during development. Differentiation in developmental level among body parts can be influenced by selection and ecological factors. The flight capability, e.g., degree of flight muscle development and fuel storage, can be in trade–off relationship with fitness components, e.g., reproduction [145], typically resulted from ontogenetic regulation of energy allocation, such as in polymorphism related to dispersal and migration [119, 34, 33]. On the other hand, body parts may play important roles at the functional level of wing reduction. In normal flight performance, body (head, thorax and abdomen segments) and legs can contribute with both inertial and aerodynamic forces. For example, abdomen inertia can be used for maneuvering [7, 138, 28], and all extruded body parts can add drag and lift forces to the insect. With the changes in thoracic structure and wing kinematics under disproportionate wing size reduction, the coordination among all body parts during flight is presumably altered.

Furthermore, performance is the mechanistic link between organismal design and the ecological and evolutionary consequences [5, 50]. Animal use flight for various purposes, e.g., locating resources, escaping, and dispersal. On one hand, the design of flight apparatus determines the limits of performance; on the other hand, flight performance in three–dimensional space reflects its utilities at fitness level in specific environment. For these reasons, the diversity of designs and performances have adaptive significance in specific habitats. For example, wing morphology and flight mode are correlated with habitat usage and prey types in bats [92]. Given the lack of empirical studies on the performance gradient associated with wing size reduction, we predict that the lack of wing area and the reduction of wing stroke

movements may together cause insufficient force production for offsetting body weight and for thrust generation. As a result, reduced wings may cause flight trajectories with greater negative incline, such that aerodynamic drag exerted through body and legs can support an additional portion of whole–insect weight. Flight trajectory with negative incline with respect to horizon can possibly be useful in elevated habitats. Recent studies on controlled aerial behaviors in wingless arthropods have suggested the possible ecological niche for insects with reduced wings to perform similarly in arboreal environments [142, 36, 140, 37].

A stick insect, *Asceles tanarata*, native to Malay Peninsula exhibits disproportionate wing size reduction, accompanied with body miniaturization and sexual dimorphism, along the altitudinal gradient. Three populations from three altitude ranges show distinctive differences in relative wing size. Such a scenario may be associated with the environmental factors in the montane environments. Three subspecies have been designated based on similar morphological characteristics, e.g., genitalia design and egg morphology, and differences in body size and relative wing size [113]. With the altitude and sex as two sources of variation, a total of six distinctive flight morphologies are shown within the species group. We use abbreviated codenames to represent each flight morph hereafter (highland population, *A. tanarata tanarata*, AT1; intermediate population *A. tanarata amplior*, AT2; lowland population, *A. tanarata singapura*, AT3; female, F; male, M. E.g., AT1F represents *A. tanarata tanarata* female.).

In order to demonstrate the gradient of morphological variation, we first addressed the intersexual and interpopulational variation in design of flight morphology. The complexity of flight apparatus design was expected to be reduced as a consequence of miniaturization [53]. Furthermore, we used comparative biomechanics to describe wing kinematics, wing–body coordination and flight performance in living specimens of three populations, and used the quantitative results to correlate interpopulational variation in wing design, kinematics and flight capabilities with ecology. Particularly, the scaling relationship between relative wing size and wing kinematics was addressed. Moreover, this case of intraspecific variation in wing size is compared with the spectrum of wing size variation of all stick insects in a phylogenetic context. By integrating evidence from morphological and performance levels, We aim to understand the details of wing reduction process, and the role of fitness gradient in evolutionary transition between flight–capable and flightless morphologies.

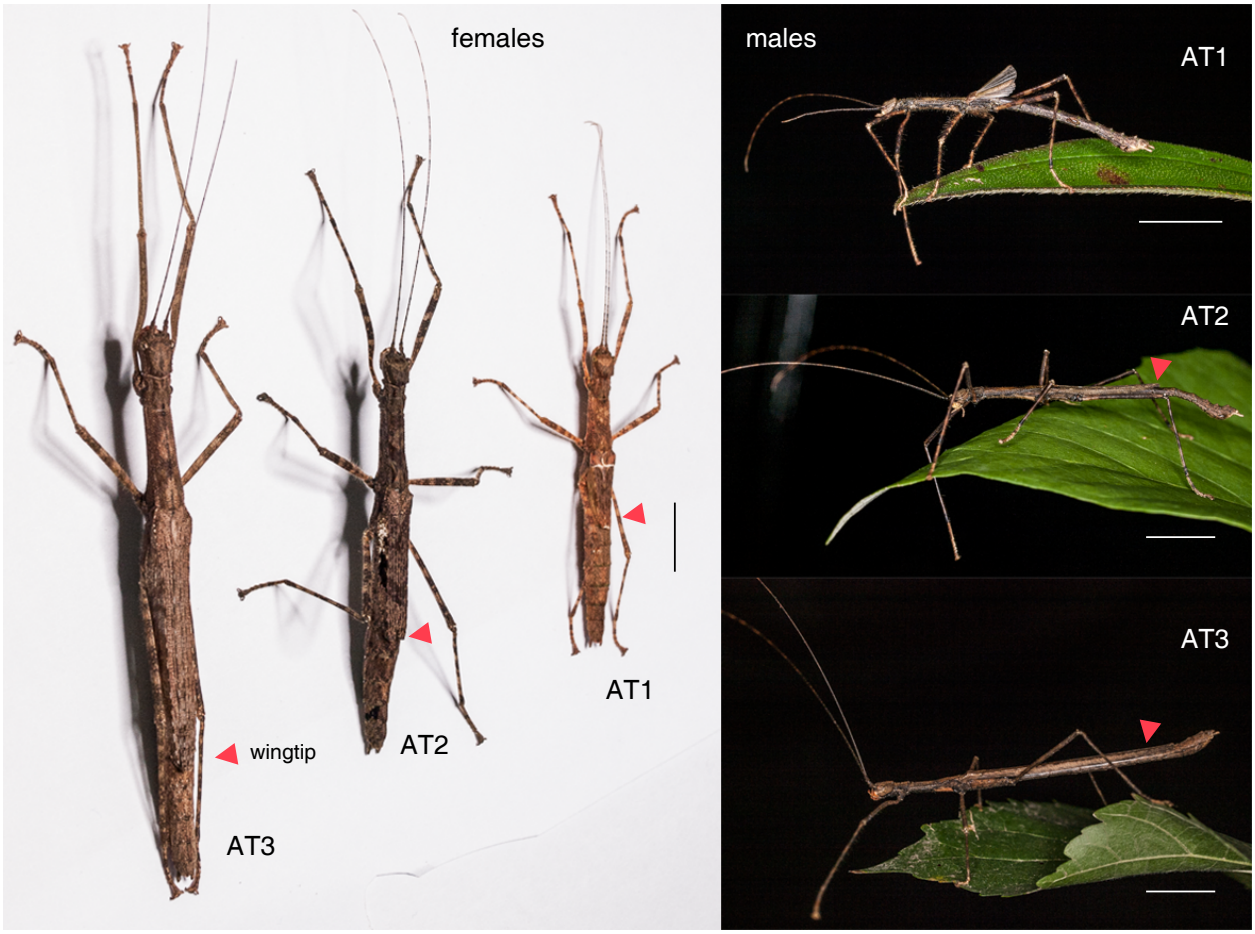

Figure 4.1: Live specimens of each flight morph. All scale bars are 1 cm. The position of wingtips are pointed by red triangles.

4.2 Materials and Methods

Insects were collected in night surveys during August 2008, July 2010 and August 2011 (Figure 4.1). Individuals were housed in individual plastic containers with sufficient space and fresh leaves of food plants (*Macaranga sp.* or *Melastoma sp.*). All housing were kept in an air-conditioned room at 22–26°C prior to filming or experimental treatments. Statistical analyses were conducted using R [101].

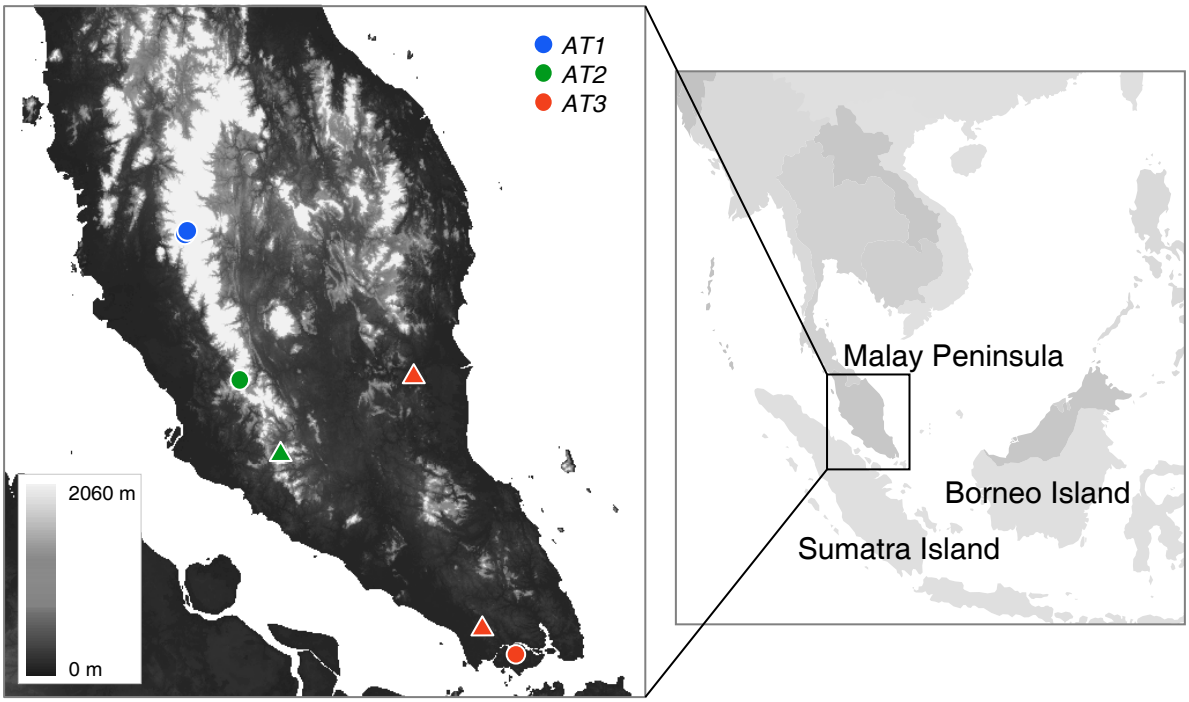

Figure 4.1: Altitudinal distribution of each subspecies. Dots denote sites visited by this study, and triangles denote other reported localities.

4.2.1 Morphometrics

Individual insects were anesthetized with a 2–min low temperature (0–4°C) treatment, and then laid right-side-up on a flat surface with legs fully expanded. High–resolution digital images were taken in dorsal view, and then profiles of different body parts were extracted using PhotoShop (Adobe Inc.). Segment dimensions and projected planform area were measured with ImageJ [2]. Whole–insect mass (m) was measured with an electronic balance (Sartorius R200D). Mass distribution was sampled by dividing the insect body into 8 sections, including 6 legs, an anterior body section (head and all thoracic segments) and a posterior section (abdomen). Two body sections were connected with the 1st abdominal joint (Figure 4.1).

The mass of each body section was measured on deep frozen samples after experiments. The center of mass (COM) of the body section was estimated based on images taken in lateral view of frozen specimens orthogonally balancing on a horizontal razorblade.

The morphology of hindwings (denoted by 'wings' hereafter) was sampled based on images of fully–unfolded specimens. The basic descriptions followed Ellington [41]. To compare relative wing sizes, we used wing size index (WSI) to represent the ratio of wing length to body length. Wing mass was measured on fresh samples from euthanized specimens. The mass of thoracic musculature was measured adopting previously established methods [81], in which the period of NaOH treatment was adjusted according to the size of thoracic chamber in each species (AT3, 12–hr; AT2, 2–hr; AT1, 30–min).

4.2.2 Experimental filming

Filming was conducted indoor in still air under a temperature range of 26–29 $°C$. All insects were exposed to the environmental temperature at least 2 hours prior to filming. All flight performances were recorded with a high-speed camera (1280 × 1024 pixel; HighSpec1, FasTec Imaging). Sufficient lighting was provided to ensure the video quality. We used a free–dropped sphere as the vertical reference in all setups. Five minutes was provided for resting between trials. All flights were initiated by manually dropping the insect into air, with the insect body orthogonal to the camera axis.

Two performance arenas were used for filming according to the space need of flight performances. (1) To film trajectories of parachuting and gliding flight in AT1 and AT2, we constructed a gliding arena, which consists of a columnar space (2.5 m, height; 80 cm, diameter) circled by white cloth with a side opening (80 cm, width; Figure 4.2. We assessed the functionality of wings in AT1 and AT2 by comparing flights with and without free wings. We used narrow stripes of paper tape (0.7 mm, width; Fisher Brand; <1% of body mass), carefully wound at wing base to constrain the wings from opening. Treated insects were then dropped following the same protocols described above, and 3 to 5 trials were filmed for each individual. (2) A flight arena was set as a rectangular space (2.5×2.5×2 m, length×height×depth) with background of white cloth (Figure 4.2. The flight arena was used to film gliding and flight AT3 females were released from 2 m above floor, with the longitudinal body axis parallel with the screen plane. AT3 males were either stimulated to takeoff from a platform or directly released by manually dropping. With both setups, the camera was calibrated to face the screen at a right angle in the horizontal direction. The distance from camera front to the screen was adjusted in each trial depending on the range of movement to be filmed, e.g., the camera was placed closer to the screen for filming detailed wing and leg kinematics. Arena floor was covered with multiple layers of cloth to prevent injuries when landing.

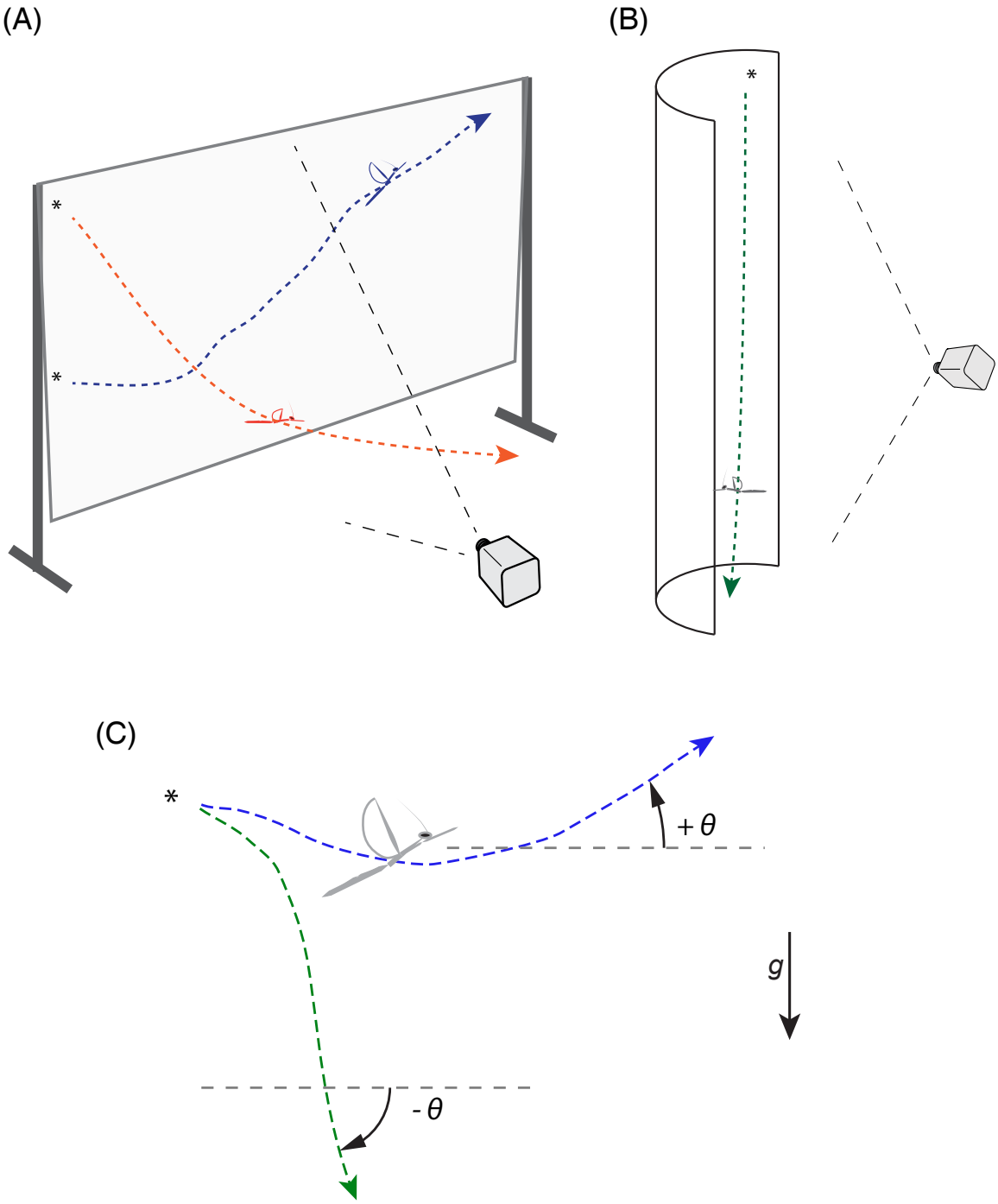

Figure 4.2: (A) Arena for filming gliding and flapping flight trajectories in both sexes of AT3. (B) Arena for filming gliding and parachuting flight in AT1 and AT2. (C) Configuration of trajectory incline angle relative to horizontal.

4.2.3 Kinematics

We used commercial software (ProAnalyst, Xcitex Inc.) to track morphological landmarks for motion reconstruction (Figure 4.3-A). Digitization error was first minimized by using a single person for digitizing and by proof–reading for all frames. To further assess the effect of digitizing error, a single trial was digitized 5 times. The mean of the standard deviation for each data point was $< 0.20\%$. We used a quintic spline to fit each set of positional data, and this method has root mean square (RMS) errors of positional data $< 4.0\%$ in all coordinates [128]. All further analyses were conducted with custom-written scripts in MatLab [82]. Motion reconstruction was conducted based on 90°lateral projections.

A body–fixed frame is centered at the 1st abdominal joint and defined by an x-axis parallel to longitudinal axis of anterior body pointing posteriorly, a dorsally oriented z-axis and an y-axis which is the cross-product of the first two (Figure 4.3). The body–fixed frame was used as a reference to quantify the position of wings, legs and COM.

4.2.3.1 Flight trajectories

Trajectories were described as translation of whole–insect COM (see Section 4.2.3.3) in space. To describe and compare all performances from parachuting to flapping flight on a continuous base, we used trajectory incline angle (θ), which was defined as the angle between body velocity vector and horizontal vector in the heading direction (Figure 4.2-C). For example, all ascending flights have positive trajectory incline angle, and gliding trajectories have negative incline angle, negative of conventionally used glide angle. Our assessment of trajectory dynamics was based on videos taken in lateral view when the insect body perpendicular to the camera axis. Body velocity is defined as a vector with respect to spatial frame, $U_b = \left[U_x, U_y, U_z\right]$.

Equilibrium intervals of trajectories were characterized by low changes of acceleration ($dU/dt < 5\%$ sampled at a minimum of 100 Hz). For equilibrium performance of parachuting flight (both sexes of AT1), the drag coefficients were calculated based on: $mg = 0.5\rho A C_D U_b^2$, where ρ is air density, A is projected planform area in flow direction, and U_b is body velocity. For equilibrium intervals of gliding, lift-to-drag ratio (L/D) was calculated as $tan(\theta)$.

4.2.3.2 Wings

The mobility of wings was first assessed by comparing the variation of wingtip position among flight morphs. Wingtip position was described within a local coordinates originated at the wing base with all axes parallel to those of the body frame (Figure 4.3). Wing position angle (ϕ) and deviation angle (ψ) together describe the angular position of wingtip with respect to the wing base frame. Wingtip position then is $p_W = \left[\psi, \phi, 0\right]$, and angular speed is $\omega_W = \left[\dot{\psi}, \dot{\phi}, 0\right]$.

Wingbeat frequency f was calculated based on periods between endpoints of up– or downstrokes. Wing stroke amplitude Φ was calculated as the angular distance between endpoints of up– and downstrokes. The period of up– and downstrokes (T_{up} and T_{dn}) were used to calculate the mean flapping velocities at wingtip of each half–stroke, e.g., upstroke velocity with respect to wing base:

$$U_{up,wb} = R\omega/T_{up}, \tag{4.1}$$

where R is wing length. Furthermore, a conservative estimate of the wind velocity at wingtips, excluding induced velocity, in flight performance was calculated as the vector sum of flapping velocity and body velocity:

$$U_{up} = U_{up,wb} + U_b. \tag{4.2}$$

As 5 out of 6 flight morphs exhibit advance ratio greater than 1, the we used such conservative estimates for a primary comparison.

For half–strokes, Reynolds number was sampled at wing chord at 70% wing length as:

$$Re = \frac{\rho R \bar{U}_c}{\mu}, \tag{4.3}$$

where μ is air viscosity, and $U_c = \omega 0.7R + U_b$ is the wind speed at 70% wing length.

Advance ratio J was calculated as

$$J = \frac{U_b}{2fR\Phi}, \tag{4.4}$$

based on average body speed, mean frequency and amplitude sampled during equilibrium intervals.

4.2.3.3 Body sections and legs

Based on preliminary observation of aerial behaviors of body and legs, the insect body excluding wings was divided into a combination of two body sections and legs. Anterior body section covers head to metathorax, and the posterior body section cover all abdominal segments posterior of the 1st abdominal joint. Two sections are connected with 1st abdominal joint (Figure 4.1). Rotation and angular velocities of body–fixed frame were calculated with respect to the spatial frame based on the transformation matrix from spatial frame to the body–fixed frame [89]. Also, an abdomen–fixed frame was set with a center at the distal end of abdomen, with x-axis parallel to the longitudinal axis of abdomen, y-axis parallel to that of the body–fixed frame. Both body sections have position angle χ relative to horizontal (Figure 4.3). Abdomen position with respect to anterior body section is also described by

its deviation from the x-axis of body–fixed frame.

The configuration of leg posture is similar to that for the wings. Each leg was treated as one section with 2 degrees of freedom. The positions of each leg was described by the sweep angle ϕ and elevation angles ψ with respect to the x-y plane of a local coxa–fixed frame with all axes parallel to those of the body frame. We calculated the angle of attack of body sections and legs based on average postures during equilibrium performances. The angle of attack α was calculated as the angle between wind velocity and the longitudinal axis of chosen section:

$$\alpha = acos(U_{wind} \cdot \hat{n}/|U_{wind}||\hat{n}|), \tag{4.5}$$

and

$$\hat{n} = R_b R_{b-s} \left[1, 0, 0\right]^T \tag{4.6}$$

is a unit vector parallel to the longitudinal axis of a given section converted into spatial frame, R_{b-s} is the rotation matrix converting body–fixed frame to the section's frame, and $U_{wind} = -U_b$ is wind velocity. Reynolds number was also calculated based on body length and average body width for all flight morphs during equilibrium intervals.

Whole–insect COM with respect to the body–fixed frame during flight is estimated as

$$COM = \sum m_i p_i / m, \tag{4.7}$$

where i denotes each segment, and

$$p_i = R_{b-s} P_{COM}, \tag{4.8}$$

is the position of a section's COM with respect to body frame, and P_{COM} is the longitudinal COM position of each section. Wing mass of all flight morphs are <1% of total body mass and was ignored in this calculation (Table 4.2).

4.3 Results

4.3.1 Morphological correlates of flight reduction

We observed whole–insect miniaturization correlated with increasing altitude, shown as significant reduction in body mass and body length in each sex (Figure 4.2). This variation is also significant if considering the interaction between sex and altitude ($P < 0.01$, $F = 20.64$, ANCOVA). The mass proportions of different body parts follow different allometries against increasing altitude. Thoracic muscle mass and wing mass reduce with increasing altitude. Notably, the mass percent of abdomen increases with altitude in females (Figure 4.2). An overall reduction in sexual differences of these characters is seen along the altitudinal gradient.

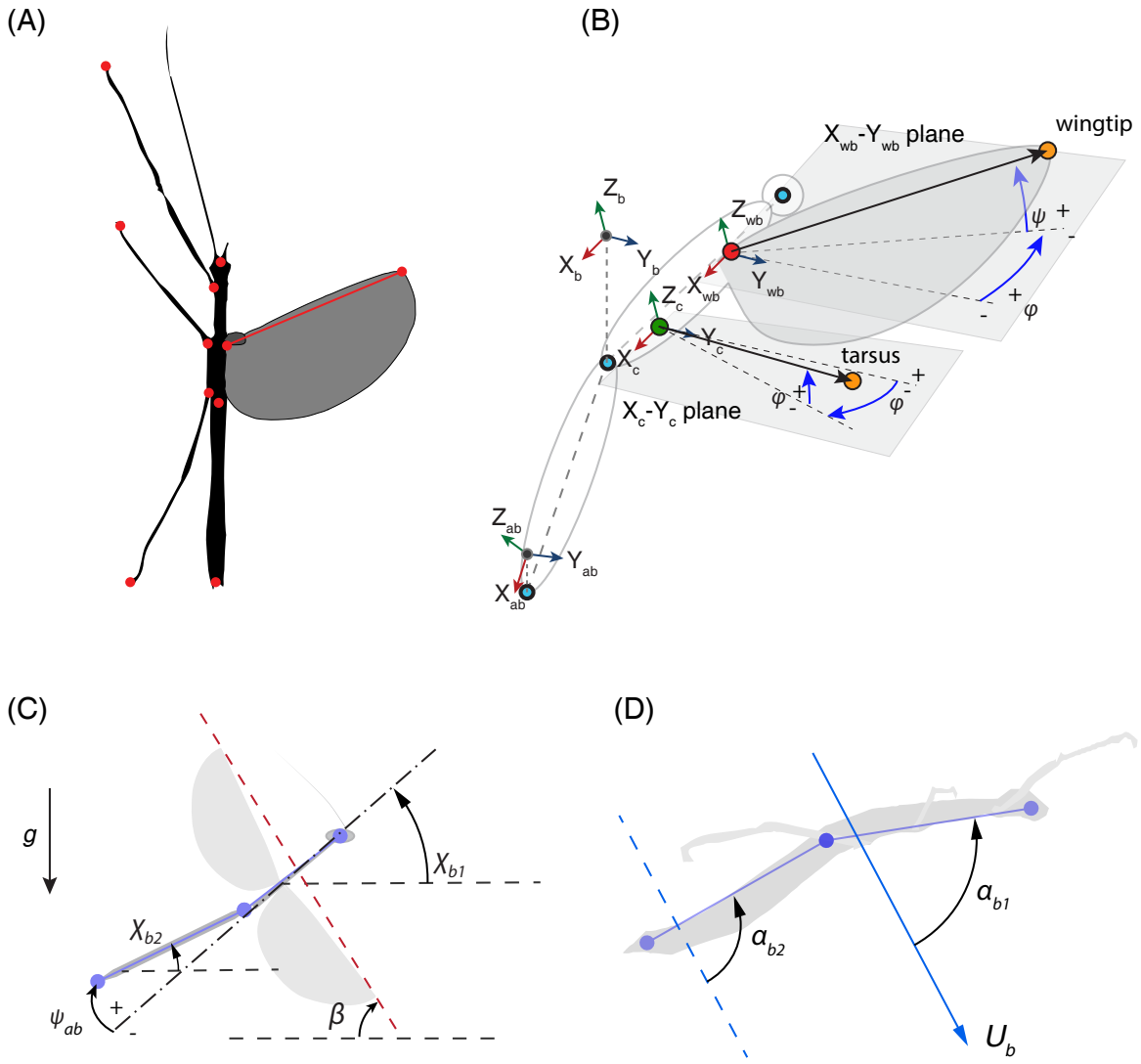

Figure 4.3: Configuration of kinematics. (A) Landmarks used for motion reconstruction. (B) Configuration of body–fixed frame, abdomen–fixed frame, wingtip position and leg position with respect to local coordinates. (C) Configuration of position angle relative to horizontal of body sections, abdomen deviation and stroke plane angle. (D) Angles of attack of both body sections.

Furthermore, flight morphology is also affected by changes in relative sizes of body parts. The overall trend is the elongation of head and thorax sections and shortening of abdomen (Table 4.5, Figure 4.3). On the other hand, the basic wing design is consistent across different flight morphs. All wings have elytronized anterior region and membranous anal region. The percent area and vein number of anal region reduces with relative wing size (WSI). Also, wing size and shape change substantially with respect to WSI. Changes of wing morphology follow different trends in two sexes (Figure 4.1, Figure 4.4). Females wings generally have lower aspect ratio than males , but this difference also reduces with wing size.

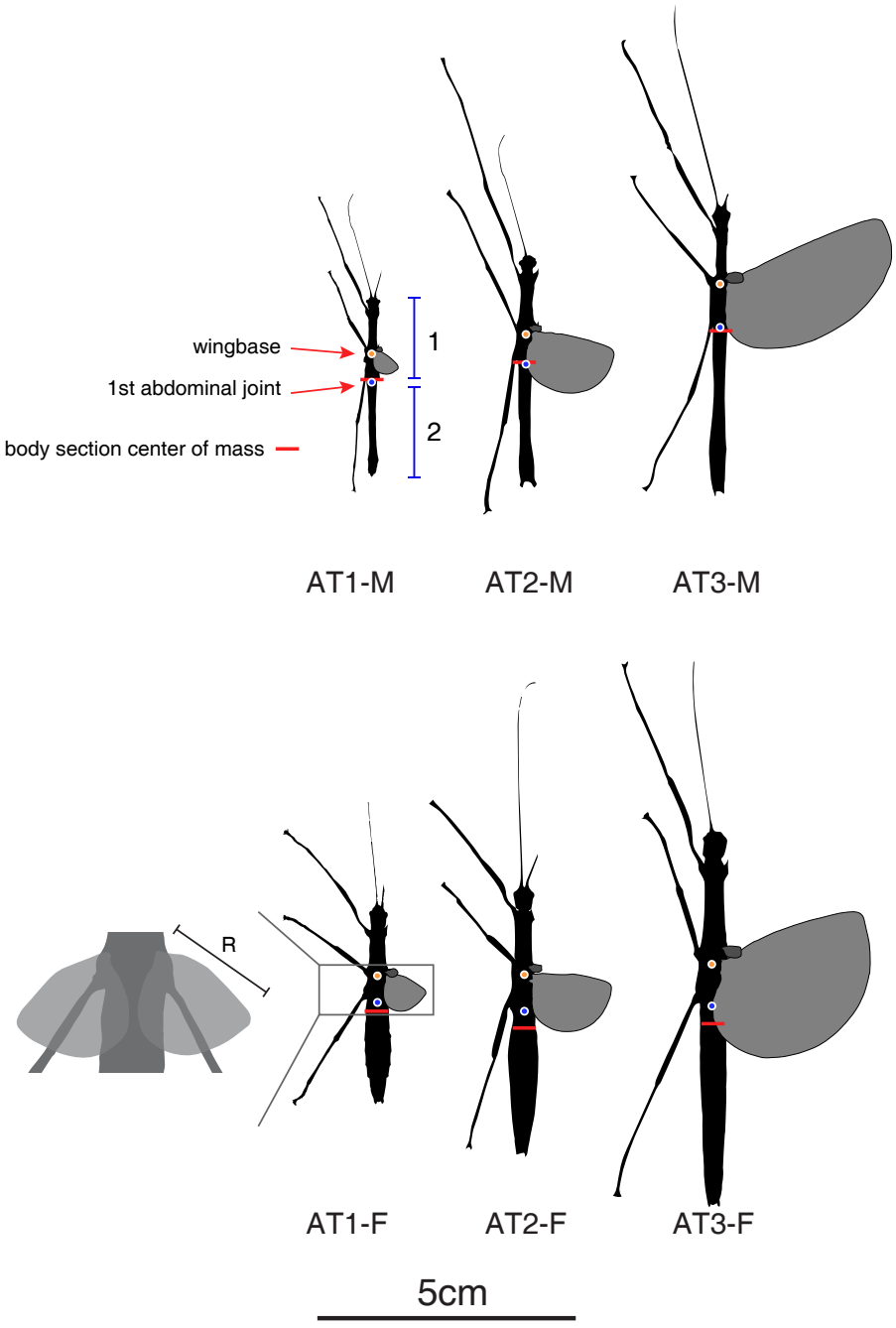

Figure 4.1: Comparison of planform profiles among flight morphs.

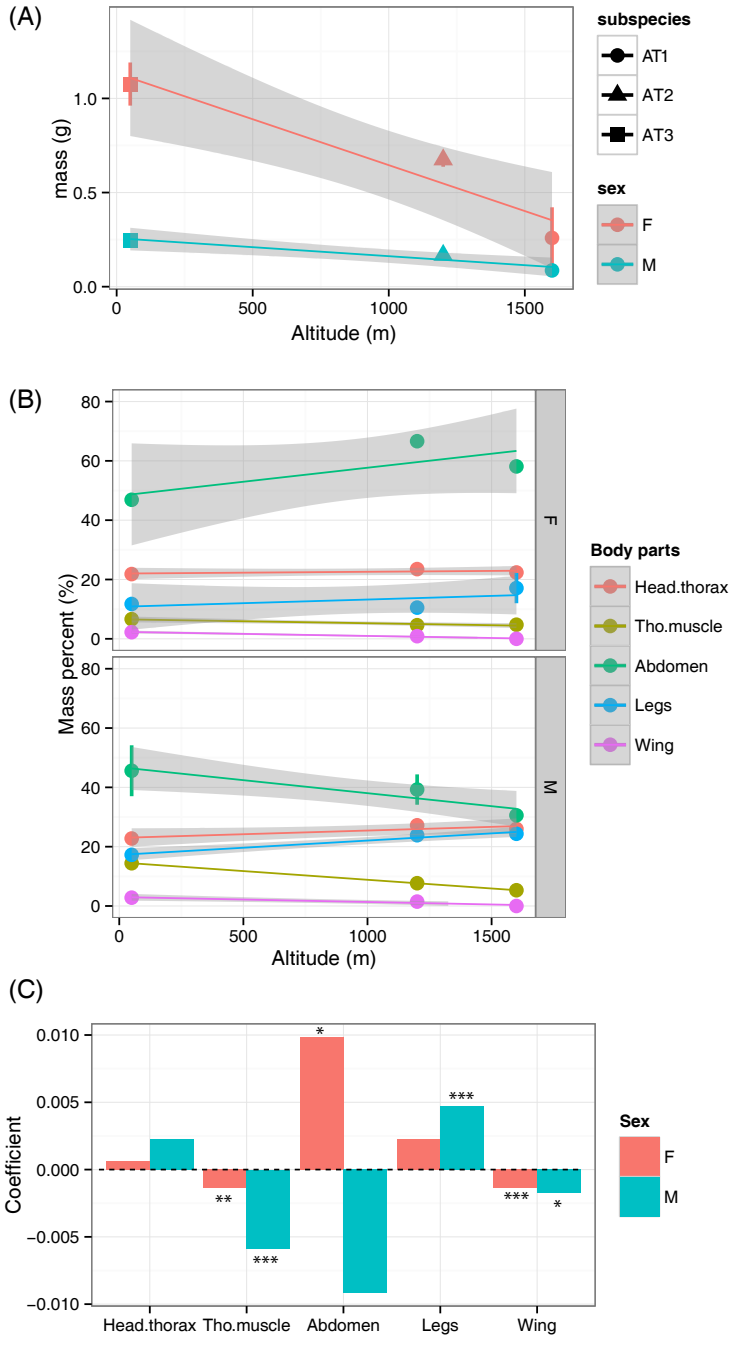

Figure 4.2: (A) Altitudinal variation of whole–insect mass. (B) Altitudinal variation in mass percentage of body parts. Shaded area indicate 95% CI. (C) Correlation coefficients of each body part's mass percent against altitude based on linear regression models. *, $P < 0.05$; **, $P < 0.01$; ***, $P < 0.001$; ns, non–significant.

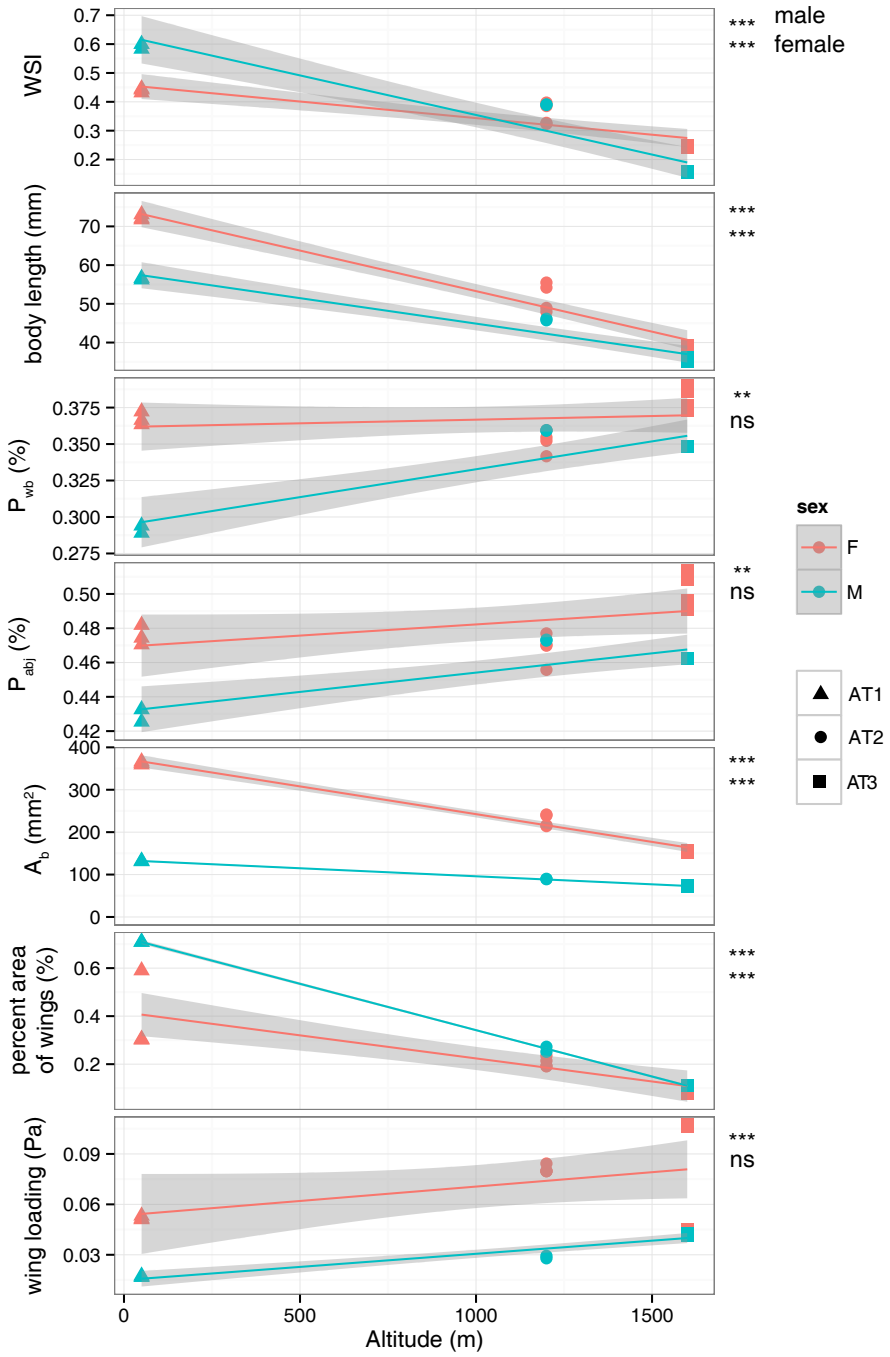

Figure 4.3: The relationships between selected filght–relevant morphological variables and altitude. WSI, wing size index. P_{wb} and P_{abj} are body length–normalized position of wing base and 1st abdominal joint, respectively. A_b is projected planfrom area of body sections. Trendlines are based on linear model, and shaded areas indicate 95% CI. *, $P < 0.05$; **, $P < 0.01$; ***, $P < 0.001$; ns, non–significant.

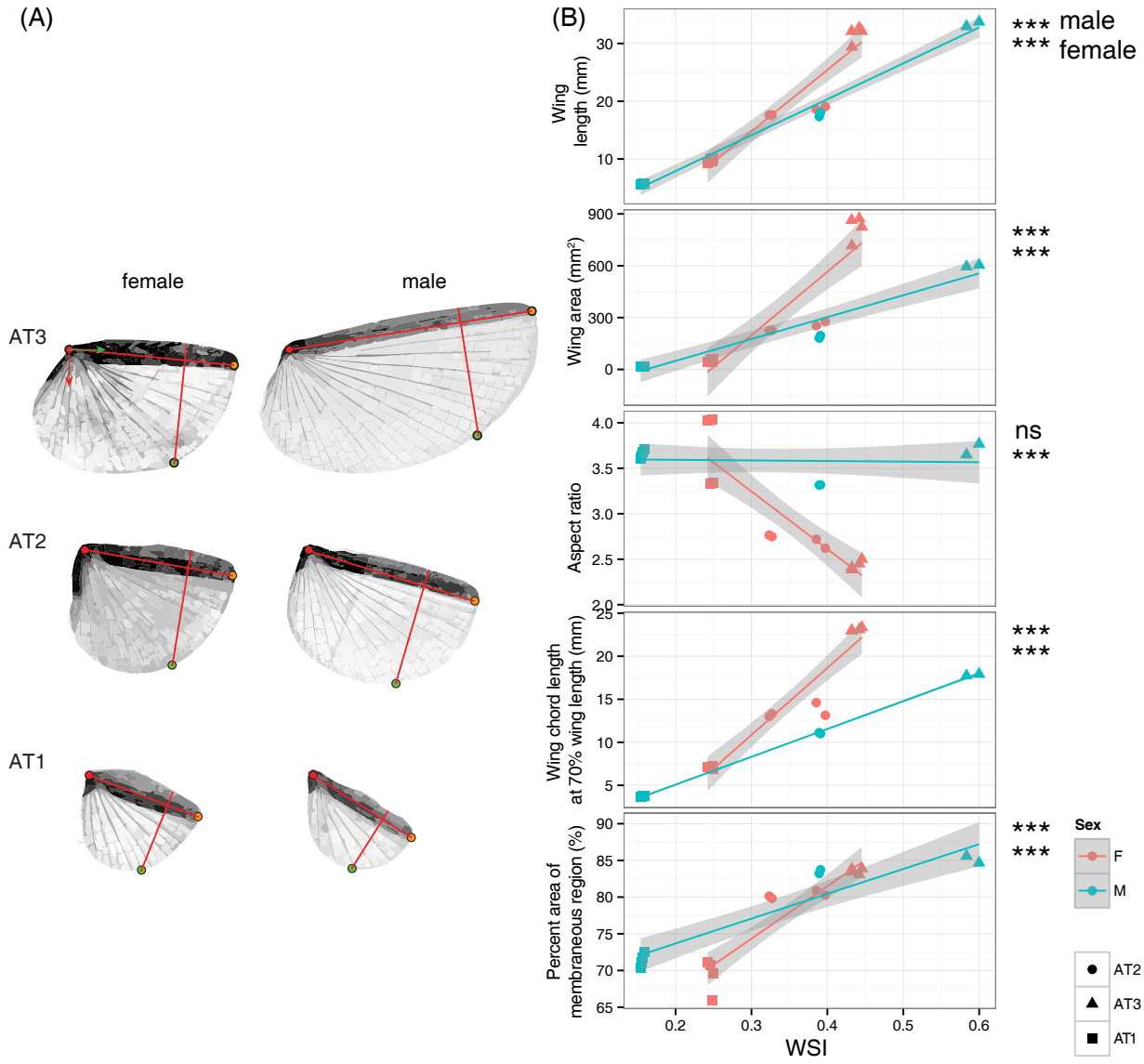

Figure 4.4: (A) 2D profiles of wings. Wing chord marked at 70% wing length. (B) The relationship between selected wing morphology variables and wing size index (WSI). Trendlines are based on linear model, and shaded areas indicate 95% CI. *, $P < 0.05$; **, $P < 0.01$; ***, $P < 0.001$; ns, non–significant.

		total mass		forelegs		midlegs		hindlegs	
	n	mean	sd	mean	sd	mean	sd	mean	sd
AT1F	3	259.00	162.63	11.00	0.00	11.00	0.00	14.00	1.41
AT1M	5	86.33	11.72	6.67	1.53	6.67	0.58	7.67	0.58
AT2F	3	674.50	37.48	23.50	2.12	19.50	0.71	28.00	2.83
AT2M	3	167.50	14.85	13.50	2.12	12.00	1.41	14.50	0.71
AT3F	3	1076.33	114.53	45.33	6.03	33.67	5.69	47.67	7.02
AT3M	3	246.50	10.61	16.00	0.00	11.00	0.00	15.50	0.71

Table 4.1: Mass distribution. Unit, *mg*.

		B.S. total		B.S. 1		T.M.		wings		B.S. 2	
	n	mean	sd	mean	sd	mean	sd	mean	sd	mean	sd
AT1F	3	223.00	135.76	60.50	44.55	13.00	9.90	< 1	–	153.50	103.94
AT1M	5	61.00	8.72	22.33	2.08	4.67	1.53	< 1	–	26.33	3.06
AT2F	3	608.00	36.77	159.00	25.46	31.00	4.24	6.00	0.00	449.00	11.31
AT2M	3	122.00	7.07	45.50	2.12	13.00	4.24	2.50	0.71	65.00	11.31
AT3F	3	943.33	106.21	235.00	27.22	71.67	12.10	24.00	2.00	506.33	78.81
AT3M	3	193.00	2.83	56.00	1.41	35.50	0.71	7.00	4.24	111.50	37.48

Table 4.2: Mass distribution (continued). Unit, *mg*. B.S., body section; T.M., thoracic musculature.

	body section 1	thoracic muscle	body section 2	legs	wings
AT1F	22.4	4.8	58.1	17.1	< 0.1
AT1M	26.0	5.3	30.6	24.3	< 0.1
AT2F	23.5	4.6	66.6	10.5	0.9
AT2M	27.2	7.7	39.3	23.9	1.5
AT3F	21.8	6.6	46.9	11.7	2.2
AT3M	22.8	14.4	45.6	17.3	2.8

Table 4.3: Mean percent mass of different body parts.

	R		A		AR		c		membrane (%)		WSI	
	mean	sd	mean	sd	mean	sd	mean	sd	mean	sd	mean	sd
AT1F	9.74	0.35	52.4	9.3	3.682	0.401	7.06	0.15	69.4	2.3	0.247	0.003
AT1M	5.64	0.07	17.4	0.2	3.657	0.047	3.71	0.05	71.4	0.9	0.156	0.002
AT2F	18.21	0.71	245.1	24.9	2.713	0.065	13.52	0.74	80.3	0.4	0.358	0.039
AT2M	17.68	0.50	188.7	10.6	3.316	0.002	11.06	0.08	83.5	0.4	0.390	0.001
AT3F	31.58	1.49	819.5	71.8	2.437	0.051	23.10	0.17	83.6	0.4	0.438	0.007
AT3M	33.33	0.56	599.5	6.6	3.707	0.084	17.83	0.13	85.1	0.7	0.592	0.012

Table 4.4: Wing morphology. R, wing length; A, wing area; AR, aspect ratio; c, chord length at 70% wing length; membrane(%), percent area of membranous portion relative to whole–wing; WSI, wing size index. Length unit, mm. Area unit, mm^2.

	L_b		P_{wb}		P_{abj}		A_b		A_l	
	mean	sd	mean	sd	mean	sd	mean	sd	mean	sd
AT1F	38.8	0.3	14.8	0.2	19.5	0.3	155.3	2.0	76.4	1.0
AT1M	35.6	0.5	12.4	0.2	16.5	0.2	72.8	0.9	66.9	0.9
AT2F	51.6	3.8	18.2	1.6	24.2	2.1	227.9	14.6	115.6	7.3
AT2M	45.9	0.3	16.5	0.1	21.7	0.2	89.5	0.6	81.8	0.6
AT3F	72.1	0.7	24.1	4.9	31.3	6.2	294.8	136.0	174.2	0.68
AT3M	56.4	0.3	16.5	0.1	24.2	0.2	131.7	0.9	114.4	0.8

Table 4.5: Flight morphology. L_b, body length; P_{wb}, wing base distance from head; P_{abj}, distance of 1st abdominal joint from head; A_b, area of body section; A_l, total area of legs. Length unit, mm. Area unit, mm^2.

4.3.2 Flight performances

All flight morphs performed flight in right–side–up body orientation with opened wings, and the horizontal travel distance is positively correlated with wing size. Both sexes of AT1 performed parachuting flight, which trajectories resembled that of free fall. Both sexes of AT2 and AT3 female performed gliding flight with reduced wing flapping in various degrees of negative trajectory incline. AT3 males performed flapping flight with large variations in flight speed and trajectory incline (Figure 4.5). Both parachuting and gliding flights initiated with a non–equilibrium descent prior to reaching a equilibrium state (Figure 4.7,4.8, Table 4.6). The height loss and time cost for non–equilibrium phases is negatively correlated with relative wing size (Figure 4.6). In AT3M, body speed is negatively correlated with trajectory incline angle. Furthermore, wing–binding caused significant increase of terminal velocity in all tested flight morphs, and disabled lateral traveling ability in AT2 (Figure 4.7, Figure 4.8). Generally speaking, a performance gradient between flapping and parachuting flight was found to be correlated with the wing size gradient, and all size–reduced wings at least generate aerodynamic drag in flight.

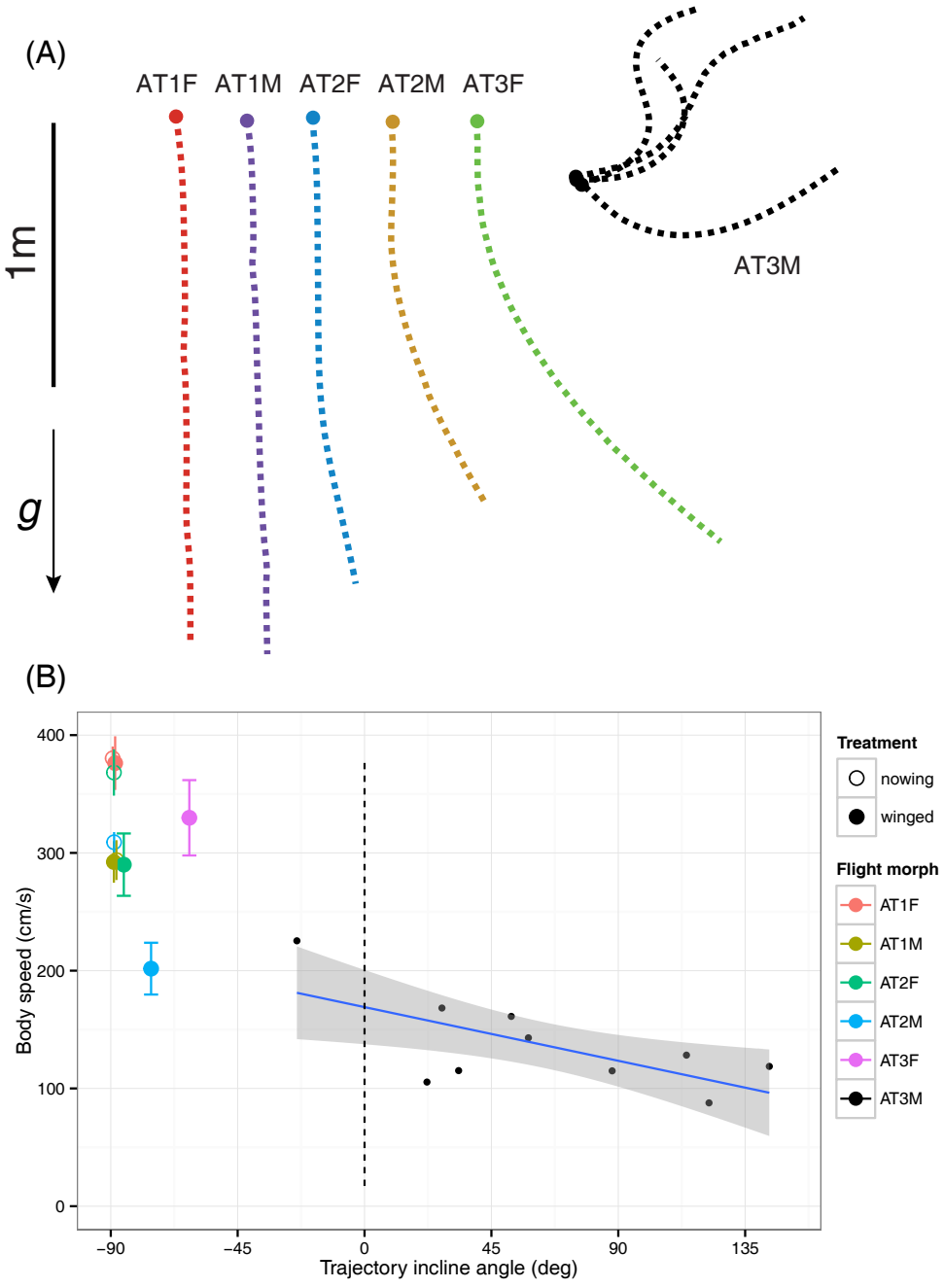

Figure 4.5: (A) Sample trajectories. (B) The relationship between body speed and trajectory incline angle. Values are averages of equilibrium phases for parachuting and gliding flight. For AT3M, values are based on equilibrium intervals from 7 flight trials, with significant correlation (R^2=0.45, P<0.05). Sample size is reported in Table 4.6.

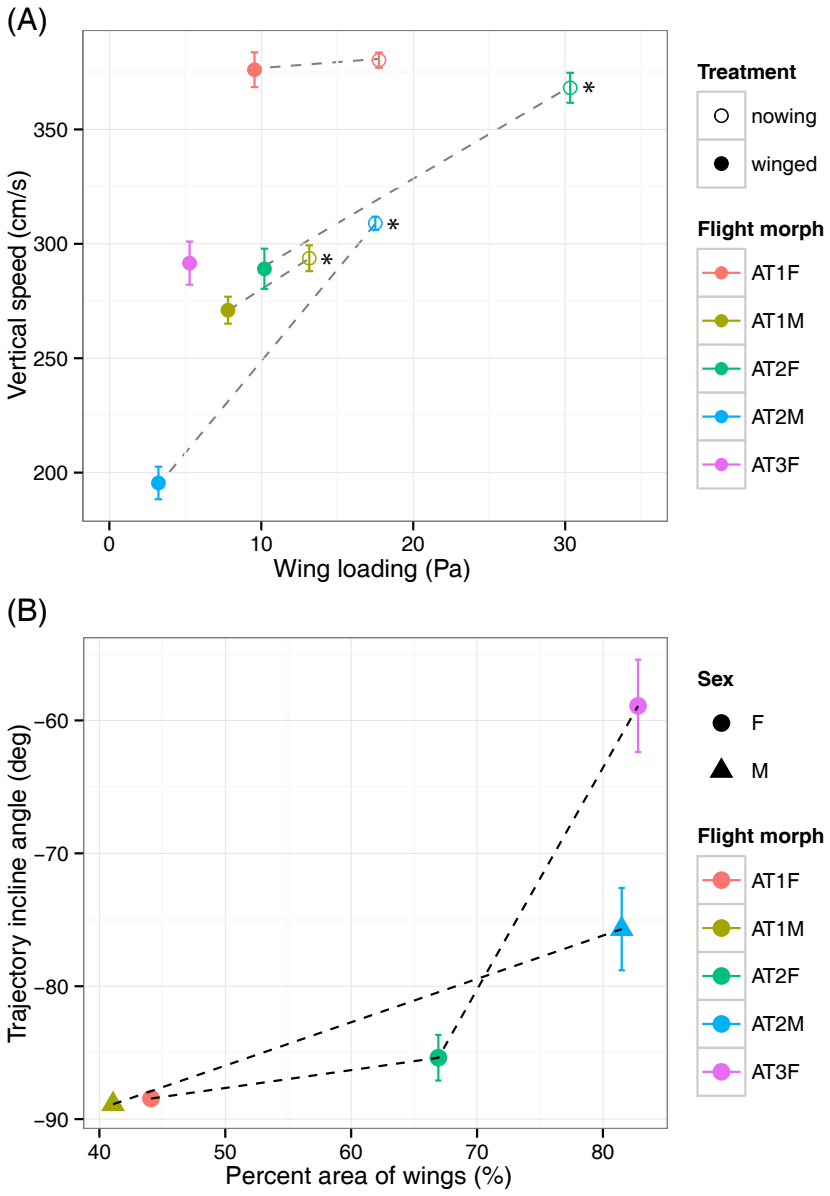

Figure 4.6: (A) The relationship between vertical speed and wing loading. Asterix symbols denote significant increase of vertical speed caused by wing–binding treatment. (B) The relationship between trajectory incline angle and percent wing are relative to total projected planform area.

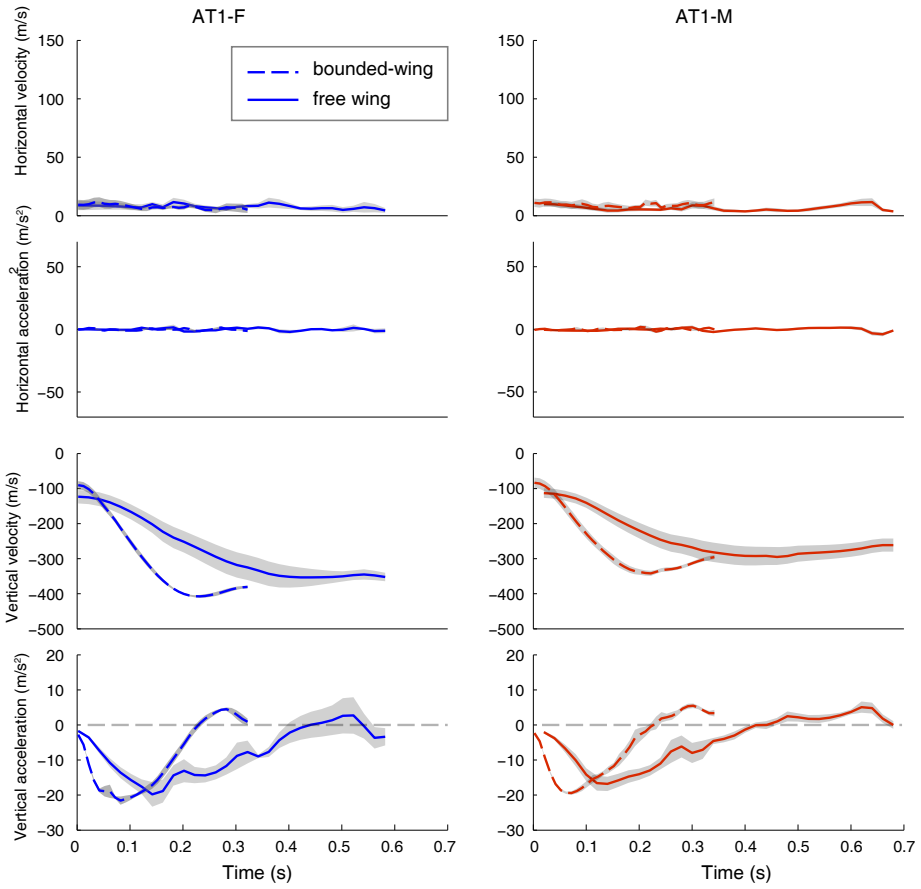

Figure 4.7: COM speed and acceleration in horizontal and vertical of AT1. Wing-binding caused greater vertical acceleration. Curves are mean±s.e.m. based on multiple trials. AT1F free–wing, N=6; AT1F bound–wing, N=5; AT1M, free–wing, N=8; AT1M, bound–wing, N=7.

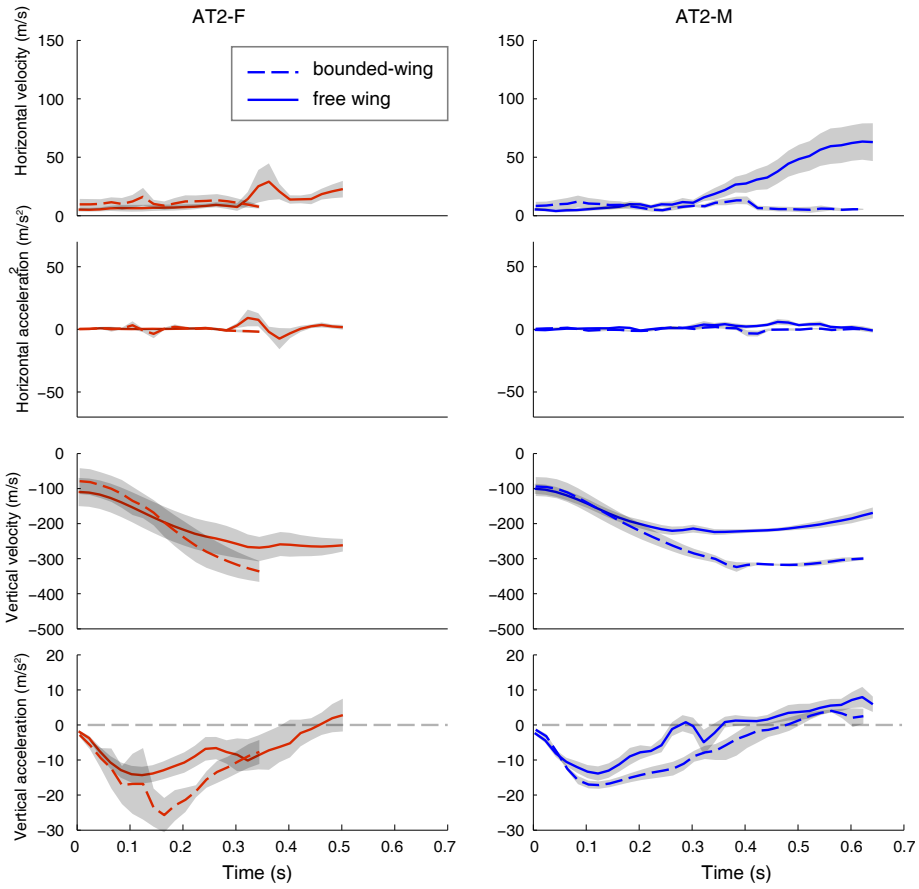

Figure 4.8: COM speed and acceleration in horizontal and vertical of AT2. Wing-binding caused greater vertical acceleration, greater vertical speed and the loss of horizontal travel. Curves are mean±s.e.m. based on multiple trials. AT2F free–wing, N=4; AT2F bound–wing, N=6; AT2M, free–wing, N=6; AT1M, bound–wing, N=10.

flight morph	N	Non–equilibrium phase			Equilibrium phase				
		$t0$ (s)	$H0$ (cm)	$H0_{bL}$	U_b (cm/s)	θ(deg)	Re_{bL}	L/D	C_D
AT1-F	6	0.352±0.030	-92±8	23.0	376±22	-88.5±0.8	10000	< 0.05	0.9
AT1-F, b-w	5	0.307±0.012	-183±8	45.8	380±10	-89.3±0.8	10000	< 0.05	1.3
AT1-M	8	0.310±0.016	-93±38	25.8	271±60	-88.9±0.5	6500	< 0.05	1.1
AT1-M, b-w	7	0.317±0.017	-161±18	44.7	294±16	-88.0±1.7	7000	< 0.05	1.2
AT2-F	4	0.415±0.070	-97±34	19.4	290±27	-85.4±4.2	10000	0.08	
AT2-F, b-w	6	0.487±0.130	-104±22	20.8	368±20	-88.9±0.7	12000	< 0.05	2.4
AT2-M	6	0.323±0.027	-56±7	12.2	202±22	-75.7±10.0	6000	0.26	
AT2-M, b-w	10	0.380±0.074	-77±10	16.7	309±9	-88.8±0.5	9000	< 0.05	1.7
AT3-F	6	0.30±0.004	-62±5	8.6	310±47	-58.9±7.0	14400	0.6	
AT3-M		-	-	-	100 to 200	-42 to 140	160000 to 320000	-	

Table 4.6: Comparison of selected variables of trajectory dynamics. $t0$, time cost prior to equilibrium. $H0$, height loss prior to reaching equilibrium. $H0_{bL}$, $H0$ normalized by both length. U_b, COM speed. Re_{bL}, Reynolds number based on body length. L/D, lift–to–drag ratio. "b-w", bounded-wing.

4.3.3 Wing kinematics

Wing kinematics was sampled in 5–7 wingbeat cycles from 5–10 trails of each flight morph that performs parachuting or gliding. The data of AT3M is from 10 flight trials in 3 individuals. First, the mobility and activity levels of wings are correlated with their relative sizes. The range of wing posture, quantified as position (ϕ) and deviation (ψ) angles, increases with relative wing size. All size–reduced wings have more reduced position angle than fully–developed wings of AT3M. Only both sexes of AT3 had wing positions exceeded 0°(Figure 4.10). The same trend is found in the range of deviation angles, and therefore wing stroke amplitude is correlated with relative wing size (Figure 4.9-B). Notably, both sexes of AT1 held wings in constant positions and didn't perform significant wing stroke movement in flight. On the other hand, wingbeat frequency was negatively correlated with relative wing size in flapping wings of both sexes. The smallest wings in AT1 had frequencies of 0 given no stroke movement (Figure 4.9-A). Stroke plane angle (β) decreases with trajectory incline angle among flight morphs (Figure 4.12). The same trend is found in the wing strokes sampled from flight trajectories of AT3M.

Furthermore, variation of aerodynamic characteristics is induced along the gradient of performance as consequences of the differences in wing size, stroke movement and whole–insect translation. In gliding flight performed with reduced flapping, wing speed is overcome by body translation, largely in the vertical direction, and thus wing velocity with respect to the space of both half–strokes are dominated by downward components. This relationship was shown in different degrees among four wing–flapping flights (Figure 4.13). The negative correlation between advance ratio (J) and θ clearly shows this pattern (Figure 4.16).

The variation in asymmetry of half–strokes along the performance gradient is shown by the differences in the differences of mean velocities between up– and down–strokes, in both magnitude and direction (Figure 4.14-A). The ratio of V_{dn}/V_{up} increases with θ in reduced flapping flight morphs, but decreases with θ in AT3M. On the other hand, angular differences between air velocities of up– and downstrokes generally increases with θ, with the highest in AT3M (Figure 4.14-B). However, no significant correlation is found between $\Delta\phi$ and θ in AT3M.

Reynolds number (Re) based on wing chord size generally increases with θ in both sexes, with greater differences between up– and downstrokes towards greater θ. In AT3M, Re_{dn} is larger than Re_{up} in low θ, but both Re_{dn} and Re_{up} follow opposite trends along increasing θ and converges at high θ (Figure 4.15).

Overall, we observed positive correlation between wing mobility and relative wing size along the wing size gradient, and continuous variation of parameters describing wing–flow interactions, e.g., (J); on the other hand, wing kinematics, e.g., f and V_{dn}/V_{up} ratio, follow non–linear correlation with the gradients in morphology and performance.

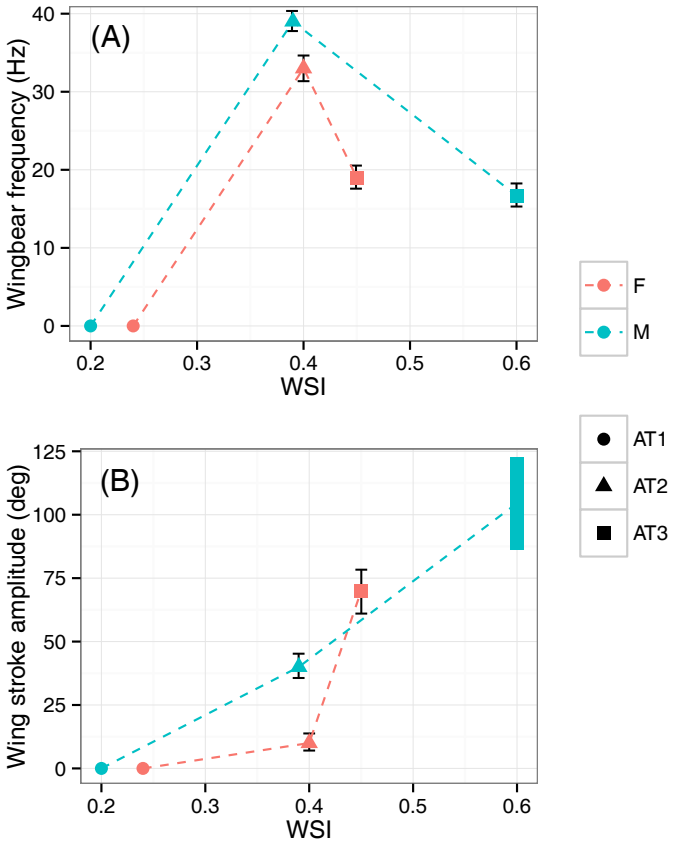

Figure 4.9: The relationships between relative wing sizes and basic wing kinematics. (A) Wingbeat frequency. (B) Wing stroke amplitude. Values are mean±s.d. (AT2F, N=20 wingbeat cycles; AT2M, N=25; AT3F, N=33; AT3M, N=53.)

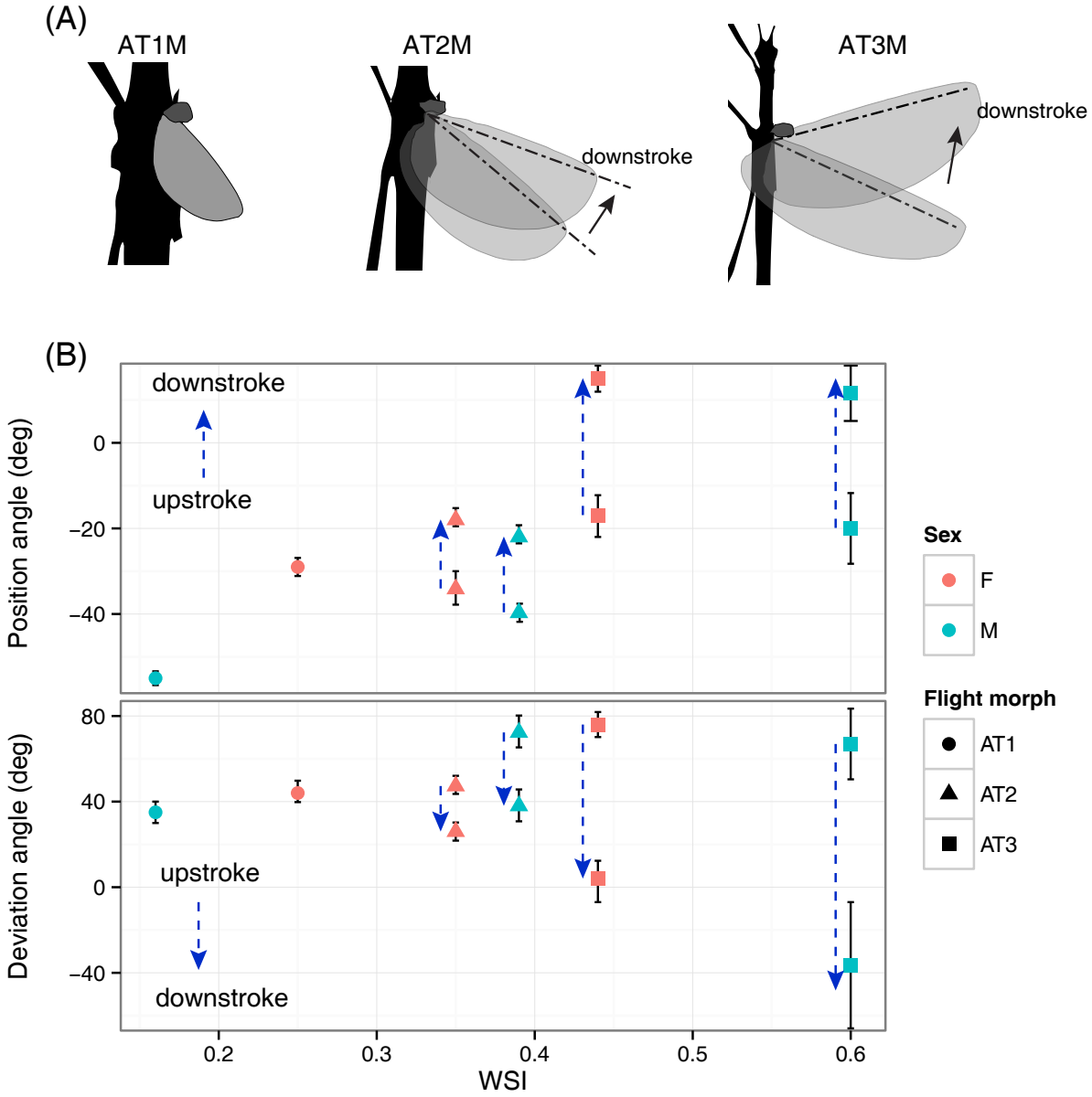

Figure 4.10: (A) Schematic diagram of the variation of wing position in different sized wings, using males as an example. (B) Position and deviation angles during up– and downstrokes, contrasting the range of motion in different sized wings. Values are mean±s.d., sample sizes are the same as in Figure 4.9.

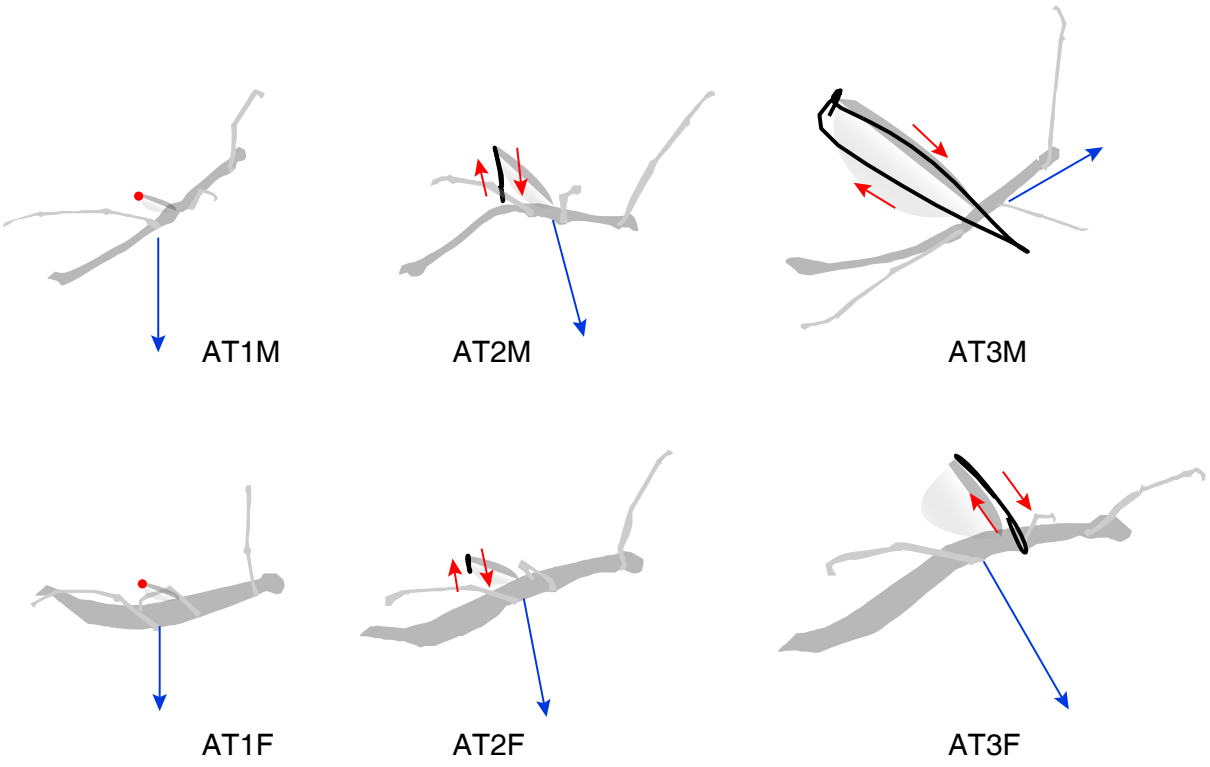

Figure 4.11: Sample wingtip path during flight in lateral view.

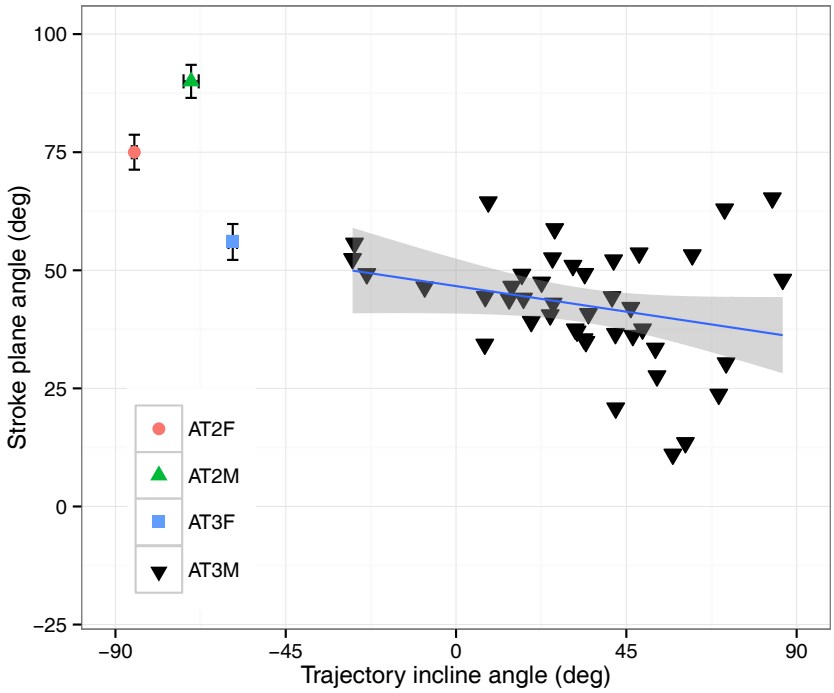

Figure 4.12: The relationship between stroke plane angle and trajectory incline angle in all wing–flapping flight modes. Values are mean±s.e.m. for gliding flight. Trajectory incline angle of AT3M was sampled as the mean during the corresponding wing strokes, and it was tested with a linear regression model, which suggested significant correlation. $R^2 = 0.44$, $P < 0.00001$. N=10 trials in 3 individuals.

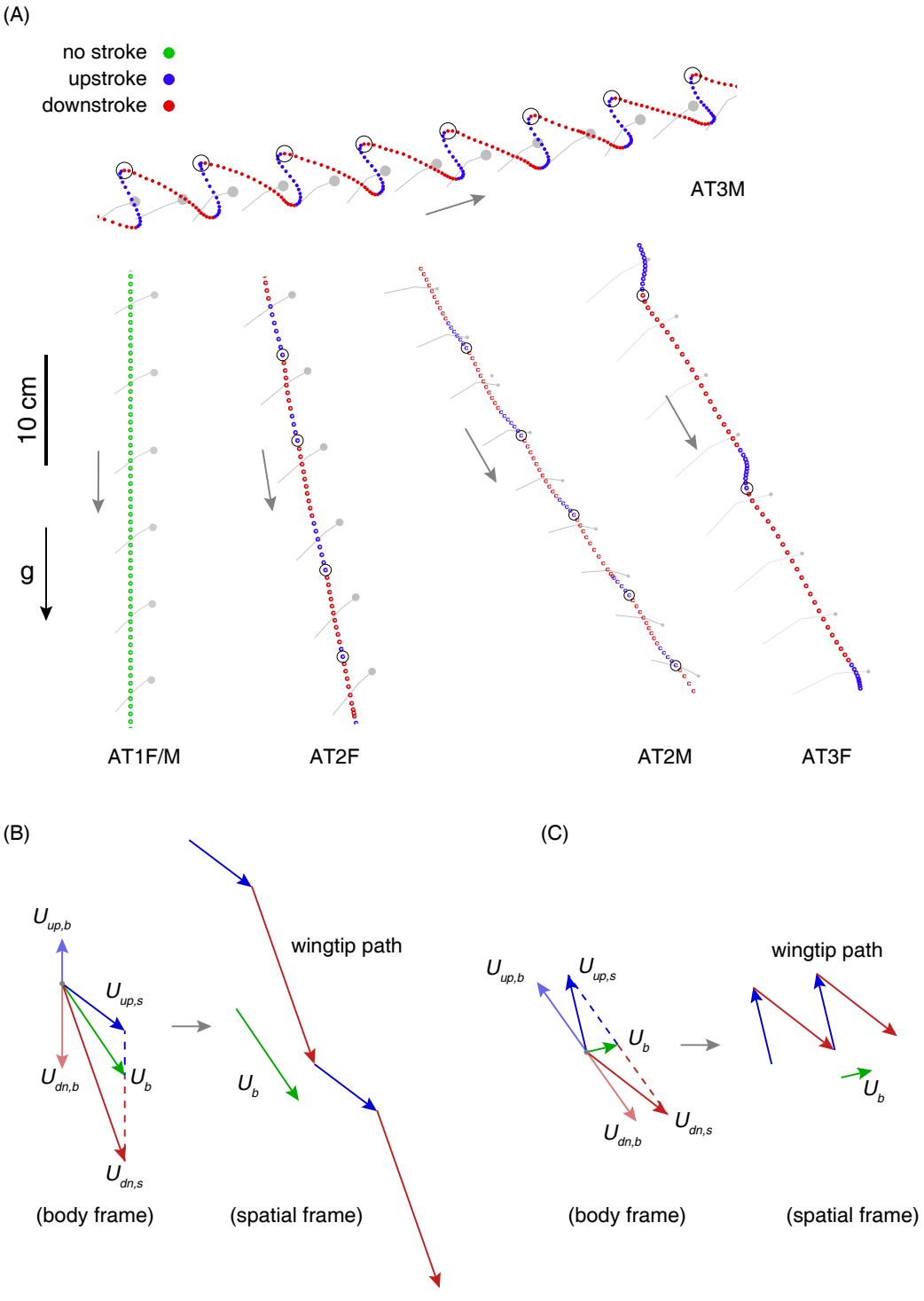
(A)
no stroke
upstroke
downstroke
AT3M
10 cm
g
AT1F/M
AT2F
AT2M
AT3F
(B)
$U_{up,b}$
$U_{up,s}$
$U_{dn,b}$
U_b
$U_{dn,s}$
wingtip path
U_b
(body frame)
(spatial frame)
(C)
$U_{up,b}$
$U_{up,s}$
U_b
$U_{dn,b}$
$U_{dn,s}$
wingtip path
U_b
(body frame)
(spatial frame)

[p]

Figure 4.13 *(preceding page)*: (A) Wingtip paths of different flight morphs in lateral view, showing the differences in speed of half–strokes. Graph was produced based on example trials sampled at 500 Hz. (B) and (C), schematic diagrams showing the underlying mechanism for observed wingtip paths in gliding and ascending flights.

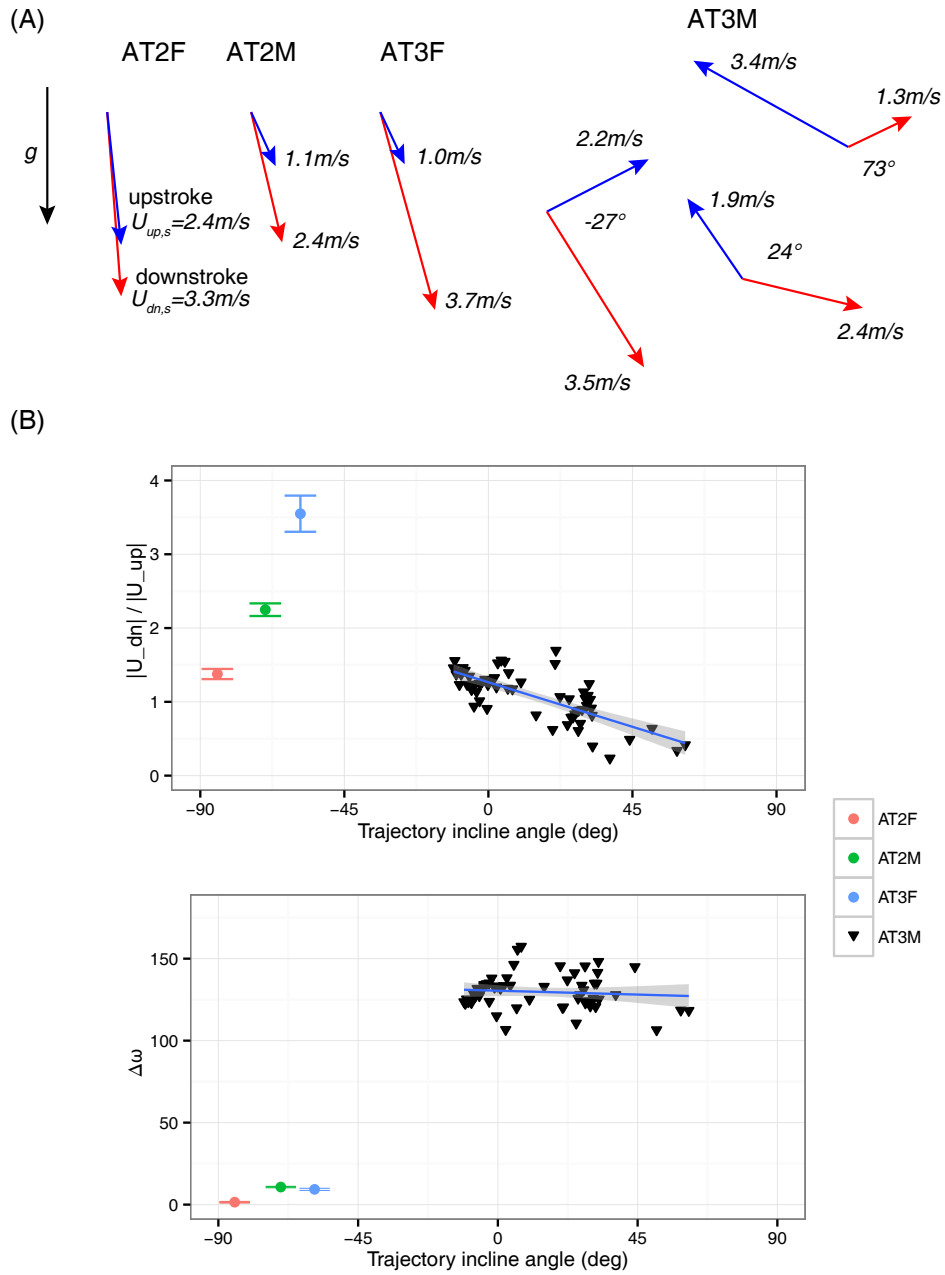

Figure 4.14: Comparison of half–stroke asymmetries. (A) Comparison of velocity vectors of up– and downstrokes. (B) (Top) Differences in wing speed. For AT3M, there is a significant correlation between U_{dn}/U_{up} ratio and trajectory incline angle, R^2=0.23, P<0.0001. (Bottom) Differences in half–stroke directions. Values are mean±s.e.m. Sample sizes are the same as in Figure 4.9. For AT3M, there is no significant correlation between $\Delta\omega$ and trajectory incline angle, P=0.28.

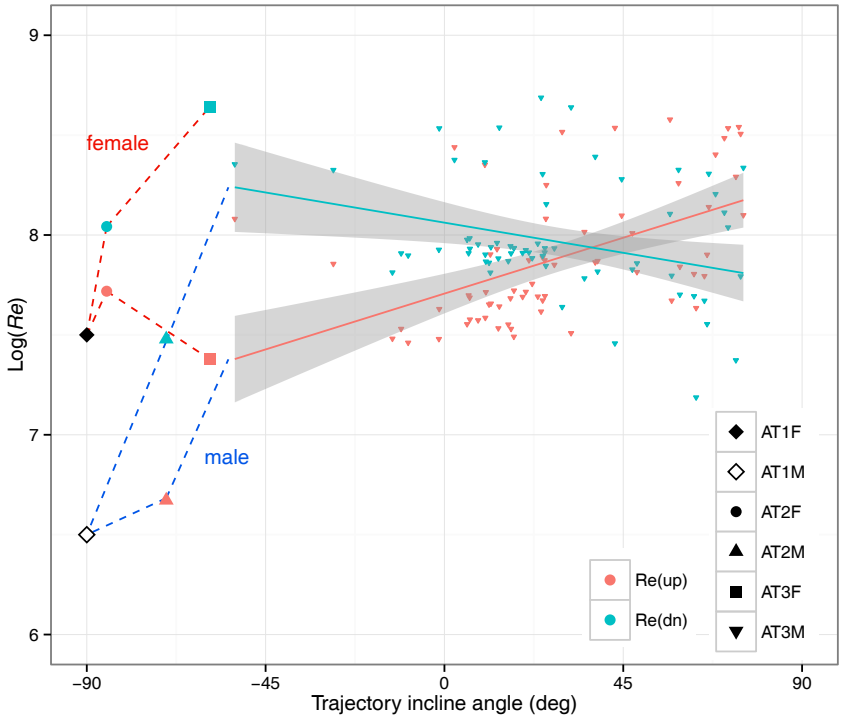

Figure 4.15: The relationship between log–transformed Reynolds number and trajectory incline. For AT3M, the correlations between trajectory incline angle and the Reynolds number associated with each of up– and downstrokes are significant. $P < 0.0001$ for both, R^2=0.23 for Re_{up}, and R^2=0.29 for Re_{dn}.

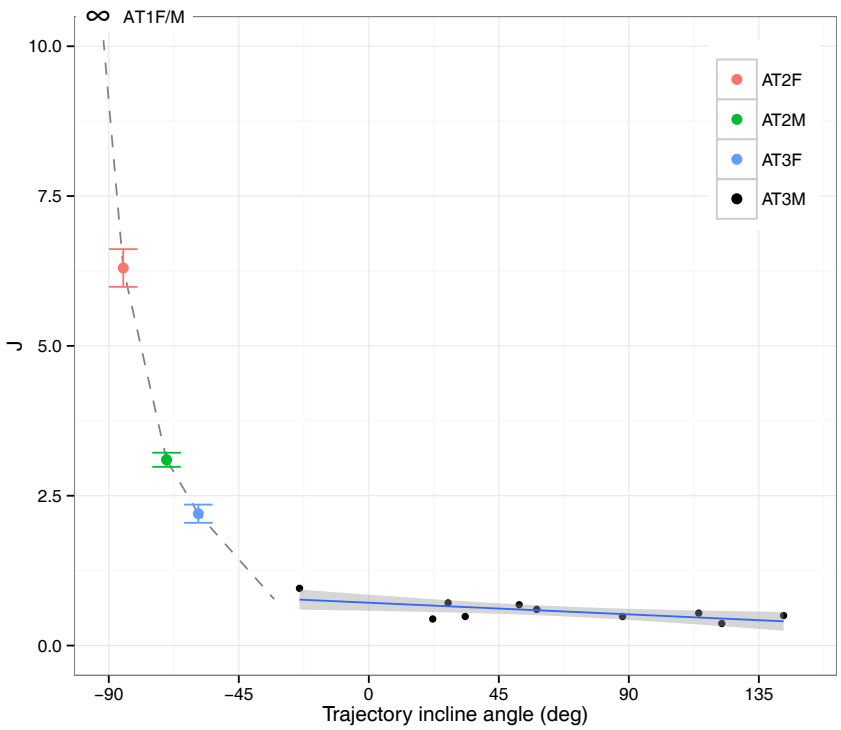

Figure 4.16: The relationship between advance ratio and trajectory incline. Values are mean±s.e.m. Sample sizes are the same as in Figure 4.9. For AT3M, the correlations between trajectory incline angle and the Reynolds number associated with each of up– and downstrokes are significant. $P < 0.05$, R^2=0.44.

4.3.4 Body and leg kinematics

For averaged body and leg postures, the sampling was conducted at a minimum of 50Hz from 3–6 trials in each parachuting and gliding flight morph. For AT3M, it sampled from 4 flight trials. Orientation of body sections during equilibrium flight differ across flight morphs (Figure 4.17-A). Comparing among flight morphs performing gliding and parachuting, greater anterior body section angle, which means greater positive pitch (nose–up), is associated with the reduction of trajectory incline angle θ. On the other hand, the posterior body section angle increases with increasing θ among the females, and decreases among males (Figure 4.17-B). Angle of attack of anterior body section (α_{b1}) is negatively correlated with θ, and the same trend was found for that of posterior body section (α_{b2}) in males. (α_{b2}) of AT2F is significantly greater than other two female morphs (Figure 4.17-C).

In flapping flight of AT3M, both body sections oscillate with wingbeat movements, and thus angular position and angle of attack of both body sections change instantaneously. Both body sections rotate to dorsal direction about 1st abdominal joint during wing downstrokes and rotates in the opposite direction during upstroke (Figure 4.18). In general, mean position angles of body sections are correlated with trajectory incline angle (Figure 4.17), and the angles of attack were maintained relatively constant across different trajectory incline angles and significantly less than all other flight morphs (Figure 4.17-C).

Also, leg postures changes along the gradient of performance. In females, both elevation angle (ϕ) and sweep angle (ψ) varies significantly. Elevation angle of hindlegs increases with α_{b1}, exhibiting the greatest range of variation. The same general trend is found in males, with the elevation of mid– and hindlegs increasing with α_{b1}. In AT3M, legs also oscillate with wingbeat movement (Figure 4.19, Figure 4.20). Clear trend of angle of attack of legs in females, more sophisticated pattern in males. Overall, following the gradient from flapping flight to parachuting, legs tend to be more elevated and more posteriorly oriented.

Different body and leg postures cause differences of the location of whole–insect COM. Estimation based on average postures suggested the COM locate near the center of longitudinal axis in all flight morphs, and have more anterior location in males (AT1F, 49.9% ; AT1M, 40.8%; AT2F, 55.3%; AT2M, 42.4%; AT3F, 41.4%. Figure 4.19). In AT3M, the body oscillation causes dorsoventral shift of COM of about 1.2 mm, which is about x% body length.

Furthermore, different postural configurations in specific trajectories cause different projected area in the flow direction. The percent of projected planform area, including both body sections and legs, in flow direction show different trends with increasing trajectory incline angle between males and females: it increases slightly in females but decreases in males. Also, the proportion of body sections in total projected area changes with trajectory incline angle in both sexes, with the intermediate one being the greatest (Figure 4.21).

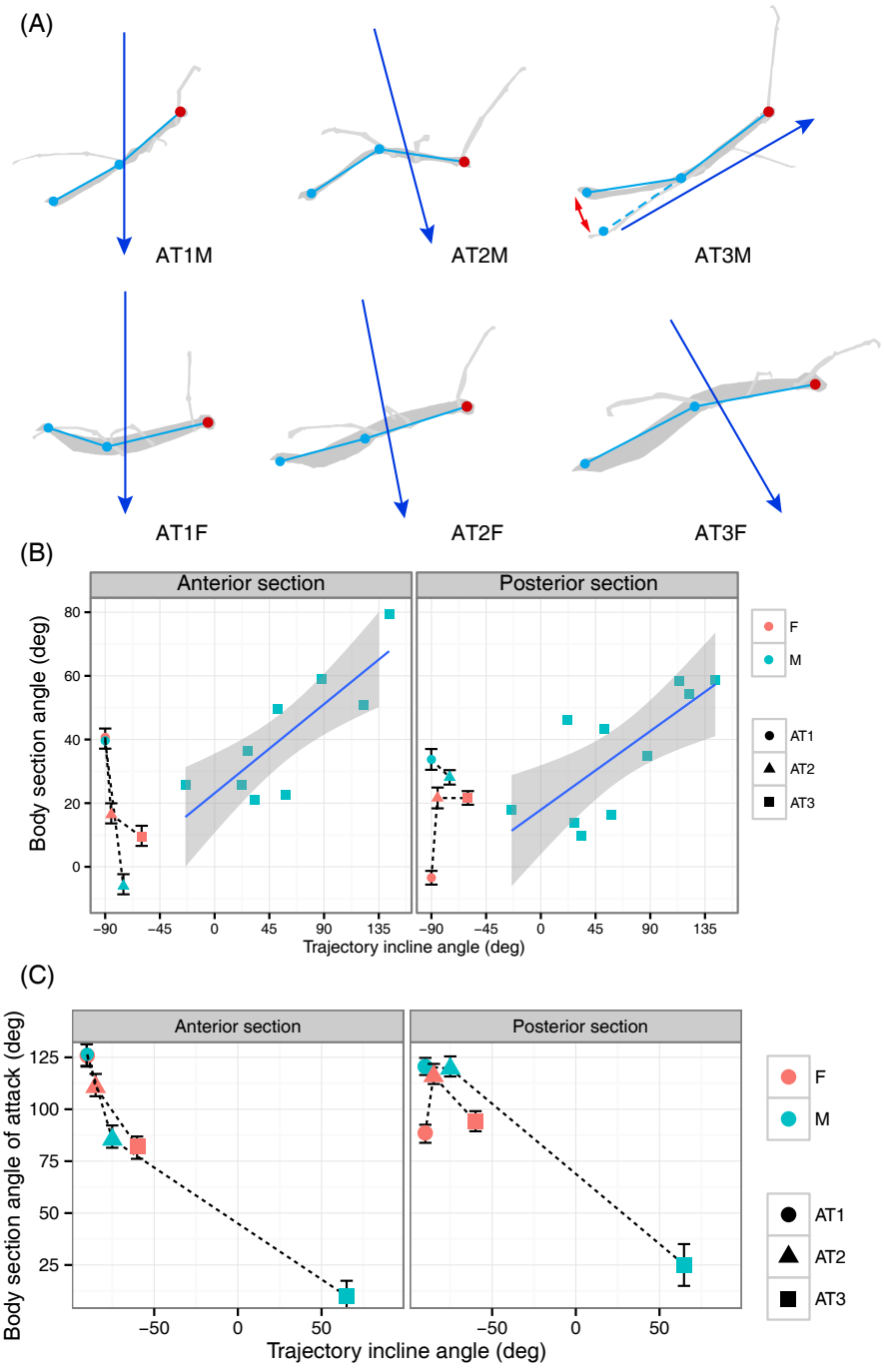

Figure 4.17: Comparison of body posture. (A) Posture in lateral view. Arrows denote flight direction. (B) Body section angle and body section angle of attack from the same trial.

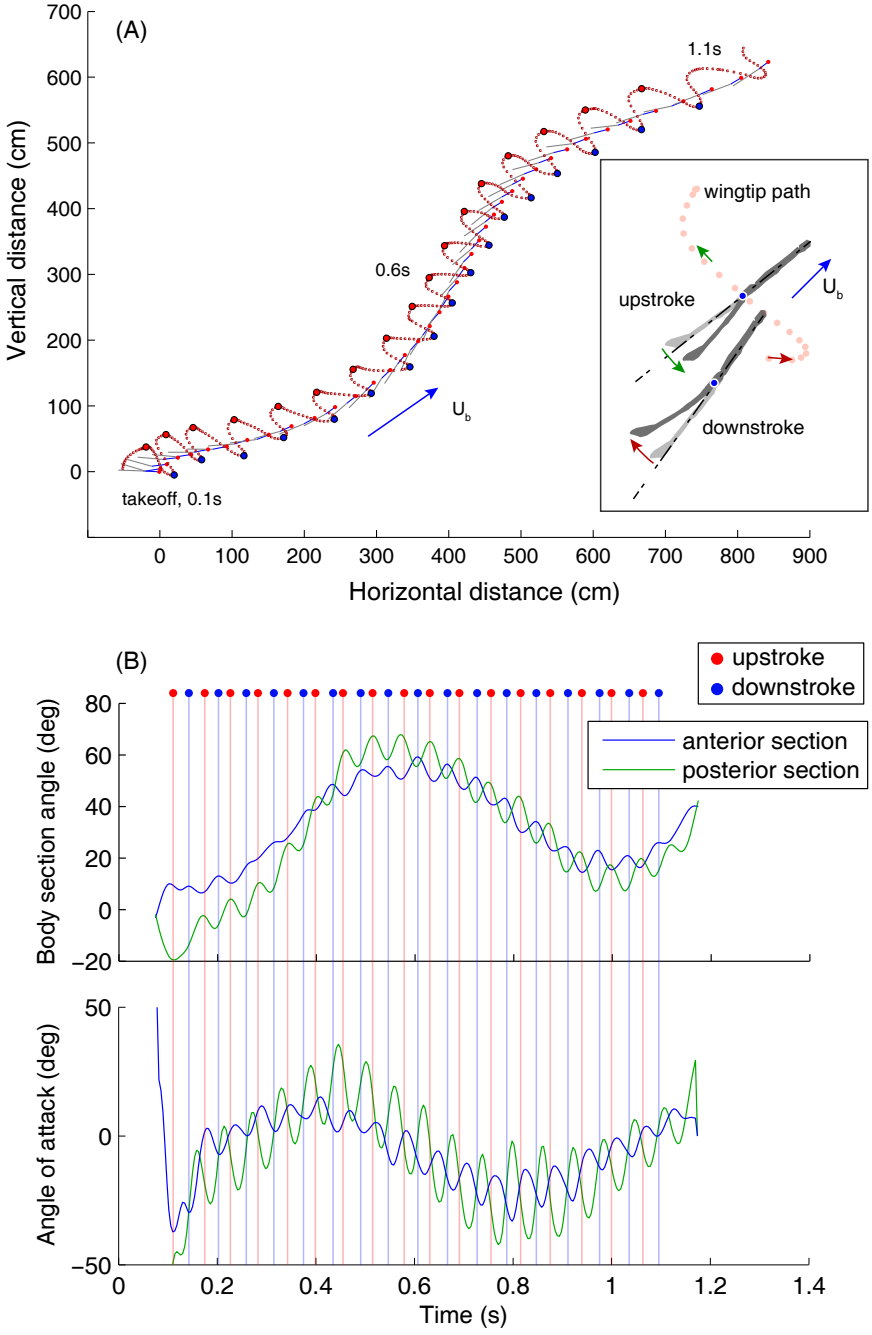

Figure 4.18: Body oscillation of AT3M flight. (A) The paths of near wingtip and body sections in lateral view, with upstrokes and downstrokes highlighted by colored dots. Insertion shows the up–and–down deviation of abdomen section in rhythm with wingbeat movement. (B) Position angle of body sections with respect to horizontal (top) and corresponding angle of attack based on the same trial in (A) (bottom).

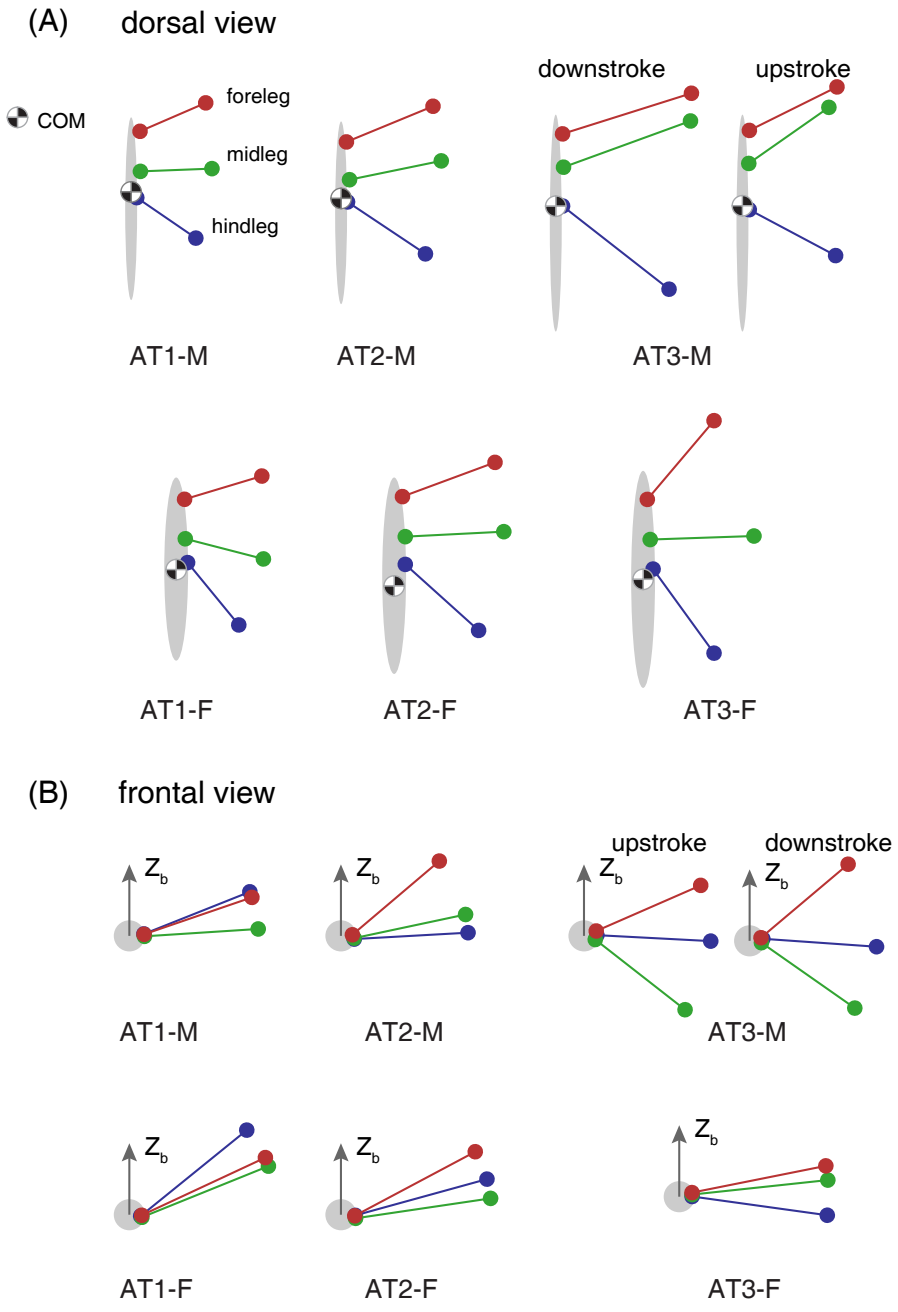

Figure 4.19: Comparison of mean leg postures in equilibrium performance. Body sections and legs are shown in smiple geometries for clarity. (A) Dorsal view of right–side legs, showing variation in sweep angle, accompanied by longtitudinal location of COM. (B) Frontal view of left–side legs, showing variation in elevation angles.

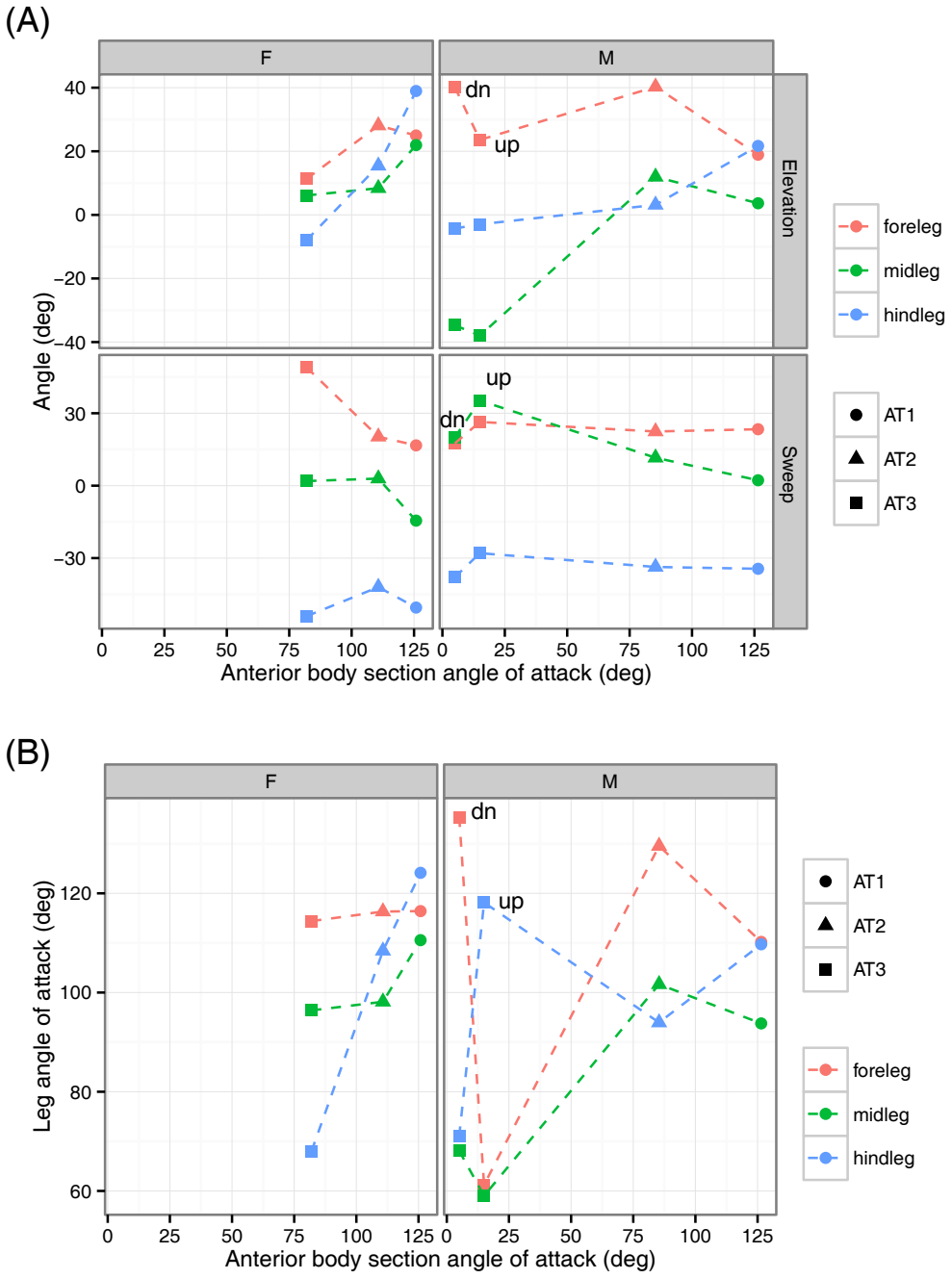

Figure 4.20: Comparison of mean leg posture, corresponding with Figure 4.19. (A) Comparison of sweep and elevation angles, corresponding with Figure 4.19. (B) Comparison of legs' angle of attack. "F" and "M" denote female and male, respectively. Leg postures at endpoint of up– and downstrokes of AT3M are denoted as "up" and "dn", respectively.

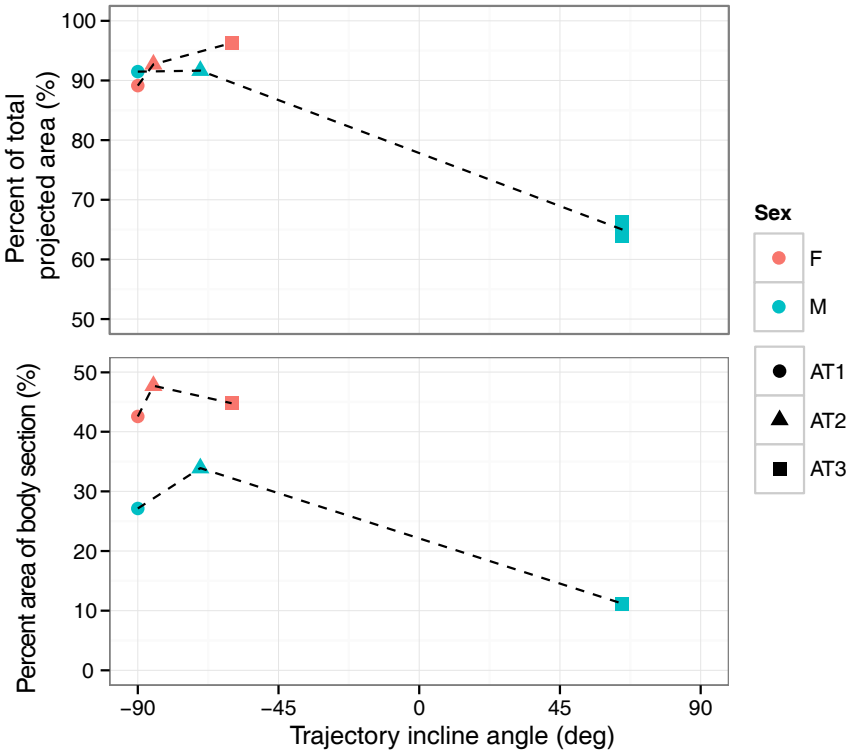

Figure 4.21: (Top) The percentage of projected planform area of body sections and legs combined in flow direction. (Bottom) The area percent of body section relative to total projected planform area in flow direction.

4.4 Discussion

The flight morphology and biomechanics in *A. tanarata* are sexually dimorphic and vary between different altitudes. Along the gradient of increasing altitude, the insects undergo body size miniaturization and an allometric reduction of flight apparatus. Quantitative comparison of flight trajectories suggested the reduction in flight performance is closely correlated with wing size reduction, but detailed wing kinematics suggested more complex and non–linear correlations among morphology, kinematics and aerodynamics. Also, the coordination of body and legs showed transition of roles in flight.

4.4.1 Morphological correlates of flight reduction

First, whole–insect morphology changes with both altitude and sex. Body size miniaturization on high altitude is likely associated with the gradient of lowland to montane climate [98, 100]. Body parts follow different size allometries with changing altitude. The increase in mass percent of abdomen in females reflects the conservation of developmental input for fecundity, which may limit the minimal size of reproductive organs. For example, the egg size and mass was found to be extremely conservative among three populations (unpublished data). Differentiated allometries suggest potential trade–off relationships among body parts and changes in developmental regulation. Also, flight apparatus undergo reduction with increasing altitude. The structural simplification of wingbase design and reduction in mass percent of thoracic musculature is likely responsible to the variation in wing kinematics discussed below.

Secondly, size–reduced wings retain the basic structural plan. It is the reduction of anal veins, which form the majority of membranous region, causes reduction in wing mobility, e.g., maximum forward sweep position, and changes in wing shape. Reduction in vein density likely changes the aeroelastic properties and is, along with reduction in wingbase stiffness, responsible for reduced wing flapping kinematics and the complete loss of wing strokes under extreme conditions, i.e., in both sexes of AT1.

Third, given the changes in morphological setting, flight biomechanics is fundamentally affected in three major aspects: (A) increase of wing loading due to wing size reduction, which predicts increased impact of body weight to flight performance, weakened maneuverability, and greater aerodynamic pressure exerted to unit body area, including both wings and other parts; (B) structural reduction and simplification of flight apparatus may alter wing kinematics and trigger novel wing behaviors and aerodynamics different from traditionally recognized flapping; (C) changes in mass distribution and relative size of body sections and legs potentially influence the strategies of coordination in different flight performances.

4.4.2 Gradient of flight performance

Different flight trajectories form a continuum of performance from highly maneuverable flapping to parachuting, correlated with the trend of wing loading increase from fully–developed to miniaturized–wing flight morphs. Only AT3M exhibited flight performance that matches conventional definition, e.g., 3D maneuverability, capability of ascending. Parachuting and gliding observed in all other flight morphs are the maximum performance. A gradient of performance, e.g., quantified as different L/D ratio, is correlated with the gradient of relative wing size and whole–insect morphology associated with wing reduction. In parachuting flight, the combination of miniaturized wings, body sections and legs generates mostly aerodynamic drag that offsets body weight. Significant lift production is shown in different gliding flights. We also showed the loss of effective lift production and increase of terminal speed in 4 flight morphs with constrained wings, which indicates the functional significance of miniaturized wings. Fitting flight performance against relative wing size, the enhancement of lift production is largely associated with relatively larger wings, and the extremely reduced wings have limited ability of lift generation. The variation in flight performance largely influences the aerodynamics of wings and how stability is maintained, which are discussed below.

Parachuting and gliding are adaptive locomotion types found in many arboreal animals [36, 37]. Here they are shown in a sequence, in both sexes, as secondarily derived reduced forms of flapping flight, reflection a gradient of selective pressure for flight reduction along the ecological gradient. Escape through airborne drop is common among arboreal stick insects. Although voluntary takeoff was only observed in males, but active dropping from trees and falling into understory in response to disturbance was frequently observed in all subspecies, including full–winged AT3M, during our field survey. Free fall can be more efficient than flight under certain circumstances, e.g., at night.

4.4.3 Wing kinematics and implications for aerodynamics

The degree of freedom and mobility are reduced in wings of reduced sizes, which limits the variability of flapping kinematics from the perspective of design. This is likely due to the structural simplification of wing base. Two basic wing kinematics parameters, wingstroke amplitude and wingbeat frequency, change with relative wing size. The variation in stroke amplitude is likely associated with both aforementioned structural reduction and the reduction in muscle strength. Higher wind speed in parachuting and gliding also can restrict the maximum downstroke position in flight. On the other hand, wingbeat frequency increase in intermediately reduced wings (AT2 and AT3F). This is likely due to decreased wing inertia, aeroelastic interaction, body size, thoracic stiffness, and changed neural activation of flight muscle [35]. The loss of wing strokes in miniaturized wings may also be attributed to many factors. It can be due to the loss of flight musculature. Another likely reason is that aerodynamic force overcome potentially small–scale stroke movements by damping effects. To

determine which factor leads to the loss of wing strokes, future investigation may use electromyography to examine the neural activities of flight muscle, and record wing kinematics in still air with wind simulation to wind–sensing organs [60].

Wings in reduced flight showed advance ratio that much larger than those associated with conventionally recognized insect flight. The advance ratio characterizes the relative magnitude of translational to flapping motion, and is an indicator of the steadiness of aerodynamic flow around the flapping wings [42, 35]. For example, hovering flight has advance ratio nearly 0, and for forward flight in most insects it is estimated to be around 0.25. Depending on the advance ratio, same flapping kinematics may have different aerodynamic outcomes [31]. Nonetheless, the variation of advance ratio among winged insects is not well known. Different from flapping flight with fully developed wings, parachuting and gliding flight are predominated by vertically downward translation due to large wing loading. In our study, the large advance ratio associated with reduced flapping wings suggests different aerodynamics: (A) steady aerodynamic flow is associated with the functioning of size–reduced wings, which can mostly produce drag; (B) the unsteadiness increases as the flapping activities is enhanced, which involves the combined effects of wing size, wingbeat frequency and stroke amplitude; (C) our result suggest the gradient of advance ratio does not only represents the intrinsic changes of aerodynamic interactions between wings and flow but also well correlates with the capabilities of overall lift generation, as shown by the progressive increase of L/D ratio with larger wings. In other words, reduced flapping has long wave length of flapping, and its aerodynamics may be more similar to airfoils with low flapping frequencies and amplitudes, e.g., sails [126]. Both reduction in aspect ratio and flapping amplitude may contribute to the differences in aerodynamics [46, 124].

Furthermore, half–stroke behaviors of reduced flight differ from flapping flight. With high advance ratio, upstrokes have downward velocity and likely serve similar function as downstrokes. Also, half–stroke asymmetries in both speed and direction is correlated with relative wing size. In gliding flights of negative incline, half–stroke speed and Reynolds number asymmetries increases with trajectory incline angle, suggesting differences in the force magnitude of half–strokes. The reduction of downstroke flapping speed in size–reduced wings is likely resulted from the weakening of flight musculature. These results indicate the functional partitioning between up– and downstrokes is positively correlated with the relative wing size in flight.

Overall, our results showed a progressive pattern of re–organization of basic wing kinematics in size–reduced wings. Wing design, wing kinematics and flight trajectories together determine the transition of wing aerodynamics along the performance gradient. Various hypotheses regarding the transition of wing kinematics in a functional context, e.g., gliding–flight transition, have been proposed [91, 137], our results provide empirical data for further studies on this topic. To address the aerodynamics of reduced flapping with large advance ratio, future studies may first describe 3D wing kinematics in greater details and evaluate the force production under various combinations of wing kinematics and advance ratio using

model–based measurements.

4.4.4 Body and leg kinematics along the performance gradient

The variation of body and leg kinematics in different flight morphs also reflects how other body parts accommodate different levels of wing reduction at performance level. In both sexes, the angle of attack of anterior body section generally decreases with increasing trajectory incline angle, suggesting a shift towards greater lift production. For instance, theoretical study suggests the L/D ratio of insect–sized cylinder is maximized at angle of attack near 30°at $Re = 5000$ [43]. Similar trend is observed in the trend of how posterior body section's angle of attack changes with trajectory incline angle in males. However, posterior body section's angle of attack in females are maintained around 90°, which is characterized by large portion ($> 95\%$) of drag generation. The interrelations between anterior and posterior body sections also indicate different strategies for maintaining the longitudinal stability. Both sexes of AT1 showed dorsiflexion of body sections, which is advantageous for staying stable by raising the center of aerodynamic pressure while lowering the center of mass. On the other hand, AT3M exhibits oscillation of both body sections. Such behavior is common in insects with elongated body, e.g., locust and mantis [138]. This observation suggests the use of abdomen for providing inertial counter torque, which stabilizes the anterior body section with flapping wings [35, 39]. Together, our results generally suggest the transition of aerodynamic and inertial roles of body sections along the gradient of flight performance, and such transitional process is paralleled in both sexes with subtle differences.

Furthermore, the transition in leg posture along the performance gradient is likely associated with pitch and roll stability. The changes in 3D configuration of legs suggest changes of their roles. An dorsally bended posture of appendages ensures greater stability in parachuting, as in 'pendulum stability' found in other gliding animals [122]. As the trajectory incline angle increases, mid– and hindlegs are more ventrally oriented and further away from the deviation position of forelegs. The degree of backward sweep, especially in mid– and hindlegs, is correlated with more negative trajectory incline, which is likely for balancing the nose–up pitching torque associated generated by the anterior section. As focusing on the average posture during equilibrium performance, we did not address the asymmetry of postures and how it contributes to flight maneuvering with different sized wings. In order for a more accurate assessment of the functional significance of these postures, future studies can measure moment coefficients based on physical models of different postural configurations, and evaluate the result together with estimates of wing forces.

4.4.5 Ecology and evolution of flight reduction

This study demonstrated how flight is reduced with increasing altitude, such a scenario is common among montane insects [109], and likely exists in other lineages local to SE

Asia [114, 14]. Different environmental factors change with altitude in SE Asian forests, such as climate [98, 100], tree ecology [93, 69], and the spatial structure of the forest [3, 100]. Our morphometrics results, e.g., body miniaturization and allometries, suggest the flight reduction in *A. tanarata* is likely a byproduct associated with truncated development. The variation of climatic factors at different altitude ranges, especially temperature and precipitation cycles (unpublished data), likely directly influenced the growth cycle of *A. tanarata* and through other indirect effects, e.g., host plants. On the other hand, canopy height reduces along the altitudinal gradient [3, 100], which likely leads to reduced space for aerial performances and affects the adaptive significance of flight. However, we think it is unsupported to attribute the flight loss to changes in forest structure alone. Substantial canopy height for gliding performance is still observed in host trees of *Asceles*, e.g. $>$ 10m, at the native forest of mini–winged AT1. Also, several sympatric species do not show strong wing reduction as in *A. tanarata*. Our field sampling Was conducted at previously known localities. Given the continuous environmental gradient, future work may reveal morphologies with greater wing loss at higher altitude or other intermediate forms at median altitudes.

Our study showed how one species responds to a gradient of selection towards flightlessness with different sized wings and various levels of reduced flapping flight. Gliding and parachuting are shown as consequences of flight reduction yet maintain certain levels of control for wing, body and legs. This result supports that the arboreal environments are an evolutionary arena for transitions between flight and flightlessness [36]. These reduced flight performances provide opportunities for the re–organization of wing and body kinematics. As wing aerodynamics is determined by both physical laws and the morphology and kinematics of wings, the aerodynamic outcome may be sensitive to how morphological and kinematic variables are correlated. Our observation suggests the transitional process from small to large wings is accompanied with non–linear changes, e.g. wingbeat frequency, and differentiation of size–dependent effects, e.g. Reynolds number. Here the great variability of wing size and flight performance are shown among populations of the same species with relatively short genetic distance. For this reason, our conclusion is limited. Nonetheless, the transitional pattern of flight biomechanics along the gradient of wing size can be more accurately assessed and generalized by analyzing the correlations among relevant parameters sampled from different species in a phylogenetic framework.

References

[1] M. Abdullah, S. Siddiqui, and R. Roohi. Geotaxis in the desert locust *Scbistocerca gregaria* (Orthoptera: Acrididae). *Zeitschrift für angewandte Entomologie: zugleich Organ of the Deutsche Gesellschaft für Angewandte Entomologie*, 67:49, 1970.

[2] M. D. Abràmoff, P. J. Magalhães, and S. J. Ram. Image processing with ImageJ. *Biophotonics international*, 11(7):36–42, 2004.

[3] S. Aiba and K. Kitayama. Structure, composition and species diversity in an altitude-substrate matrix of rain forest tree communities on Mount Kinabalu, Borneo. *Plant Ecology*, 140(2):139–157, 1999.

[4] C. Allen. *Astrophysical quantities*. Athlone Press, London, 1973.

[5] S. J. Arnold. Morphology, performance and fitness. *American Zoologist*, 23(2):347–361, 1983.

[6] E. Baird, E. Kreiss, W. Wcislo, E. Warrant, and M. Dacke. Nocturnal insects use optic flow for flight control. *Biology Letters*, 7(4):499–501, 2011.

[7] P. Baker. The wing movements of flying locusts during steering behaviour. *Journal of Comparative Physiology A: Neuroethology, Sensory, Neural, and Behavioral Physiology*, 131(1):49–58, 1979.

[8] J. Bell, D. Bohan, E. Shaw, and G. Weyman. Ballooning dispersal using silk: world fauna, phylogenies, genetics and models. *Bulletin of Entomological Research*, 95(02):69–114, Mar. 2007.

[9] W. Bell. Searching behavior patterns in insects. *Annual Review of Entomology*, 35(1):447–467, 1990.

[10] E. Binns. Take-off and the 'tarsal reflex' in *Aphis fabae*. *Physiological Entomology*, 2(2):97–102, 1977.

[11] O. Bjorkman and M. Ludlow. Characterization of the light climate on the floor of a Queensland rainforest. *Carnegie Institution of Washington Yearbook*, 71:85–94, 1972.

[12] N. Blüthgen, A. Metzner, and D. Ruf. Food plant selection by stick insects (Phasmida) in a Bornean rain forest. *Journal of Tropical Ecology*, 22(01):35–40, 2006.

[13] D. Bowman, B. Wilson, and L. McDonough. Monsoon forests in northwestern Australia I. Vegetation classification and the environmental control of tree species. *Journal of Biogeography*, 18(6):679–686, 1991.

[14] P. E. Bragg. *Phasmids of Borneo*. Natural History Publications (Borneo),Malaysia, 2001.

[15] A. Briscoe and L. Chittka. The evolution of color vision in insects. *Annual review of entomology*, 46(1):471–510, 2001.

[16] P. Brock. Studies on the Australasian stick-insect genus *Extatosoma* Gray (Phasmida: Phasmatidae: Tropoderinae: Extatosomatini). *Journal of Orthoptera Research*, 10(2):303–313, 2001.

[17] P. Brock and J. Hasenpusch. *Complete Field Guide to Stick and Leaf Insects of Australia*. Commonwealth Scientific and Industrial Research Organisation, 2009.

[18] P. D. Brock and R. Fry. *The Amazing World of Stick and Leaf Insects*. Amateur Entomologists' Society, 1999.

[19] A. Brockmann and G. Robinson. Central projections of sensory systems involved in honey bee dance language communication. *Brain, behavior and evolution*, 70(2):125–136, 2007.

[20] A. Büschges, J. Schmidt, and H. Wolf. Sensory processing in invertebrate motor systems. *eLS*, 2001.

[21] G. Byrnes, T. Libby, N. Lim, and A. Spence. Gliding saves time but not energy in Malayan colugos. *The Journal of Experimental Biology*, 214(16):2690–2696, 2011.

[22] U. Calberg. An analysis of the secondary defense reactions in stick insects (Phasmida). *Biologisches Zentralblatt*, 100:295–303, 1981.

[23] U. Calberg. External morphological postembryonic development in *Extatosoma tiaratum* (MacLeay) (Insecta: Phasmida). *Zoologische Jahrbücher. Abteilung für Anatomie und Ontogenie der Tiere*, 110(3):365–372, 1983.

[24] U. Calberg. Sizes of Eggs and Oviposition Females of *Extatasoma tiaratum* (MacLeay) (Insecta: Phasmida). *Zoologischer Anzeiger*, 212:226–228, 1984.

[25] U. Carlberg. Hatching-time of *Extatosoma tiaratum* (Macleay) (Phasmida). *Entomologist's Monthly Magazine*, 117:199–200, 1981.

[26] U. Carlberg. A review of the different types of egglaying in the Phasmida in relation to the shape of the eggs and with a discussion on their taxonomic importance (Insecta). *Biologisches Zentralblatt*, 102(5):587–602, 1983.

[27] U. Carlberg. Hatching rhythms in *Extatasoma tiamtum* (MacLeay) (Insecta: Phasmida). *Zoologische Jahrbuecher Abteilung fuer Allgemeine Zoologie und Physiologie der Tiere*, 88 (4):441–446, 1984.

[28] B. Cheng, X. Deng, and T. L. Hedrick. The mechanics and control of pitching manoeuvres in a freely flying hawkmoth (*Manduca sexta*). *The Journal of Experimental Biology*, 214(24):4092–4106, 2011.

[29] H. Cruse and C. Bartling. Movement of joint angles in the legs of a walking insect, *Carausius morosus*. *Journal of Insect Physiology*, 41(9):761–771, 1995.

[30] A. Dafni, M. Lehrer, and P. Keyan. Spatial flower parameters and insect spatial vision. *Biological Reviews*, 72(2):239–282, 1997.

[31] W. B. Dickson and M. H. Dickinson. The effect of advance ratio on the aerodynamics of revolving wings. *Journal of Experimental Biology*, 207(24):4269–4281, 2004.

[32] H. Dingle. Flight and swimming reflexes in giant water bugs. *Biological Bulletin*, pages 117–128, 1961.

[33] A. Dixon, S. Horth, and P. Kindlmann. Migration in insects: cost and strategies. *Journal of Animal Ecology*, pages 182–190, 1993.

[34] A. F. Dixon and P. Kindlmann. Cost of flight apparatus and optimum body size of aphid migrants. *Ecology*, 80(5):1678–1690, 1999.

[35] R. Dudley. *The biomechanics of insect flight: form, function, evolution*. Princeton University Press, 2002.

[36] R. Dudley, G. Byrnes, S. Yanoviak, B. Borrell, R. Brown, and J. McGuire. Gliding and the Functional Origins of Flight: Biomechanical Novelty or Necessity? *Annual Review of Ecology, Evolution, and Systematics*, 38:179–201, 2007.

[37] R. Dudley and S. P. Yanoviak. Animal aloft: the origins of aerial behavior and flight. *Integrative and comparative biology*, 51(6):926–936, 2011.

[38] J. Dyhr and C. Higgins. The spatial frequency tuning of optic-flow-dependent behaviors in the bumblebee *Bombus impatiens*. *Journal of Experimental Biology*, 213(10):1643–1650, 2010.

[39] J. P. Dyhr, K. A. Morgansen, T. L. Daniel, and N. J. Cowan. Flexible strategies for flight control: an active role for the abdomen. *The Journal of experimental biology*, 216(9):1523–1536, 2013.

[40] M. Edwards. Zero angular momentum turns. *American Journal of Physics*, 54:846, 1986.

[41] C. Ellington. The aerodynamics of hovering insect flight. II. Morphological parameters. *Philosophical Transactions of the Royal Society of London. Series B, Biological Sciences*, 305(1122):17–40, 1984.

[42] C. Ellington. The aerodynamics of hovering insect flight. III. Kinematics. *Philosophical Transactions of the Royal Society of London. Series B, Biological Sciences*, pages 41–78, 1984.

[43] C. Ellington. Aerodynamics and the origin of insect flight. *Advances in Insect Physiology*, 23:171–210, 1991.

[44] J. A. Endler. The color of light in forests and its implications. *Ecological monographs*, pages 2–27, 1993.

[45] A. R. Ennos. The inertial cause of wing rotation in Diptera. *Journal of experimental biology*, 140(1):161–169, 1988.

[46] A. R. Ennos. Inertial and aerodynamic torques on the wings of Diptera in flight. *Journal of Experimental Biology*, 142(1):87–95, 1989.

[47] K. Fent and R. Wehner. Oceili: A celestial compass in the desert ant *Cataglyphis*. *Science*, 228(4696):192–194, 1985.

[48] F. E. Fish, A. J. Nicastro, and D. Weihs. Dynamics of the aerial maneuvers of spinner dolphins. *The Journal of experimental biology*, 209(Pt 4):590–8, Feb. 2006.

[49] J. W. Flower. On the origin of flight in insects. *Journal of Insect Physiology*, 10(1):81–88, 1964.

[50] T. Garland and J. B. Losos. Ecological morphology of locomotor performance in squamate reptiles. *Ecological morphology: integrative organismal biology*, pages 240–302, 1994.

[51] K. G. Götz. Flight control in Drosophila by visual perception of motion. *Kybernetik*, 4(6):199–208, 1968.

[52] P. Haemig. Effects of birds on the intensity of ant rain: a terrestrial form of invertebrate drift. *Animal behaviour*, 54(1):89–97, 1997.

[53] J. Hanken and D. B. Wake. Miniaturization of body size: organismal consequences and evolutionary significance. *Annual Review of Ecology and Systematics*, pages 501–519, 1993.

[54] J. Hasenpusch and P. D. Brock. Macleays Spectre *Extatosoma tiaratum* - taking camouflage to an extreme! *The Newsletter of The Phasmid Study Group*, March:11–12, 2009.

[55] J. Hateren and C. Schilstra. Blowfly flight and optic flow. II. Head movements during flight. *Journal of Experimental Biology*, 202(11):1491–1500, 1999.

[56] T. L. Hedrick. Damping in flapping flight and its implications for manoeuvring, scaling and evolution. *The Journal of Experimental Biology*, 214(24):4073–4081, 2011.

[57] D. Hochuli. Insect herbivory and ontogeny: How do growth and development influence feeding behaviour, morphology and host use? *Austral Ecology*, 26(5):563–570, 2001.

[58] B. Hölldobler. Canopy orientation: a new kind of orientation in ants. *Science*, 210(4465):86, 1980.

[59] L. Hughes and M. Westoby. Capitula on stick insect eggs and elaiosomes on seeds: convergent adaptations for burial by ants. *Functional Ecology*, 6(6):642–648, 1992.

[60] R. Hustert and R. Klug. Evolution of a new sense for wind in flying phasmids? Afferents and interneurons. *Naturwissenschaften*, 96(12):1411–1419, 2009.

[61] J. Iriarte-Díaz and S. M. Swartz. Kinematics of slow turn maneuvering in the fruit bat *Cynopterus brachyotis*. *Journal of Experimental Biology*, 211(21):3478–3489, 2008.

[62] R. Junker, T. Itioka, P. Bragg, and N. Blüthgen. Feeding preferences of phasmids (Insecta: Phasmida) in a Bornean dipterocarp forest. *Raffles Bulletin of Zoology*, 56(2):445–452, 2008.

[63] A. Jusufi, D. Goldman, and S. Revzen. Active tails enhance arboreal acrobatics in geckos. *Proceedings of the National Academy of Sciences*, 105(11):4215, 2008.

[64] A. Jusufi, Y. Zeng, R. J. Full, and R. Dudley. Aerial righting reflexes in flightless animals. *Integrative and comparative biology*, 51(6):937–943, 2011.

[65] T. Kane and M. P. Scher. A dynamical explanation of the falling cat phenomenon. *International Journal of Solids and Structures*, 5:663–670, 1969.

[66] R. Kern, M. Egelhaaf, and M. Srinivasan. Edge detection by landing honeybees: behavioural analysis and model simulations of the underlying mechanism. *Vision research*, 37(15):2103–2117, 1997.

[67] H. H. Kimball and I. F. Hand. Sky-Brightness and Daylight-Illumination Measurements. *Monthly weather review*, 49(9):481–488, 1921.

[68] J. G. Kingsolver and M. Koehl. Selective factors in the evolution of insect wings. *Annual review of entomology*, 39(1):425–451, 1994.

[69] K. Kitayama and S.-I. Aiba. Ecosystem structure and productivity of tropical rain forests along altitudinal gradients with contrasting soil phosphorus pools on Mount Kinabalu, Borneo. *Journal of Ecology*, 90(1):37–51, 2002.

[70] H. Komsuolu, K. Sohn, R. J. Full, and D. E. Koditschek. A physical model for dynamical arthropod running on level ground. In *Experimental Robotics*, pages 303–317. Springer, 2009.

[71] K. Kral and M. Poteser. Motion parallax as a source of distance information in locusts and mantids. *Journal of insect behavior*, 10(1):145–163, 1997.

[72] D. Kramer and R. McLaughlin. The behavioral ecology of intermittent locomotion. *American Zoologist*, 41(2):137–153, 2001.

[73] H. G. Krapp, R. Hengstenberg, and M. Egelhaaf. Binocular contributions to optic flow processing in the fly visual system. *Journal of Neurophysiology*, 85(2):724–734, 2001.

[74] C. C. Labandeira, B. S. Beall, and F. M. Hueber. Early insect diversification: evidence from a Lower Devonian bristletail from Québec. American Association for the Advancement of Science, 1988.

[75] M. F. Land. Visual acuity in insects. *Annual review of entomology*, 42(1):147–177, 1997.

[76] D. Lee. Canopy dynamics and light climates in a tropical moist deciduous forest in India. *Journal of Tropical Ecology*, 5(1):65–79, 1989.

[77] M. Lehrer, M. Srinivasan, and S. Zhang. Visual edge detection in the honeybee and its chromatic properties. *Proceedings of the Royal Society of London. B. Biological Sciences*, 238(1293):321–330, 1990.

[78] P. G. Lillywhite. Single photon signals and transduction in an insect eye. *Journal of Comparative Physiology A: Neuroethology, Sensory, Neural, and Behavioral Physiology*, 122(2):189–200, 1977.

[79] J. Longino and R. Colwell. Biodiversity assessment using structured inventory: capturing the ant fauna of a tropical rain forest. *Ecological Applications*, 7(4):1263–1277, 1997.

[80] J. Lough. Regional indices of climate variation: temperature and rainfall in Queensland, Australia. *International journal of climatology*, 17(1):55–66, 1997.

[81] J. H. Marden. Maximum lift production during takeoff in flying animals. *Journal of Experimental Biology*, 130(1):235–258, 1987.

[82] MATLAB. *version 7.14.0.739 (R2012a)*. The MathWorks Inc., Natick, Massachusetts, 2012.

[83] R. Matthews and J. Matthews. *Insect Behavoir*. Springer Verlag, 2009.

[84] W. Mattingly and B. Jayne. Resource use in arboreal habitats: structure affects locomotion of four ecomorphs of *Anolis* lizards. *Ecology*, 85(4):1111–1124, 2004.

[85] R. May. The dynamics and diversity of insect faunas. *Diversity of insect faunas*, pages 188–204, 1978.

[86] Merriam-Websters Online Dictionary. "stroke". `http://www.merriam-webster.com/dictionary/stroke`, 15, Aug, 2013.

[87] G. A. McCulloch, G. P. Wallis, and J. M. Waters. Do insects lose flight before they lose their wings? Population genetic structure in subalpine stoneflies. *Molecular ecology*, 18(19):4073–4087, 2009.

[88] V. Meyer-Rochow and E. Keskinen. Post-embryonic photoreceptor development and dark/light adaptation in the stick insect *Carausius morosus* (Phasmida, Phasmatidae). *Applied Entomology and Zoology*, 38(3):281–291, 2003.

[89] R. M. Murray and S. S. Sastry. *A mathematical introduction to robotic manipulation*. CRC Press, 1994.

[90] D. E. Nilsson. Optics and evolution of the compound eye. In *Facets of vision*, pages 30–73. Springer, 1989.

[91] U. M. Norberg. Evolution of vertebrate flight: an aerodynamic model for the transition from gliding to active flight. *American Naturalist*, pages 303–327, 1985.

[92] U. M. Norberg. Wing design, flight performance, and habitat use in bats. *Ecological morphology: integrative organismal biology*, pages 205–239, 1994.

[93] S. Numata, M. Yasuda, T. Okuda, N. Kachi, and N. S. M. Noor. Temporal and spatial patterns of mass flowerings on the Malay Peninsula. *American Journal of Botany*, 90(7):1025–1031, 2003.

[94] R. Olson and R. McPherson. Potential vs. realized larval dispersal: fish predation on larvae of the ascidian *Lissoclinum patella* (Gottschaldt). *Journal of Experimental Marine Biology and Ecology*, 110(3):245–256, 1987.

[95] D. Osorio. Ultraviolet sensitivity and spectral opponency in the locust. *Journal of experimental biology*, 122(1):193–208, 1986.

[96] R. Paine. Food web complexity and species diversity. *American Naturalist*, pages 65–75, 1966.

[97] R. Pearson, L. Benson, and R. Smith. Diversity and abundance of the fauna in Yuccabine Creek, a tropical rainforest stream. *Monographiae biologicae*, 61:329–342, 1986.

[98] C. A. Pendry and J. Proctor. The causes of altitudinal zonation of rain forests on Bukit Belalong, Brunei. *Journal of Ecology*, pages 407–418, 1996.

[99] J. Pringle. The reflex mechanism of the insect leg. *Journal of Experimental Biology*, 17(1):8–17, 1940.

[100] J. Proctor, Y. Lee, A. Langley, W. Munro, and T. Nelson. Ecological studies on Gunung Silam, a small ultrabasic mountain in Sabah, Malaysia. I. Environment, forest structure and floristics. *The Journal of Ecology*, pages 320–340, 1988.

[101] R Core Team. *R: A Language and Environment for Statistical Computing*. R Foundation for Statistical Computing, Vienna, Austria, 2013.

[102] M. Rankin and J. Burchsted. The cost of migration in insects. *Annual Review of Entomology*, 37(1):533–559, 1992.

[103] D. Rentz. *Grasshopper country: the abundant orthopteroid insects of Australia*. University of New South Wales Press, 1996.

[104] C. Rettenmeyer. Insect mimicry. *Annual Review of Entomology*, 15(1):43–74, 1970.

[105] G. Ribak, M. Gish, D. Weihs, and M. Inbar. Adaptive aerial righting during the escape dropping of wingless pea aphids. *Current biology*, 23(3):R102–R103, Feb. 2013.

[106] C. J. J. Richter. Aerial Dispersal in relation to habitat in eight wolf spider species. *Oecologia*, 5:200–214, 1970.

[107] L. Ristroph, A. J. Bergou, G. Ristroph, K. Coumes, G. J. Berman, J. Guckenheimer, Z. J. Wang, and I. Cohen. Discovering the flight autostabilizer of fruit flies by inducing aerial stumbles. *Proceedings of the National Academy of Sciences*, 107(11):4820–4824, 2010.

[108] A. Robie, A. Straw, and M. Dickinson. Object preference by walking fruit flies, *Drosophila melanogaster*, is mediated by vision and graviperception. *Journal of Experimental Biology*, 213(14):2494–2506, 2010.

[109] D. Roff. The evolution of flightlessness in insects. *Ecological Monographs*, pages 389–421, 1990.

[110] D. Roff. The evolution of flightlessness: is history important? *Evolutionary Ecology*, 8(6):639–657, 1994.

[111] S. Rossel. Binocular stereopsis in an insect. *Nature*, 302:821–822, 1983.

[112] T. Schowalter. *Insect ecology: an ecosystem approach*. Academic Pr, 2006.

[113] F. Seow-Choen. *An Illustrated Guide to the Stick and Leaf Insects of Peninsula Malaysia and Singapore*. Natural History Publications (Borneo), 2000.

[114] F. Seow-Choen. *Phasmids of Peninsular Malaysia and Singapore*. Natural History Publications (Borneo), 2005.

[115] E. C. Sobel. The locust's use of motion parallax to measure distance. *Journal of Comparative Physiology A*, 167(5):579–588, 1990.

[116] J. Socha. Gliding flight in *Chrysopelea*: turning a snake into a wing. *Integrative and Comparative Biology*, 2011.

[117] R. R. Sokal and F. J. Rohlf. *Biometry: the principles and practice of statistics in biological research*. WH Freeman, New York, 1995.

[118] R. Suppiah and K. Hennessy. Trends in total rainfall, heavy rain events and number of dry days in Australia, 1910–1990. *International Journal of Climatology*, 18(10):1141–1164, 1998.

[119] S. Tanaka. Allocation of resources to egg production and flight muscle development in a wing dimorphic cricket,*Modicogryllus confirmatus*. *Journal of Insect Physiology*, 39(6):493–498, 1993.

[120] C. P. Taylor. Contribution of compound eyes and ocelli to steering of locusts in flight: I. Behavioural analysis. *Journal of Experimental Biology*, 93(1):1–18, 1981.

[121] C. P. Taylor. Contribution of compound eyes and ocelli to steering of locusts in flight: II. Timing changes in flight motor units. *Journal of Experimental Biology*, 93(1):19–31, 1981.

[122] A. L. Thomas and G. K. Taylor. Animal flight dynamics I. Stability in gliding flight. *Journal of Theoretical Biology*, 212(3):399–424, 2001.

[123] D. Tomblin and J. Cranford. Ecological niche differences between *Alouatta palliata* and *Cebus capucinus* comparing feeding modes, branch use, and diet. *Primates*, 35(3):265–274, 1994.

[124] E. Vardaki, Z. Wang, and I. Gursul. Flow reattachment and vortex re-formation on oscillating low-aspect-ratio wings. *AIAA journal*, 46(6):1453–1462, 2008.

[125] K. Vernes. Gliding performance of the northern flying squirrel (*Glaucomys sabrinus*) in mature mixed forest of eastern Canada. *Journal of Mammalogy*, 82(4):1026–1033, 2001.

[126] S. Vogel. *Life in moving fluids: the physical biology of flow*. Princeton University Press, 1994.

[127] P. C. Wainwright and S. M. Reilly. *Ecological morphology: integrative organismal biology*. University of Chicago Press, 1994.

[128] J. A. Walker. Estimating velocities and accelerations of animal locomotion: a simulation experiment comparing numerical differentiation algorithms. *Journal of Experimental Biology*, 201(7):981–995, 1998.

[129] G. K. Wallace. Visual scanning in the desert locust *Schistocerca gregaria* Forskål. *Journal of Experimental Biology*, 36(3):512–525, 1959.

[130] D. R. Warrick. The turning-and linear-maneuvering performance of birds: the cost of efficiency for coursing insectivores. *Canadian Journal of Zoology*, 76(6):1063–1079, 1998.

[131] N. Weber. The nest of an anomalous colony of the arboreal ant *Cephalotes atratus*. *Psyche*, 64(2):60–69, 1957.

[132] R. Wehner, B. Michel, and P. Antonsen. Visual navigation in insects: coupling of egocentric and geocentric information. *Journal of Experimental Biology*, 199(1):129–140, 1996.

[133] W. Wheeler. The Australian honey-ants of the genus *Leptomyrmex* Mayr. In *Proceedings of the American Academy of Arts and Sciences*, volume 51, pages 255–286. JSTOR, 1915.

[134] D. M. Wilson. The central nervous control of flight in a locust. *Journal of Experimental Biology*, 38(47):l–490, 1961.

[135] J. Wolken. *Light detectors, photoreceptors, and imaging systems in nature*. Oxford University Press, USA, 1995.

[136] R. Wootton. The fossil record and insect flight. In *Symposium of the Royal Entomological Society of London*, volume 7, pages 235–254, 1976.

[137] R. I. Wootton. How insect wings evolved. In *Insect movement: mechanisms and consequences: proceedings of the Royal Entomological Society's 20th Symposium*, volume 20, page 43. CABI, 2001.

[138] D. Yager, M. May, and M. Fenton. Ultrasound-triggered, flight-gated evasive maneuvers in the praying mantis Parasphendale agrionina. I. Free flight. *Journal of Experimental Biology*, 152(1):17–39, 1990.

[139] N. Yagi. Phototropism of *Dixippus morosus*. *The Journal of General Physiology*, 11(3):297, 1928.

[140] S. Yanoviak. Directed aerial descent in tropical arboreal arthropods. *Comparative Biochemistry and Physiology Part A: Molecular & Integrative Physiology*, 146(4):S145, 2007.

[141] S. Yanoviak and R. Dudley. The role of visual cues in directed aerial descent of *Cephalotes atratus* workers (Hymenoptera: Formicidae). *Journal of Experimental Biology*, 209(9):1777–1783, 2006.

[142] S. Yanoviak, R. Dudley, and M. Kaspari. Directed aerial descent in canopy ants. *Nature*, 433:624–626, 2005.

[143] S. Yanoviak, M. Kaspari, and R. Dudley. Gliding hexapods and the origins of insect aerial behaviour. *Biology Letters*, 2009.

[144] S. Yanoviak, Y. Munk, M. Kaspari, and R. Dudley. Aerial manoeuvrability in wingless gliding ants (*Cephalotes atratus*). *Proceedings of the Royal Society B*, 2010.

[145] A. J. Zera and R. F. Denno. Physiology and ecology of dispersal polymorphism in insects. *Annual review of entomology*, 42(1):207–230, 1997.